X-615-65-296

NASA TM X-55368

THE EQUILIBRIUM ELECTRIC POTENTIAL OF A BODY IN THE UPPER ATMOSPHERE AND IN INTERPLANETARY SPACE

BY

E. C. WHIPPLE, JR.

JUNE 6, 1965

NASA — GODDARD SPACE FLIGHT CENTER —
GREENBELT, MARYLAND

THE EQUILIBRIUM ELECTRIC POTENTIAL OF A BODY IN THE UPPER ATMOSPHERE AND IN INTERPLANETARY SPACE

By Elden Cole Whipple, Jr.

B. S., June, 1955, Wheaton College, Wheaton, Illinois
M. S., October, 1958, The George Washington University, Washington, D. C.

A thesis submitted to the Faculty of the Graduate Council of The George Washington University in partial satisfaction of the requirements for the degree of Doctor of Philosophy.

June 6, 1965

Thesis directed by John Fulmer Clark, Ph. D.

BLANK PAGE

ABSTRACT

N66 17226

A body in the upper atmosphere or in space will acquire an electric charge, or potential, which must be known to determine the motion of micrometeorites, the drag on earth satellites, and to assess the behavior of certain experiments on satellites.

The equation for ion and electron currents to a sphere are available in the literature for small bodies. For large bodies, an estimate of the influence of the plasma sheath is required in an attractive field. Poisson's equation has been solved numerically for high-velocity spheres, and the ion current obtained by an analysis of the ion's distance of closest approach. Photoemission is an important charging mechanism for bodies in sunlight. Measurements of photoelectric yields are reviewed and compared with photocurrents measured above the atmosphere. Secondary electron emission upon energetic particle impact may also be an important mechanism, especial in the earth's radiation belts. The effects of cosmic rays, radioactivity, thermionic and field emission, collisions with dust grains, and the influence of radio-frequency electric fields are generally negligible. A magnetic field induces a potential gradient in a moving body; in addition, the restriction of electrons to a spiralling motion along the field line decreases the body's effective collection area.

These charging mechanisms are evaluated for conditions in the upper atmosphere and in interplanetary space, and are combined into expressions from which the equilibrium potential may be determined. In the ionosphere the equilibrium potential is typically a few tenths of a volt negative. At higher altitudes the potential may become positive in the sunlight as photoemission predominates over positive ion collection. In the earth's magnetosphere the potential is sensitive to the ratio of electron flux to photoemission, and may vary widely. Positive values are limited to a few volts, but large negative values are possible. In interplanetary space positive potentials due to both photoemission and the solar wind protons are expected.

The equilibrium potential of the satellite Explorer VIII has been measured in both darkness and sunlight. There is general agreement with theoretical values at higher altitudes. At low altitudes the measured potentials are more negative than anticipated. This is shown to be due to a radio-frequency plasma impedance experiment carried on the satellite.

Author

BLANK PAGE

ACKNOWLEDGMENTS

I would like to thank the National Aeronautics and Space Administration for their support of my graduate work, and for their permission to use data obtained while at the Goddard Space Flight Center for the thesis. I would especially like to thank Dr. John F. Clark for his advice and guidance during the preparation of the thesis, and also my colleague Dr. Eugene J. Maier for his careful reading of the manuscript and his helpful comments. I also would like to acknowledge the helpful discussions with my other colleagues: Mr. Robert E. Bourdeau, Mr. John L. Donley, Mr. Gideon P. Serbu and Mr. Ballard E. Troy.

I am indebted to Mr. David Quinn for his many hours of data plotting, calculating, and computer programming. Mr. Daniel Elliot also assisted in some computer programming and Mr. William Zadell in some of the plotting and calculations. The staff of the Physical Science Laboratory of the New Mexico State University assisted with the Explorer VIII data reduction.

Finally, I would like to thank my wife, June, for her encouragement and for her help in proof-reading the final text.

BLANK PAGE

TABLE OF CONTENTS

TABLE OF CONTENTS (Continued)

LIST OF TABLES

BLANK PAGE

LIST OF FIGURES

LIST OF FIGURES (Continued)

LIST OF FIGURES (Continued)

CHAPTER I

INTRODUCTION

1. The Concept of Equilibrium Charge. A body in the upper atmosphere or in space, such as a satellite, a meteor, or a dust grain, is continually bombarded by environmental particles of which a proportion will be electrically charged, such as electrons, ions or cosmic rays. When such an encounter occurs there is, in general, a transfer of charge either to or from the body. Other processes may also occur that can effect a charge transfer. Incident photons of sufficient energy will induce the emission of photoelectrons. Under the proper conditions thermal emission or field emission of electrons could occur. Other mechanisms of charge transfer include radioactivity of the material composing the body, secondary emission of electrons and collisions with other bodies such as micrometeors (dust grains).

The rate at which charge transfer proceeds for a given mechanism depends both upon characteristics of the body such as its surface area and material and on the environmental conditions such as the number density of charged particles. In particular, this rate of change of charge on the body depends on the net charge already residing on the body. This is merely saying that the motion of charged particles in the vicinity of the body is influenced by the electric field arising from the charge distributed on the body. A positive charge will attract electrons and repel ions. Secondary or photoelectrons may not escape but may return to the body.

These statements may be summarized in a differential equation for the charge on such a body. If we let I denote the total current to the body, we have

$$I = \frac{dQ}{dt} = f\ (Q,\ \text{body characteristics, environmental conditions}) \quad (1.1)$$

where Q is the total charge on the body. A complete understanding of the charge as a function of time requires a solution of (1.1) where the right hand side expresses the sum of the various currents to the body as a function of Q and t. However, it turns out that typical charging or discharge times are small compared with the time in which significant changes in the environmental conditions usually occur. For example, the period of revolution or tumbling of a satellite will be on the order of a second or greater, whereas discharge times will be on the order of milliseconds or less, as will be shown later when the various mechanisms are discussed in detail. Consequently, it is a good approximation to assume that the environmental conditions remain constant during the time that it takes for a body to acquire a charge; hence, the right hand side of equation (1.1) will not be explicitly dependent upon time. One exception to this assumption occurs when the effect of radio frequency voltages on current collection is considered, as discussed in Chapter V.

With this approximation it is convenient to discuss equation (1.1) by referring to a "phase diagram" similar to the kind employed in describing the behavior of oscillatory systems. Figure 1 is such a plot of the current I versus charge Q for a hypothetical but typical body in space. Such a curve is typical, for instance, of the case in which the positive current is due to positive ion collection and the negative current is due to electron collection from the environmental plasma.

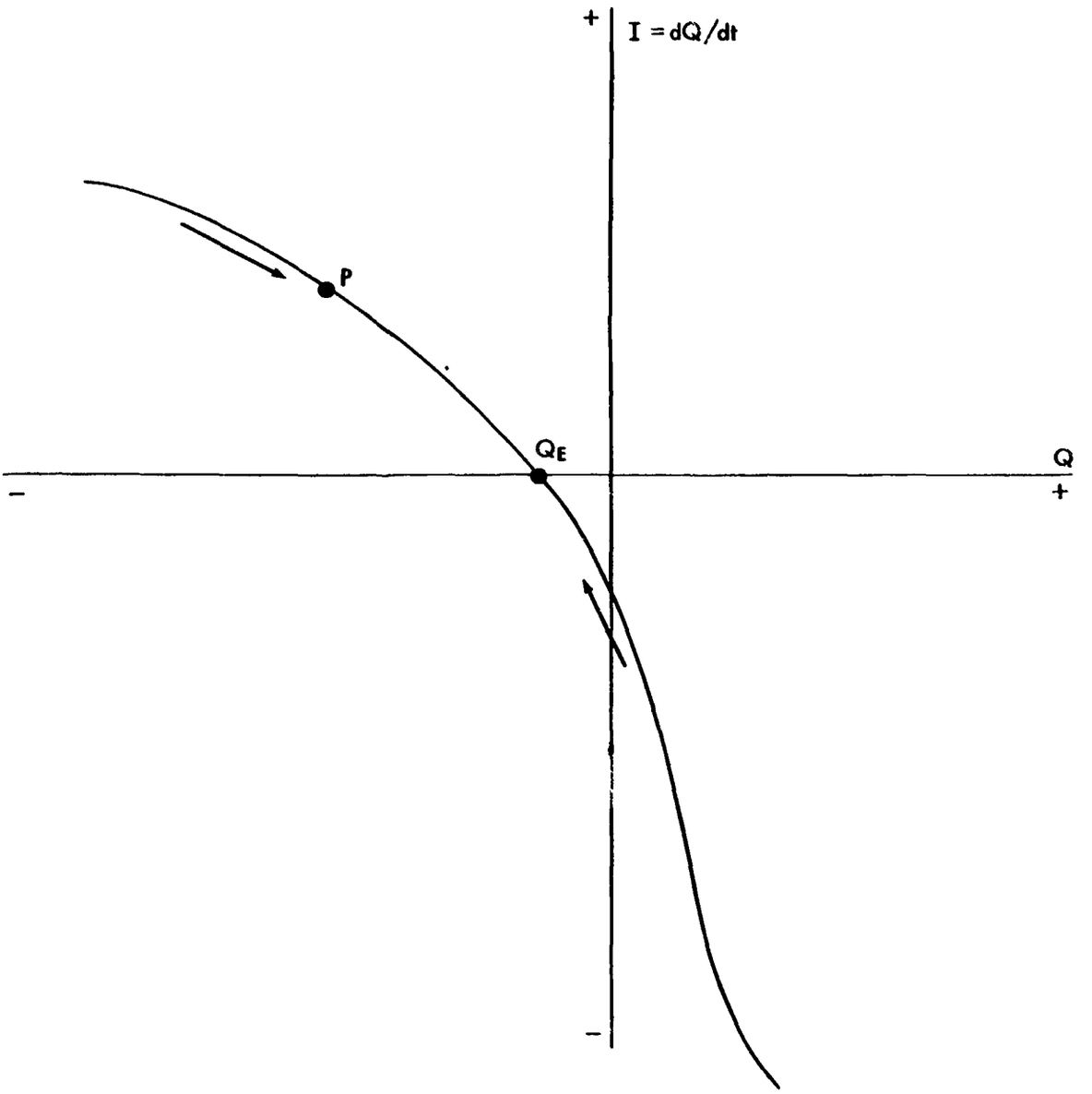

Figure 1. Phase Diagram Illustrating Typical Dependence of Current on Charge

The behavior of the system can be described by the motion of the representative point P. For positive I, P will move to the right, as shown by the arrow indicating an increase in Q. For a negative current P will move to the left. When P arrives at the point on the abscissa marked Q_E its motion will cease; the current is zero and hence Q remains constant: Q_E is the so-called equilibrium charge. It is important to note that this is a point of stable equilibrium, since if P is displaced from Q_E the direction of the arrows is such as to restore the system to equilibrium.

The curve in Figure 1 is also typical of most natural current mechanisms in that it is monotonic – the slope of the curve is everywhere negative. A negative slope indicates a positive (but not necessarily linear) resistance between the medium and the body, with a steeper slope indicating a lower resistance.

The existence of a stable equilibrium point depends upon this resistive character of the charging mechanisms involved. To see this, consider a hypothetical mechanism exhibiting 'negative' resistance. Such a mechanism is physically feasible although unlikely. For example, a material with secondary emission characteristics can be imagined with a secondary emission yield which increases at some threshold energy of the incident primary electrons to a value greater than unity with increasing energy. If, in addition, the secondaries were all emitted with an energy distribution centered at an energy sufficient for escape, one would have a phase diagram similar to that shown in Figure 2.

This system has three possible equilibrium points as indicated by Q_1, Q_2, Q_3. Only two of these are stable, however. The point Q_2 on the negative resistance portion of the curve is unstable. Even though dQ/dt

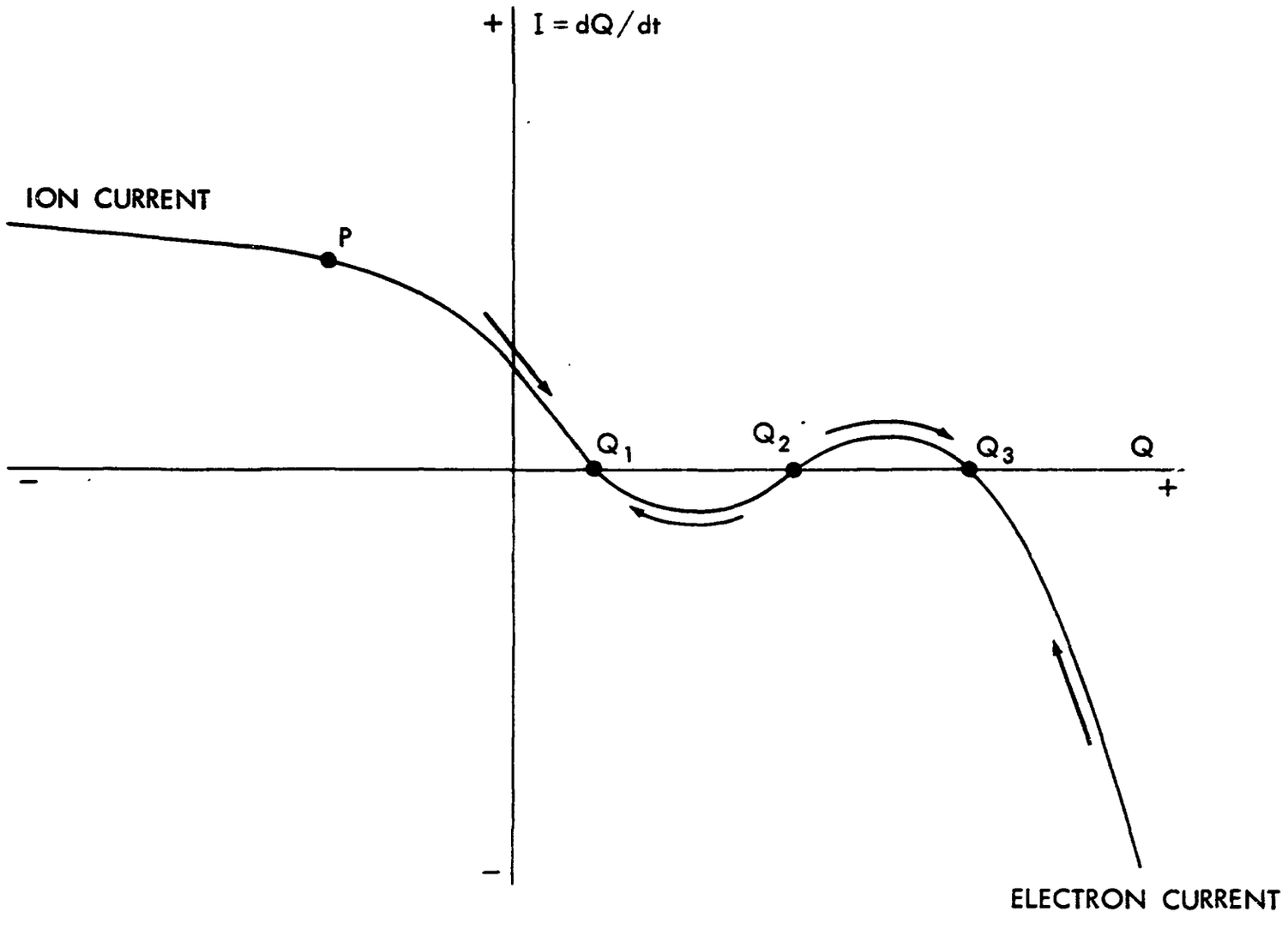

Figure 2. Phase Diagram Illustrating the Effect of a Negative Resistance Mechanism

is zero at Q_2, a slight fluctuation of the charge will cause the system to move to one of the two stable equilibrium points as indicated by the direction of the arrows.

The question arises: might not a current mechanism be possible such that an oscillatory solution could be obtained? It is difficult to think of any natural mechanism of this type; but it would be simple to construct such a device which could be placed in a satellite. For example, an electric field meter to sense the polarity and magnitude of the satellite charge could be combined with an ion gun in such a way that the curve of current versus charge of Figure 3 would be obtained. The ion gun would be turned on when $Q = Q_2$ and turned off when $Q = Q_1$. If the initial (non-equilibrium) charge were sufficiently negative the equilibrium point Q_E would never be reached; the ion gun would cycle on and off as the representative point P travels around the closed loop ABCD. This demonstrates the fact that for an oscillatory solution of (1.1), when the righthand-side does not explicitly depend upon time, the current must be at least double-valued as a function of Q. In other words, the current mechanism must involve at least two states in such a way that the system can alternate between the two or more states.

2. Applications of Equilibrium Char[illegible]ations. Knowledge of the equilibrium charge on a body is im[illegible]o several areas of investigation. In the ionosphere and also in [illegible]erplanetary and interstellar space the flux of ions and electrons to a body such as a dust grain constitutes a loss mechanism for the charged particles in the medium.[1] Electrons striking the body are usually captured, while ions in striking the body ordinarily pick up an electron and rebound as a neutral atom or molecule. Since the fluxes of ions and electrons are influenced by

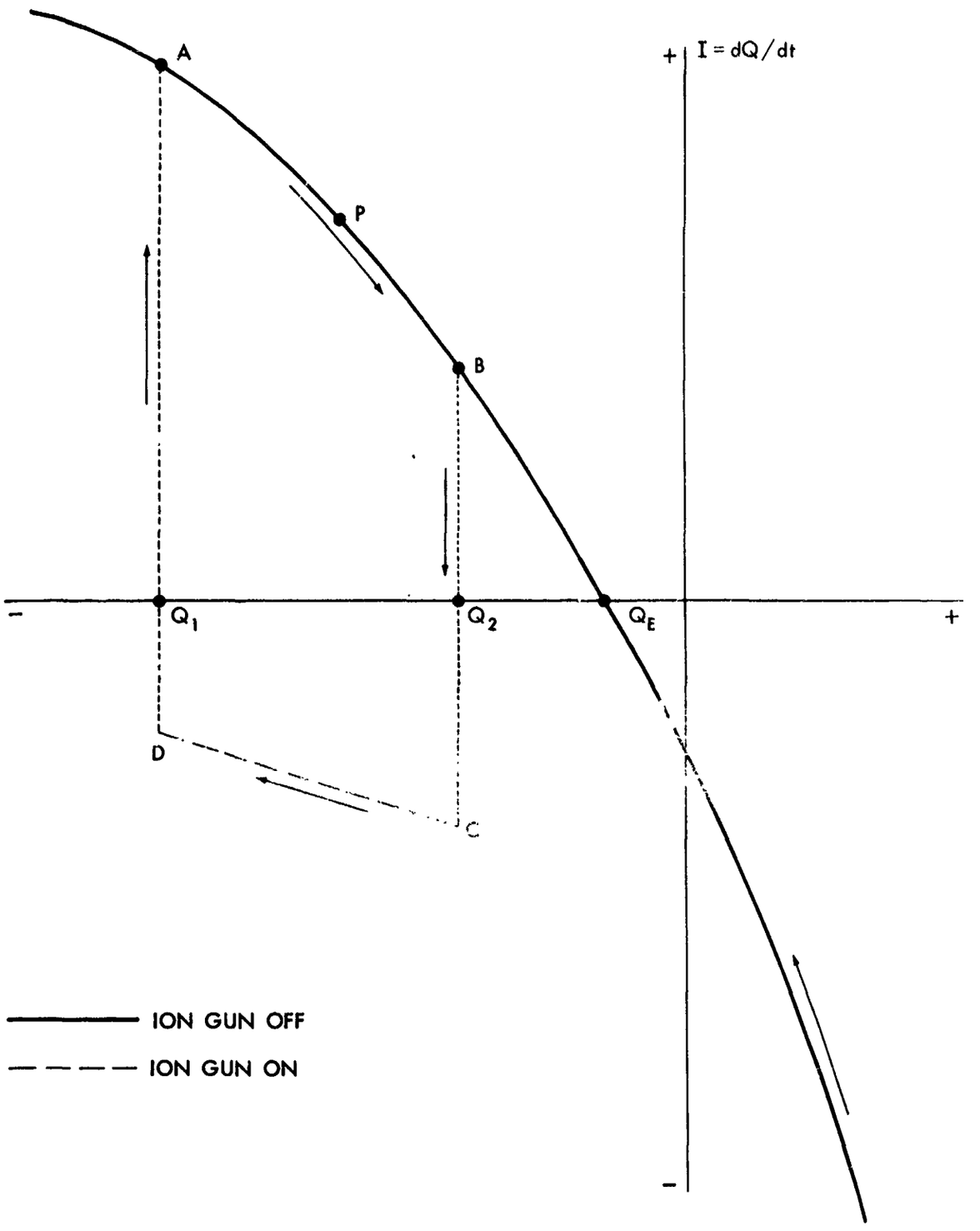

Figure 3. Phase Diagram Illustrating Oscillatory Behavior of Satellite Charge

the grain's charge, this information is necessary to determine the ionization balance of the medium.

Spitzer has shown that photoemission from interstellar grains is a source of kinetic energy for the interstellar medium.[2] Since the amount of energy carried away from the grain depends upon the grain's charge, this quantity needs to be estimated.

In interplanetary space the motion of micrometeorites, if they are charged, will be influenced by the interplanetary magnetic field originating from the sun,[3,4] and also by the earth's magnetic field.[5]

The electric charge on a satellite increases the atmospheric drag by attracting ions of opposite polarity to the satellite which otherwise would not have impacted. Momentum is also transferred to ions which do not impact directly but are deflected by the satellite's electric field.[6,7,8] It is also possible that the motion of a charged satellite through the ionosphere will excite plasma waves which can carry away energy from the satellite.[9,10]

The charge on a rocket or satellite may have an important influence on the behavior of experiments designed to measure the properties of charged particles in the atmosphere. Johnson and Meadows have discussed the effect of a vehicle charge on the performance of a rocket-borne ion mass spectrometer.[11] The interpretation of data from ion and electron traps and from Langmuir probes must take into account the effects of the potential between the vehicle and the medium.[12,13] Conversely, the vehicle potential may be determined from the characteristics of the data from such experiments, as will be illustrated later.

It is frequently advantageous to discuss the charge on a body in terms of the corresponding potential with respect to the surrounding

medium. The charging currents to a body depend upon the body's potential rather than charge; also, the potential is more easily measured on a satellite. The relation between the equilibrium charge and potential – i.e. the body's capacitance – is, in general, a strong function of the environment, which is another way of saying that a body in a plasma behaves quite differently electrically from a body in a vacuum. For example, consider Poisson's equation in spherical coordinates for the potential ϕ, where the space charge ρ, is given by (See also Appendix A.)

$$\rho = N_0 e(1 - e^{\phi e/kT}) \tag{1.2}$$

Here N_0 is the ion or electron density at a great distance, e is the elementary charge, k is Boltzmann's constant and T the plasma temperature. The first term gives the ion density and the second the electron density in front of a fast moving spherical satellite with a negative potential, ϕ_R. If $\left|\frac{\phi_R e}{kT}\right| << 1$, we may write Poisson's equation as

$$\frac{d^2\phi}{dr^2} + \frac{2}{r}\frac{d\phi}{dr} = +\frac{N_0 e}{\epsilon_0}\frac{\phi e}{kT} \tag{1.3}$$

where ϵ_0 is the permittivity.

The solution of (1.3) is the well-known Debye potential

$$\phi = \frac{\phi_R R}{r} e^{-(r-R)/L} \tag{1.4}$$

where R is the satellite radius and L is the Debye length,

$$L = \left(\frac{\epsilon_0 kT}{N_0 e^2}\right)^{1/2} \tag{1.5}$$

The "capacitance" may be determined from the field at the surface of the satellite and the potential ϕ_R. We obtain

$$C = \frac{Q}{\phi_R} = - \frac{\epsilon_0 \, 4\pi R^2 \left(\frac{d\phi}{dr}\right) R}{\phi_R}$$

or

$$C = 4\pi \epsilon_0 \, R^2 \left(\frac{1}{R} + \frac{1}{L}\right). \tag{1.6}$$

This is simply the capacitance for two concentric spheres with a separation distance L. Thus the Debye length, L, gives the screening distance or sheath thickness about a charged body in a plasma.

The subject of this investigation is the value of the equilibrium potential of a body in the upper atmosphere and in interplanetary space as a function of environmental conditions and various body characteristics. Only naturally occurring mechanisms will be considered, and it is anticipated that for a body in a given environment there will exist only one stable equilibrium point. This investigation will be concerned mainly with simple bodies in the sense that the body surface is considered to be a good conductor. Clearly one can imagine a satellite consisting of two metallic portions connected by an insulator such that each portion would reach its own independent equilibrium potential. Indeed, such "double probes" have been treated in the literature and flown in the upper atmosphere.[14,15] Recently some satellites have been coated with thermal blankets which are also good electric insulators, so that each point on the outer surface would reach its own equilibrium potential determined by the local conditions, orientation of the surface at that point, etc.

Chapter II surveys what has been done on this problem and indicates its present status. Chapters III, IV and V contain discussions of various mechanisms of charge acquisition, and Chapter VI examines the effects of a magnetic field. Chapter VII combines the results of Chapters III through VI to calculate expected potentials for a body in various environments. Finally, Chapter VIII presents the results of measurements of satellite potential made on Explorer VIII and compares them with the predicted calculations.

BLANK PAGE

CHAPTER II

HISTORICAL SURVEY AND PRESENT STATUS OF THE PROBLEM

1. Historical Survey. Apparently the first paper to discuss the problem of the equilibrium electric charge to be expected on a body in space was one by Jung in 1937, entitled "The Origin of Solid Particles in Interstellar Space."[16] Jung obtained equations for fluxes of positive ions or electrons to an interstellar grain as a function of the potential of the grain. He concluded that in interstellar space the effective processes are photoemission and electron accretion. An efficiency (yield) of 100% was assumed for photons with sufficient energy to remove an electron completely from the solid particle. He arrived at values for the potential of about one to a few volts positive.

Spitzer in 1941 took up the problem in a paper, "The Dynamics of the Interstellar Medium."[17] He showed that the effects of cosmic rays on charging an interstellar dust grain are negligible. The effects of grain collisions with protons and electrons along with photoemission were considered. Using an efficiency of 10^{-3}, he concluded that photoemission does not predominate in its effect on the grain charge in interstellar space. In H II regions (where hydrogen is ionized and n_e equals about $1/cm^3$) he obtained a grain potential of about -2 volts independent of its composition or radius. In H I regions where n_e is smaller (10^{-3} / cm^3 and hydrogen is not ionized) the effect of photoemission is noticeable and reduces the potential by about 50% but does not make it positive. The charge on a grain in the vicinity of a star was not considered. The effects of dust in "de-ionizing," (providing a recombination surface for ions) was mentioned but not discussed in detail.

Cernuschi criticized Jung for using too high a value for the photoelectric yield, and both Spitzer and Jung for assuming metallic grains only.[18] Cernuschi claimed that not every electron incident on the particle surface is captured, especially for dielectric substances, and assumed a sticking probability of 10% for small negative potentials. In H II regions the grains are then slightly positive near stars and slightly negative in regions far from stars (-0.7 volts). In H I regions the potential is positive – about 0.8 volts. For dielectric materials the potential is very nearly zero or perhaps slightly positive.

Spitzer treated the subject very thoroughly in "The Temperature of Interstellar Matter," considering the following factors in detail[2]: (1) The sticking probability for electrons, which he takes to be between 0.1 and 0.5, depending on the nature of the substance; (2) The neutralization probability for ions, which because of lack of information could be anywhere from 1 to 10^{-4}; (3) The fraction of available photon energy converted to photoelectron kinetic energy. This involved an average over the photoelectron kinetic energy spectrum. He arrived at a figure of 0.55 for this fraction representing a value midway between the empirical value of 0.45 and the theoretical value of 0.67; (4) The threshold frequency which corresponds to the work function and is dependent on the nature of the substance; (5) The photoelectric efficiency or yield which is a function of both the incident frequency and the substance; (6) And finally, the relative absorption cross section for photons which differs from the geometrical cross section for particles with diameters comparable to the photon length. He obtained equations which can be used to determine the equilibrium electric charge involving all these factors as well as the density and frequency distribution of interstellar photons.

In a companion paper Spitzer and Savedoff in 1950 concluded that if the sticking probability for electrons is equal to the neutralization probability for ions, then in H II regions the potential $V = -2.2(T/10{,}000^\circ)$ volts for non-metallic substances.[19] If the neutralization probability is less than 10^{-4}, then the potential may reach -3 volts where field emission of electrons is likely to occur. For highly photosensitive materials (which are unlikely) positive charges are expected, especially close to hot stars. Metallic surfaces have moderate potentials as computed by Cernuschi. In H I regions low temperatures for the gas yield low potentials if photoemission is weak – only a few electrons per grain. Especially sensitive or metallic grains may have positive potentials up to 10 volts if photoemission is important.

Johnson and Meadows postulated a negative rocket potential of 20 volts above 120 km to explain the results of an ion mass spectrometer experiment flown in 1954.[11] They suggested that the potential could be due to energetic electrons or to absorption of X-rays and subsequent ionization of the gas evolving from the rocket.

The first calculation of electric charge on a macroscopic body was apparently made by Lehnert in 1956.[6] Anticipating the orbiting of earth satellites, Lehnert took into account the increased positive ion current to the satellite on its forward surface due to the high satellite to ion velocity ratio. The resulting potential was about -0.7 to -1.0 volts. Photoemission may change this value depending on the type of surface. The electric field caused by polarization of the satellite in the earth's magnetic field was said to be small compared to the field from the net charge on the satellite. The satellite was shielded electrically at about one Debye length.

In 1956 Singer discussed the charge on micrometeorites near the earth.[5] He assumed a power law for the photon energy distribution and balanced photoemission against electron accretion. He computed a potential of -8 volts in the dark (neglecting the ram effect on the positive ions). Assuming a mean energy of 1.5 volts for electrons and a photoelectric yield of unity, he obtained a potential of about 100 volts positive for particles in the sunlight.

In 1957 Opik calculated the expected charge on interplanetary dust particles.[20] He assumed that the radiation effective for photoemission comes largely from the solar corona rather than the photosphere. Rather than estimating photoemission currents from assumed yields and work functions, he used Saha's equation for an ionization equilibrium applied to a diluted solar corona and the solid grains. He arrived at values of grain potential ranging from 50 to 220 volts positive for interplanetary electron densities from one to 600 per cm^3.

In 1957 Jastrow and Pearse estimated the charge on a satellite in order to find the additional drag.[7] They neglected photoemission but took into account the ram effect of the satellite's velocity on the positive ion current plus the attraction of a negative satellite for positive ions. The equilibrium potential was computed to be from -10 volts on the night side of the earth to -60 volts on the day side because of the high energy assumed for the electrons (1.5 volts with a tail at higher energies). They showed that the satellite is effectively screened at a distance of a few Debye lengths.

In anticipation of the first Soviet Sputnik, Gringauz and Zelikman[21] in 1957 discussed the distribution of charged particles around a satellite and derived an equation for the equilibrium satellite potential taking into account the satellite's velocity and photoemission:

$$\phi = -\frac{kT_e}{e} \ln\left(\frac{I_e}{I_+ + I_\phi}\right) \qquad (2.1)$$

Here k is Boltzmann's constant, T_e the electron temperature, e the value of the electron charge, and I_e, I_+ and I_ϕ the electron current, ion current and photoemission current to the satellite. The induced potential gradient caused by the satellite's motion in the earth's magnetic field was estimated.

In a companion paper Imyanitov discussed the problems of measuring an electric field in the ionosphere from a satellite.[22] The field due to the charge on the satellite must be eliminated; its magnitude was estimated at several volts/cm by computing the satellite potential in a manner similar to that of Gringauz and Zelikman and estimating the sheath thickness from plasma probe theory.

Fred Whipple in 1958 used Spitzer's method of computation and Hinteregger's data on solar ultraviolet flux and yield.[23] With a mean wavelength of 1000 Å and an efficiency of 0.2, he obtained a photoemission rate of 5.7×10^{10} electrons/cm^2 sec (9.1×10^{-9} amp). If the electron temperature is 500,000°, then the potential is zero for meteoric dust if the electron density is 130/cm^3.

Chang and Smith in 1959 derived an expression for satellite potential by balancing the positive ion current (simple ram expression plus a first order correction) against the electron current.[24] Photoemission may also be included, but the authors concluded that its effect was negligible. However, their expression for photoemission is incorrect in that there is no place in the derivation where the actual solar flux is introduced.

Beard and Johnson in 1960 discussed the interaction of a satellite with the earth's magnetic field.[8] The induced potential gradient may be as high as 0.2 volts per meter which affects the distribution of the electron flow to the satellite surface and may also affect measurements of satellite potential. Equilibrium potentials (at the midpoint of the satellite) are on the order of one volt negative for an electron temperature equivalent to 0.1 volts. Photo- and secondary emission were felt to be unimportant.

Results of measuring the potential of Sputnik III have not been reported in detail. A summary of available statements indicates a negative potential varying from -2 volts to -7 volts with altitude and with day-night conditions.[25,26]

Chopra in a review article found an expression for the potential of a body at rest:

$$\phi = -\frac{kT_e}{2e} \ln\left(\frac{m_i T_e}{m_e T_i}\right) \qquad (2.2)$$

where m is the particle mass, the subscripts referring to ions or electrons.[10] If photoemission predominates over ion collection, then

$$\phi = -\frac{kT_e}{e} \ln\left(\frac{n_e v_e}{n_\phi}\right) \qquad (2.3)$$

where $n_e v_e$ and n_ϕ refer to the plasma electron flux and photoelectron flux respectively. At satellite velocities the ion flux is increased, but he believed that "at least in the outer parts of the terrestrial atmosphere and in the interplanetary space, the photoelectric effect is important." He observed that surface phenomena such as secondary emission are unimportant for particle impacts at ordinary gas temperatures. In a

paper in 1961, Beard and Johnson discussed ionospheric limitations on attainable satellite potentials.[27] Higher negative than positive potentials are attainable by ejecting positive ions from a source in the satellite because of the limited mobility of environmental positive ions constituting the return current.

The probability distribution for charges on lunar dust grains was considered by Grannis.[28] However, he seems to have confused the charge on a grain with the rate at which the grain acquires the charge and in addition did not take into account the effect of the grain's charge on its rate of charging.

The latter criticism was also made of Grannis' paper by Walker who derived a different probability distribution for the charges on lunar grains.[29] In another paper Singer and Walker concluded that dust on the lunar surface has a charge proportional to the exposed surface area.[30] No large potential differences can exist because free electrons above the surface conduct currents efficiently. Dust ejected from the surface by meteors may become charged by the same processes that charge dust in interplanetary space.

In a companion paper Singer and Walker calculated the screening effect of photoelectrons on bodies in interplanetary space.[31] Photoemission current density was computed using Hinteregger's results on the number of solar photons with energies greater than 8 eV. The yield was assumed to be 1 for want of better information. When applied to the lunar surface a potential of about plus 20 volts was obtained.

Gdalevich has reported some results of electric field measurements from rockets launched in 1957 and 1958.[32,33] He found a field of 0.2 to 3 volts/cm at the rocket surface corresponding for the most part to

a negative charge, although for portions of the trajectory the charge was positive. He also has derived expressions for the rocket potential similar to those of Gringauz and Zelikman and of Chopra. Imyanitov, in reporting results from more recent rockets, found rather high negative potentials (several volts) which led him to assume that a considerable number of fast negative particles was present in the atmosphere.[34] Sagalyn and others have also reported negative rocket potentials, from -0.4 volts at 150 km to -1.7 volts at 450 km.[35]

Shen and Chopra have considered the problems accompanying thermionic emission from a hot body in a plasma.[36] Solutions were obtained for the potential resulting from the balance between thermionic emission and electron accretion.

Rawer in a recent article has discussed the positive and negative particle fluxes to a satellite.[37] He has some good comments on the inductive effect of the earth's magnetic field, but states that the magnetic field has no effect on the isotropy of the electron flux apart from the induced polarization. The effect of photoemission is discussed carefully with reliable values for the solar flux and yield. He points out that in regions of low electron density the satellite potential may be determined by strong emission lines such as Lyman alpha of H or He.[+] Finally, both Walker and Bettinger discuss equilibrium potential in recent dissertations.[38,39] Walker finds a transcendental equation

$$\phi = -\frac{kT_e}{e} \ln \left[\frac{\sqrt{T_e m_i / T_i m_e}}{1 - \phi e / k T_i} \right] \qquad (2.4)$$

for the potential of a sphere at rest in a plasma. Bettinger computes the equilibrium potential for an insulated probe that emits electrons thermally. He neglects photoemission but assumes that there is a high

energy tail to the normal Maxwell-Boltzmann velocity distribution of electrons. The results of a rocket flight carrying the probe are presented and discussed in terms of the number of high energy electrons necessary to obtain the observed values of -1 to -4.5 volts.

2. Present Status of the Problem. It is apparent that a considerable amount of attention has been devoted in the literature to the problem of the equilibrium potential of a body in space. However, almost all of the treatments have been restricted to a consideration of two or perhaps three mechanisms that the author considers important for his model; one exception to this has been the discussion of the charge on interstellar grains, particularly Spitzer's work.[2] Only a few experimental data have been obtained, and in no case have these measurements been analyzed in terms of the expected potential where all the possible charging mechanisms were evaluated for the specific vehicle that carried the experiment.

In addition to Sputnik III, vehicle potentials have been measured on the satellites Explorer VIII, Ariel I and Explorer XVII. Some preliminary results have been reported from Explorer VIII.[40] No data on satellite potential have been reported in the literature yet from Ariel I or Explorer XVII.

The author believes that some of the charge acquisition mechanisms have not been treated sufficiently thoroughly. Only Rawer has attempted to evaluate the effects of photoemission by combining photoemission yields as a function of wavelength with the solar spectrum.[37] Our knowledge of the solar spectrum in the extreme ultra-violet has since been improved, and the author feels that fairly good quantitative estimates of the photoemission current can be made for certain materials.

The effects of energetic particle fluxes have been invoked as being of probable significance, but there have been no quantitative estimates based on known fluxes such as those of the Van Allen radiation belts. Such an estimate should be made, and secondary emission yields are known well enough for certain materials that this effect could also be included in the calculation.

Another effect that has only been noted in passing and then dismissed is that of the magnetic field in restricting the direction of motion of environmental ions and electrons. It will be shown that this effect can be quite significant.

Finally, there is no literature presently available should one want to make a quantitative estimate of the equilibrium potential for, say, a satellite or other body of certain dimensions and material under specific environmental conditions. It is hoped that this investigation will help to fill this gap.

CHAPTER III

COLLECTION OF ELECTRONS AND IONS

1. General Considerations. Mechanisms of charge acquisition can be classified as charge collection or charge emission. The latter consists of processes such as photoemission, thermal emission, field emission and emission of alpha or beta particles from radioactive materials in the body. There may be a combination of collection and emission as when there is secondary emission of electrons upon incidence of energetic particles. It turns out that by far the most important processes are collection of environmental electrons and ions, which will be treated in this chapter, and photoemission and secondary emission, which will be discussed in Chapter IV. Other less important processes will be considered in Chapter V.

At the outset a distinction may be made between the incidence of energetic particles and that of lower energy (thermal) particles in that only the latter are influenced by the charge on the target body. Hence, it is a straightforward calculation to determine the current to a body from energetic particles if the particle flux and directional distribution are known. The effective collection area for a unidirectional flux, for example, will simply be the cross-section of the body normal to the particle flux. The total effect of the energetic particles on the body's charge must of course take into account the amount of induced secondary emissions. This and the related problem of "sticking probabilities" for incident ions and electrons is considered in the next chapter.

Finally, a distinction should be made between large and small target bodies according to their dimensions compared to a Debye length, L:

$$L = \sqrt{\frac{\epsilon_0 kT}{n e^2}} \tag{3.1}$$

where ϵ_0 is the permittivity, k Boltzmann's constant, T the plasma temperature, n the electron or ion density and e the unit electron charge. The significance of the Debye length is that any shielding of a charged body by space charge in the surrounding plasma occurs in a distance on the order of a Debye length. Hence, for example, a spherical body that is small compared to the Debye length is effectively unshielded for many radii away from its center and the electric field is essentially coulomb. On the other hand, bodies that are large compared to L have their charge shielded in a small fraction of a radius away from the surface. Consequently, it is sometimes possible to treat the problem of particle attraction by assuming a neutral body with a slightly larger surface area.

2. Electron Collection. The problem of electron and ion currents to a probe in a plasma has been the object of considerable attention in the literature, beginning with the work of Langmuir, Mott-Smith and others three decades ago.[41,42] In the upper atmosphere and in space the situation is somewhat simpler than in the laboratory in that there are no "wall effects" such as occur in laboratory vacuum systems, and the thermal plasma is probably more nearly Maxwellian. This is particularly true for electrons since their most probable thermal velocity is much larger than typical satellite or meteor velocities.

Velocities range from about 8 km/sec for a satellite near the earth to a maximum of 73 km/sec for a meterorite approaching the earth, whereas the electron thermal velocity is on the order of 200 km/sec for a temperature of 1500°K. Therefore it is realistic to assume that in a satellite centered co-ordinate system the electron velocity distribution is still Maxwellian. This is not true for ions which have thermal velocities on the order of 1 km/sec – in general lower than typical satellite velocities.

One other simplification is that at the altitudes which are considered here, collisions between particles are unimportant. The minimum perigee altitude for a satellite that is to have a lifetime of at least a few days is about 150 km. The mean free path at 150 km is about 50 meters which is larger than most satellite dimensions and very large compared to a Debye length at that altitude.

For a repulsive potential the electron current to a body will follow the Boltzmann relation,

$$I = \frac{ne\alpha A}{2\sqrt{\pi}} e^{\phi e/kT} \qquad (3.2)$$

where α is the most probable thermal velocity defined by $1/2\, m\alpha^2 = kT$, and A is the surface area of the body. This equation is valid for any convex-shaped body of any size in contrast to the expressions for attractive potentials which depend strongly on the body's geometry.[41] There are other phenomena, however, which may modify the effective collection area A, such as the effect of a magnetic field or the presence of space charge in the wake behind a satellite, as will be shown later.

For attractive potentials both the size and shape of the body are important. Spherical, cylindrical and planar geometries have been treated in the literature. It is convenient to restrict the discussion at this point to spherical bodies for several reasons: (1) It is clearly advantageous to approximate a complex-shaped body as a sphere for simplicity of treatment. (2) This is a good approximation for small isolated bodies where the far field will be a coulomb field regardless of the details of the body's shape. (3) Most satellites are roughly spherical in that the three axes are approximately equal. Exceptions come immediately to mind such as antennas or long booms, but they may be treated separately as special cases.

A positively-charged sphere, then, whose radius is small compared to the Debye length will be surrounded by a coulomb field that is effectively unshielded. The electron current to a body in such a case is[40]

$$I = \frac{ne\alpha A}{2\sqrt{\pi}} \left(1 + \frac{\phi e}{kT}\right) \tag{3.3}$$

For a body whose radius is comparable to the Debye length the variation of the potential through the sheath is important in determining the total collected current. This means that Poisson's equation must be solved in the sheath taking into account all the sources of space charge in addition to that due to the electrons alone. In general this is an extremely complicated problem requiring numerical procedures, but in certain simplified cases an approximate analytical expression may be obtained. Mott-Smith and Langmuir derived the following expression for the current due to attracted particles in a spherical sheath:[41]

$$I = \frac{ne\,\alpha}{2\sqrt{\pi}}\,(4\pi a^2)\left[1 - \frac{(a^2 - r^2)}{a^2}\,e^{-r^2 e\phi/kT(a^2-r^2)}\right] \qquad (3.4)$$

where r is the radius of the body and a the radius of the sheath, assumed to be spherical and concentric with the body. This equation was derived by assuming a well-defined edge to the sheath so that the flux of electrons at the sheath surface is due to their random thermal motions. More recently it has been shown that the sheath boundary is not well-defined but that the electric field may penetrate "beyond" the sheath for a considerable distance.[43] However, Walker has found that the Mott-Smith-Langmuir equation may still be used if the following expressions are used to determine the sheath radius, a:[38]

$$a = r + t \qquad (3.5)$$

and

$$\frac{t}{L} = 0.83\left(\frac{r}{L}\right)^{1/3}\left(\frac{\phi_e}{kT}\right)^{1/2} \qquad (3.6)$$

where t is the "thickness" of the sheath around the body. Equation (3.4) reduces to equation (3.3) for the case when $t >> r$; when $t << r$ then

$$I = \frac{ne\,\alpha}{2\sqrt{\pi}}\,(4\pi a^2) \cong \frac{ne\,\alpha}{2\sqrt{\pi}}\,(4\pi r^2)\left(1 + \frac{2t}{r}\right) \qquad (3.7)$$

i.e., the body may be taken to be neutral with a slightly larger $(2t/r)$ surface area.

3. Positive Ion Collection. The essential difference between the treatment of electron collection and ion collection is that in general the motion of the body through the plasma cannot be neglected. In the

special case where the body is at rest with respect to the plasma, the preceding equations derived for electrons are applicable to ion collection with appropriate changes in the sign of the potential and in the quantities referring to particle characteristics. In succeeding equations the subscripts + or - will be used to denote reference to ions or electrons. These equations for the body at rest will also serve as checks on the general ion current equations since the latter must reduce to the former for zero velocity.

Mott-Smith and Langmuir[41] discussed the problem of a moving collector in a plasma but did not give equations for the current. Gringauz and Zelikman[21] showed that the ion current to a moving sphere would decrease in a nearly linear manner with an increasing retarding potential, approaching zero at a potential corresponding to the kinetic energy of the ions in the moving system, $\phi = m_+V^2/2e$, where V is the velocity of the sphere. The current is given approximately by

$$I_+ = \pi r^2 n_+ eV \left[1 - \frac{2\phi e}{m_+ V^2}\right] \qquad (3.8)$$

as long as the thermal motions of the ions can be disregarded. Two spherical ion traps, each consisting of an outer grid and an inner collector biased to repel electrons, were flown on Sputnik III. Linear current-voltage curves were obtained for repulsive potentials as predicted;[26] effects of the ion thermal motions were discussed but a general equation was not given.

Such an equation for repulsive potentials has been derived by Hinteregger[44] and later by Kanal.[45]

$$I_+ = \frac{\pi r^2}{2} n_+ eV \left\{ \left[1 + \frac{\alpha_+^2}{2V^2} - \frac{U^2}{V^2} \right] \left[\operatorname{erf}\left(\frac{V+U}{\alpha_+} \right) + \operatorname{erf}\left(\frac{V-U}{\alpha_+} \right) \right] \right.$$

$$\left. + \frac{\alpha_+}{\sqrt{\pi}\, V} \left[\left(\frac{U}{V} + 1 \right) e^{-\left(\frac{V-U}{\alpha_+}\right)^2} - \left(\frac{U}{V} - 1 \right) e^{-\left(\frac{V+U}{\alpha_+}\right)^2} \right] \right\} \qquad (3.9)$$

where

$$U = [2e\phi/m_+]^{1/2} \qquad (3.10)$$

and

$$\operatorname{erf} x = \frac{2}{\sqrt{\pi}} \int_0^x e^{-u^2}\, du \qquad (3.11)$$

Interestingly, the current is independent of sheath size or variation of potential through the sheath as long as the electric field is radial. Gringauz showed that this is because the current is limited by angular momentum considerations, and is true as long as the effective radius of the collector, given by

$$r_{eff} = r \left[1 - \frac{2e\phi}{m_+ V^2} \right]^{1/2} \qquad (3.12)$$

is less than the sheath radius. This is always true for repulsive potentials since the bracket in (3.12) is less than unity. In addition, it will be true for attractive potentials until the effective radius exceeds the sheath radius, with the consequence that (3.8) may also be used for a

limited range of attractive potentials. Equation (3.9) reduces to (3.8) as the ratio a_+/V approaches zero, and it reduces to Equation (3.2) as a_+/V approaches infinity.

An analytic expression for the general case of the ion current to a moving body in an attractive field has not yet been obtained. The problem is extremely complex because it involves a simultaneous solution of Poisson's equation and calculation of the ion trajectories. Both Kanal[45] and Walker[38] have made certain simplifying assumptions in order to obtain useful solutions. Kanal used a model for the sheath in which ions enter the sheath with zero initial velocity and obtained two equations for the ion current by means of which the unknown sheath radius was eliminated graphically. Walker integrated the ion trajectories numerically, assuming a spherical sheath edge. The shape of the collector then depends on the results of the computations, and is not in general spherical. For the case where the collector is nearly spherical, a comparison of Kanal's and Walker's currents shows a disagreement by more than an order of magnitude.

The assumption of a spherical sheath in front of the moving body is probably quite realistic as has been shown by Al'pert, Gurevic and Pitaevskij.[46] If the sheath edge were sharp it would be possible to use Equation (3.9) for the range of potentials where $r_{eff} < a$, the sheath radius. The same equation with ϕ set equal to zero, and with r replaced by a could be used for the case when $r_{eff} > a$. Unfortunately, the sheath edge is not sharp as Walker and others have pointed out. However, the precise position of the edge of the sheath will not matter greatly if the sheath thickness $t = a - r \ll r$. In this case the current will be the same as that derived by Sagalyn et al.[35]

$$I_+ = \pi a^2 n_+ eV \left[\left(1 + \frac{\alpha_+^2}{2V^2} \right) \operatorname{erf} \frac{V}{\alpha_+} + \frac{\alpha_+}{V\sqrt{\pi}} e^{-(V/\alpha_+)^2} \right] \tag{3.13}$$

In the case when the body is so small compared to the Debye length that the field may be assumed to be a coulomb field, the current for an attractive potential has been derived by Kanal.[45] He finds

$$I_+ = n_+ e \alpha_+ \sqrt{\pi}\ r^2 \left[\frac{\sqrt{\pi}\alpha_+}{V} \operatorname{erf} \left(\frac{V}{\alpha_+} \right) \left(\frac{\phi e}{kT} + \frac{V^2}{\alpha_+^2} + \frac{1}{2} \right) + e^{-(V/\alpha_+)^2} \right] \tag{3.14}$$

The current in this case reduces to that in (3.3) as the velocity of the body approaches zero, and it reduces to (3.13) for zero potential.

Because of the importance of the ion current to a negatively charged moving sphere for satellite potential calculations, a program to compute this current has been developed. Poisson's equation has been solved with the assumption of spherical symmetry and with the space charge given by

$$\rho = n_+ e \left(1 - e^{\phi e / kT} \right) \tag{3.15}$$

i.e., the ion density is constant and the electron density is described by the Boltzmann factor, the same assumptions used by Jastrow and Pearse.[7] The ion current may then be computed, without integrating the ion trajectories, by using Walker's classification of trajectories as either periastron or pericritical.[38] Details of the analysis are given in the appendix. Some typical results are given in Figure 4 in the form of current versus satellite potential curves. The linear relationship at lower voltages with a saturation effect as the effective radius of Equation (3.12) exceeds the sheath radius is apparent. The thermal motions

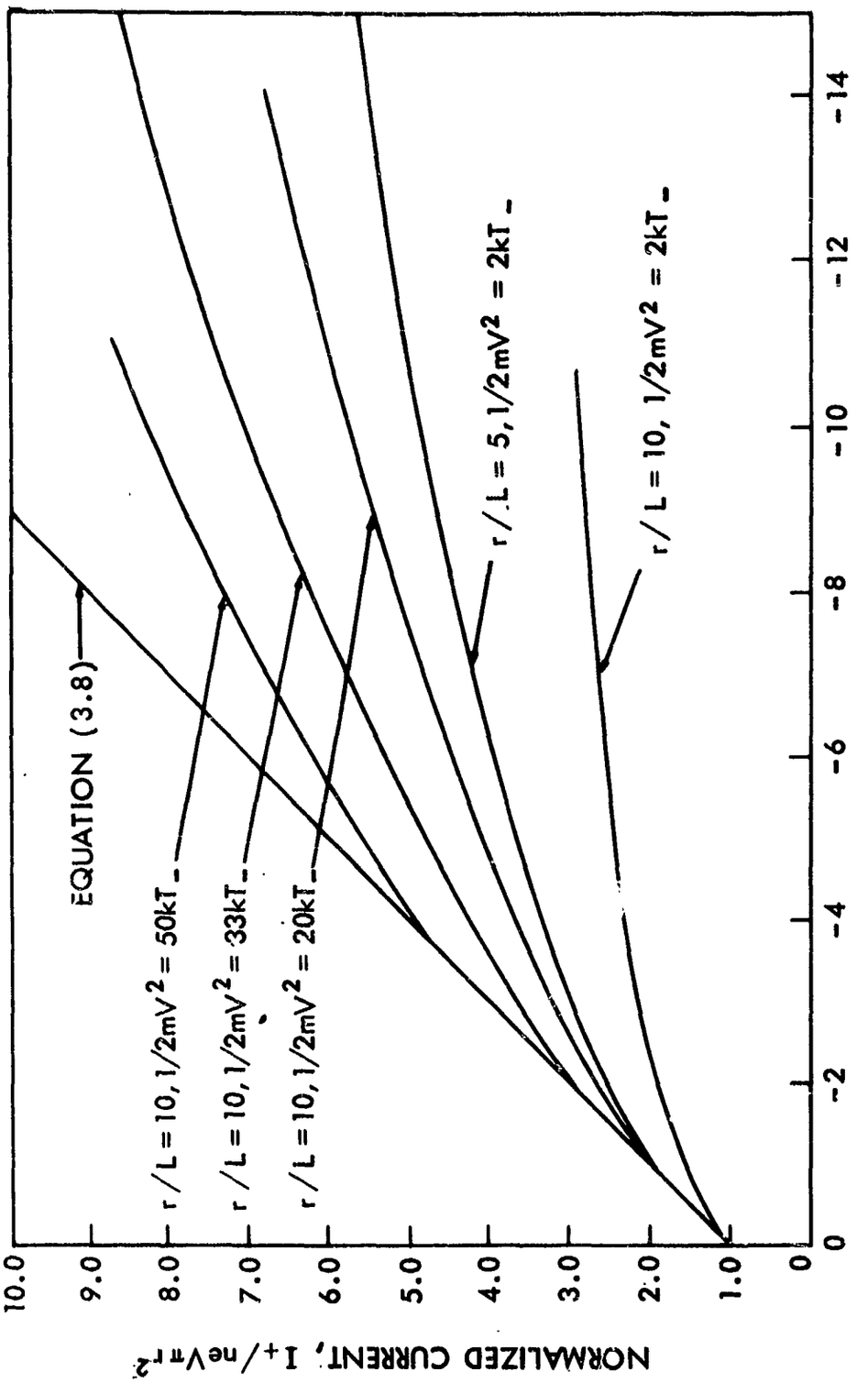

Figure 4. Ion Current to a Large, Negative, Moving Body

of the ions have been neglected, but the temperature of the plasma is taken into account through the Debye length.

The accompanying table summarizes the different situations that have been discussed and shows the appropriate equation to use in each case.

Table I

Size of Body:	Small	Intermediate	Large
	Body at Rest, $V/\alpha << 1$		
Attractive Field	Eq. (3.3)	Eq. (3.4) with (3.5) and (3.6)	Eq. (3.7)
Repulsive Field	Eq. (3.2)	Eq. (3.2)	Eq. (3.2)
	Body Moving, $V/\alpha \neq 0$		
Attractive Field	Eq. (3.14)	Fig. 4	Eq. (3.13) or Fig. 4
Repulsive Field	Eq. (3.9)	Eq. (3.9)	Eq. (3.9)

4. Effects of the Satellite Wake: A body moving rapidly through the atmosphere (in comparison with the ion thermal velocity) will have a rarified region behind it in the shape of a cone, as shown in Figure 5, with a half-angle given approximately by $\tan \theta = \alpha_+/V$. The shape of the wake and the ion and electron and potential distribution in the wake have been discussed in great detail by Al'pert, Gurevic and Pitaevskij.[46] The potential distribution in the wake does not appreciably affect the total ion current to the body because most of the ion current is incident on the front half. However, this is not the case for the electron current. Electrons will diffuse into the wake where because of the absence of ions there will be a net negative space charge. Al'pert et al. show that the potential in the wake will in general be more negative than that of the body, reaching an extremum of approximately $-2kT/e \ln (r/L)$ as

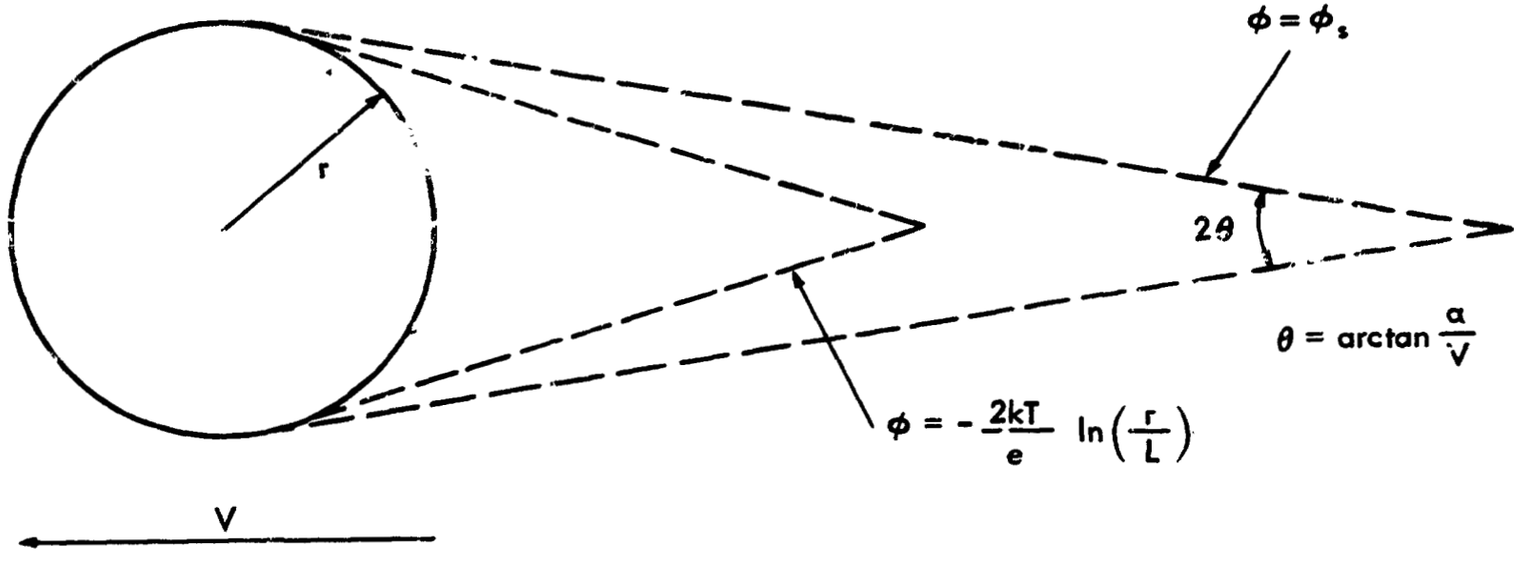

Figure 5. The Wake Behind a Rapidly Moving Body in the Upper Atmosphere

shown by the dotted line. Consequently, electrons with energies less than this will be unable to cross this potential barrier to reach the rear half of the body, and in place of Equation (3.2) one should use

$$I_- = \frac{n_- e \alpha_- (2\pi r^2)}{2\sqrt{\pi}} \left[e^{\phi_s e/kT} + \left(\frac{L}{r}\right)^2 \right] \qquad (3.16)$$

as long as ϕ_s, the satellite potential, is more positive than $-2kT/e \ln(r/L)$, but less than zero. If the satellite potential is positive, then Equation (3.7) should be used for the front half of the satellite, and

$$I_- = \frac{n_- e \alpha_- (2\pi r^2)}{2\sqrt{\pi}} \left(\frac{L}{r}\right)^2 \qquad (3.17)$$

for the rear half of the satellite.

BLANK PAGE

CHAPTER IV

PHOTOEMISSION AND SECONDARY EMISSION

1. Photoemission. Two steps are involved in estimating the effects of both photoemission and secondary emission on the equilibrium potential of a body. Only the first step is necessary if the body is negative, namely the calculation of the total emission current which depends on the energy spectrum of the primaries and the secondary electron yield as a function of primary energy. Since the body is negative all the secondaries may be assumed to escape, and it is unnecessary to know the energy spectrum of the secondary electrons.

If the body is positive not all of the secondary electrons will escape, and it is in this case necessary to know the energy spectrum of the secondaries. If the body is small (compared to a Debye length) then all electrons emitted with energies greater than that corresponding to the potential difference between the body and the environment will escape. If the body is large the equipotential surfaces will be approximately planar, and the condition for escape is that the directed kinetic energy of the electrons normal to the surface must be greater than $\Phi_s e$, where Φ_s is the satellite potential. In general, for a sphere we have

$$E > \left[V(r) + \frac{p^2}{2m_- r^2}\right]_{max} = [V'(r)]_{max} \qquad (4:1)$$

as the condition for escape, where E is the total energy (kinetic plus potential) upon emission, V(r) is the potential outside the sphere, and p is the angular momentum of the emitted electron.

The importance of photoemission in providing a charging mechanism for bodies in the upper atmosphere and in interplanetary space has emerged as a result of rather recent experimental data in two areas of investigation. First has been the demonstration of rather large photoelectric yields for metals in the extreme ultra-violet range of wavelengths—ranging up to peak values greater than 10% in some cases compared with numbers like 10^{-4} to 10^{-5} for yields in the near UV (> 2000Å). And second has been the discovery of considerable energy in this same region of the solar spectrum. Figure 6 shows the solar spectrum from 100 to 10,000Å. The ordinate is the number of photons per cm^2 per second per Angstrom interval. The data at wavelengths below 1775Å was obtained by Hinteregger, Hall and Schmidtke;[47] that above 1775Å is from Nawrocki and Papa.[48] The Lyman-α line at 1216Å is particularly important in its contribution to photoemission.

To demonstrate the effects of both photoemission and secondary emission upon the problem of equilibrium potential, two metals have been chosen: tungsten with a work function between 4 and 5 electron volts and aluminum with a lower work function between 3 and 4 volts. The choice of these materials is partly dictated by the fact that data is available for both secondary and photoemission from both. Also, aluminum is used extensively in spacecraft construction, and tungsten has been used frequently in experiment sensors so that a comparison of laboratory and flight results is possible.

Photoelectric yields for tungsten in the ultra-violet wavelengths have been measured both in the laboratory and on rocket flights in the upper atmosphere. The yields as a function of wavelength are shown in Figure 6 for both clean and dirty tungsten: "dirty" means an untreated surface, and "clean" means the surface was heated at a temperature

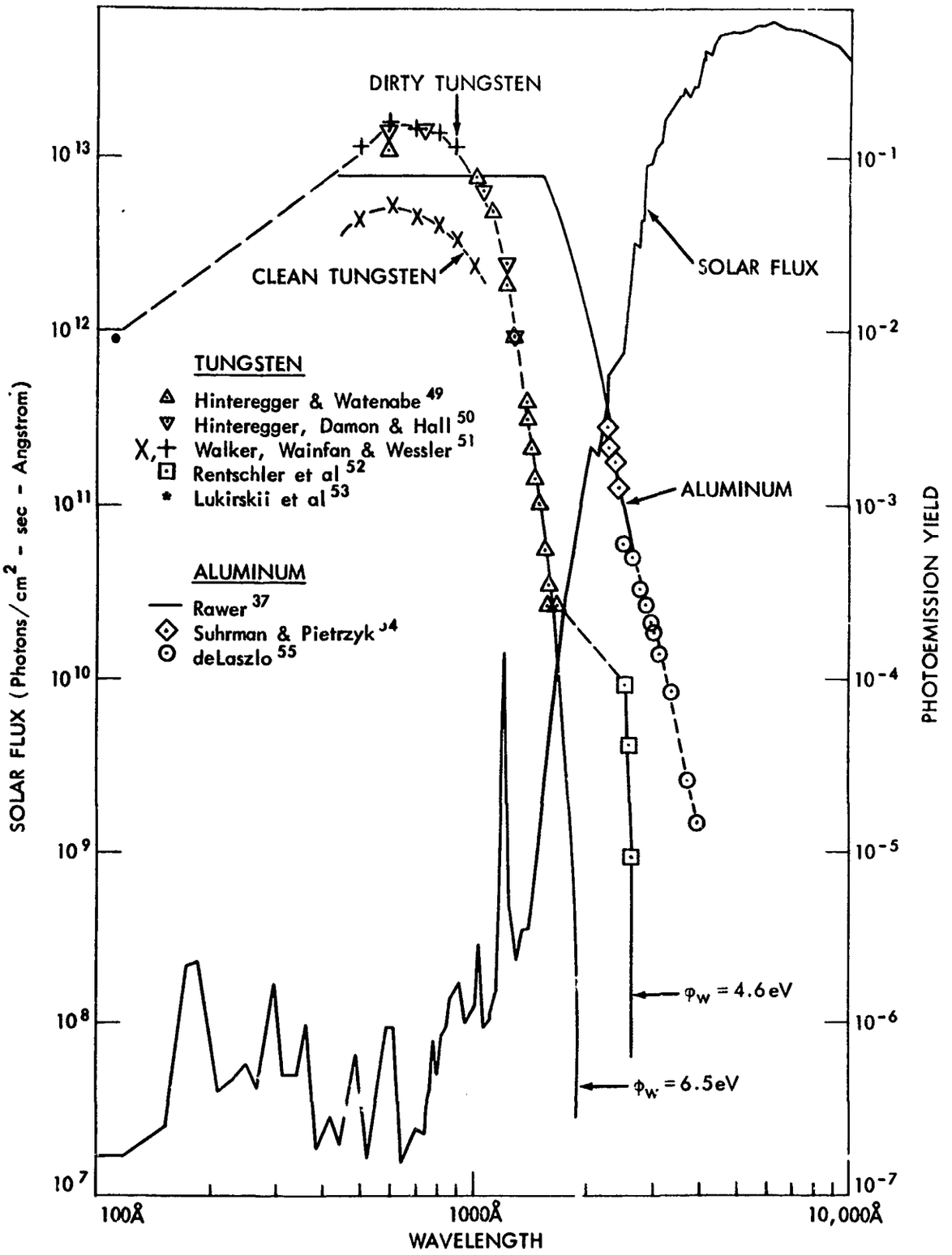

Figure 6. The Solar Spectrum and Photoemission Yields from 10^2 - 10^4 A°

greater than 1000°C in a vacuum of 10^{-5} torr until yield reproducibility was established. Hinteregger's data was obtained for an untreated surface; he states that the yields are reproducible even after exposure to air.

The solid line drawn through Hinteregger and Watanabe's experimental points to higher wavelengths is a theoretical curve for the yield according to the Fowler-DuBridge theory, with a long wavelength cut-off at 1900Å, corresponding to a work function of 6.5 eV determined by Fowler's method.[56,57] The theoretical curve through Rentschler's points corresponds to a long wavelength cut-off of 2690Å, or 4.6 eV, in good agreement with Warner's results.[58] The difference in the curves is probably due to the state of the metal surface, although it is not clear that the Fowler-DuBridge theory can be applied at wavelengths as low as 1700Å.

When the product of the yield and solar flux is integrated over the spectrum, a total current of 2.1×10^{-9} amp/cm^2 and 8.1×10^{-9} amp/cm^2 is obtained, depending on which of the two curves is used at the longer wavelengths. These values bracket experimental photoemission current densities from tungsten of 3.9×10^{-9} amp/cm^2 obtained by Hinteregger[50] and 5×10^{-9} amp/cm^2 obtained on Explorer VIII.[40]

The yields for aluminum below 2500Å are laboratory measurements by Suhrman and Pietrzyk[54] fitted to the following law by Rawer:[37]

$$Y = 5.2 \times 10^{-3} (\Phi_\lambda - \Phi_w)^3, \quad \Phi_\lambda < 8 \text{ volts}$$

$$Y = 0.077, \qquad \Phi_\lambda > 8 \text{ volts} \tag{4.2}$$

where Φ_w is the work function of 4 eV and Φ_λ is the energy of the corresponding wavelength. These values join nicely with experimental

data by de Laszlo[55] above 2500Å. These large yields, which are a consequence of aluminum's lower work function, result in a computed photoemission current density of 2.5×10^{-7} amp/cm^2 above the atmosphere—two orders of magnitude greater than that for tungsten. Such a large photocurrent would certainly be important for satellite potentials because of this metal's wide use in spacecraft construction. Consequently, an experiment was designed to measure the photoemission current from aluminum and was flown on a Nike-Apache rocket to an altitude of 193 km on Dec. 16, 1964 at White Sands, N.M. The maximum measured current at an altitude of 160 km was 2.3×10^{-9} amp/cm^2. An extrapolation to the top of the atmosphere yields a value of 3×10^{-9} amp/cm^2, in fair agreement with the result for tungsten rather than the computed value for aluminum. Probably the discrepancy is due to the state of the aluminum surface causing an increased work function—de Laszlo's results were for a carefully prepared and outgassed surface. The experimental photocurrent will be used in the calculations of satellite potential.

When a satellite or other body is positive, the energy distribution of the photoelectrons is needed. An experimental current-voltage curve for photoelectrons emitted from a positive plane tungsten surface has been obtained by Hinteregger, Damon and Hall,[50] and is reproduced in Figure 7. For small bodies where the angular momentum distribution of the electrons is needed to compute the number that escape, it will be assumed that they are emitted with a cosine distribution.

2. Secondary Emission of Electrons Upon Electron Impact. The phenomenon of secondary electron emission upon electron impact has been studied extensively and is fairly well understood according to recent reviews of the subject.[59,60,61,62,63] The electrons emitted from a

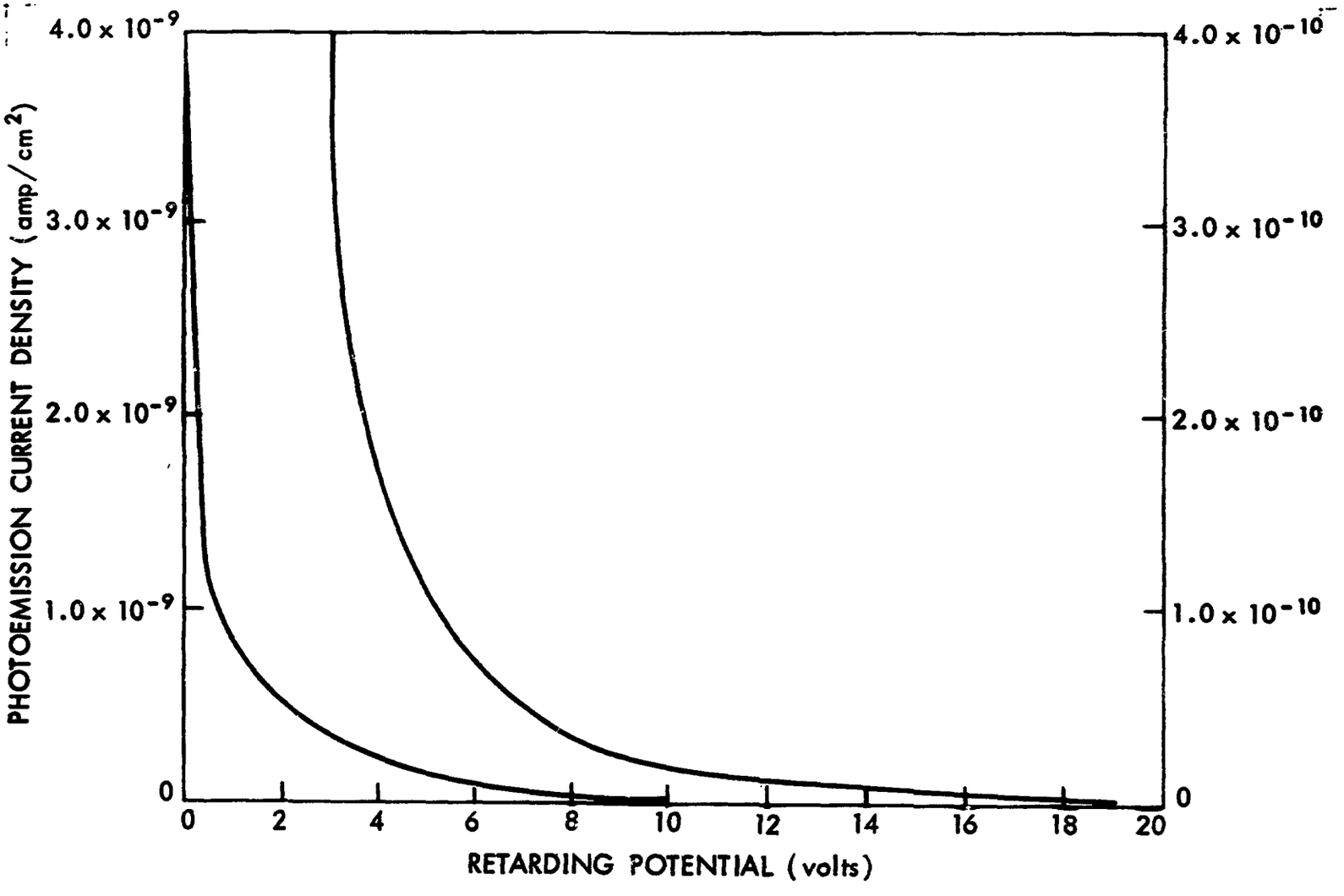

Figure 7. Experimental Current-Voltage Curve for Photoemission from Tungsten by Hinteregger et al.

target surface include, however, reflected and back-diffused primaries as well as true secondary electrons. The total yield, δ, defined as I_t/I_p, the ratio of emitted target current to incident primary current, may be written as

$$\delta = \delta_p (1 - r) + r + \eta (1 + \delta_p \beta) \qquad (4.3)$$

Here δ_p is the "true" yield of secondaries due to the primaries, r is the reflection coefficient (1-r is the "sticking factor" for electrons), η the back-diffusion coefficient and β an efficiency factor describing the increased efficiency with which the back-diffused electrons produce their own secondaries.

The shape of the true yield curve as a function of primary energy below a few keV is in effect a universal curve for metals when normalized to the maximum yield and the primary energy at the maximum. Figure 8 shows the yields for Al and W as a function of primary energy. What is plotted in Figure 8 is the effective yield given by $\delta_p(1 + \eta\beta)$, since measurements of the yield generally have been corrected for the back-diffused primaries only, with no distinction being made between slow secondary electrons caused by the incident as against the back-scattered primaries. The yields have been extrapolated to zero at 5 eV according to the observations of Shulman and Myakinin,[64] and Harrower[65] that true secondaries occur only above primary energies of 4-7 eV. The maximum yield occurs approximately at an energy where the primaries are stopped at a depth in the metal corresponding to the depth from which secondaries can escape. At higher primary energies the yield decreases in accordance with the rate at which the primaries lose energy in the escape zone; and it has been shown by Kanter[66] for energies between 1 and 20 keV and by Schultz and Pomerantz[67] at energies up

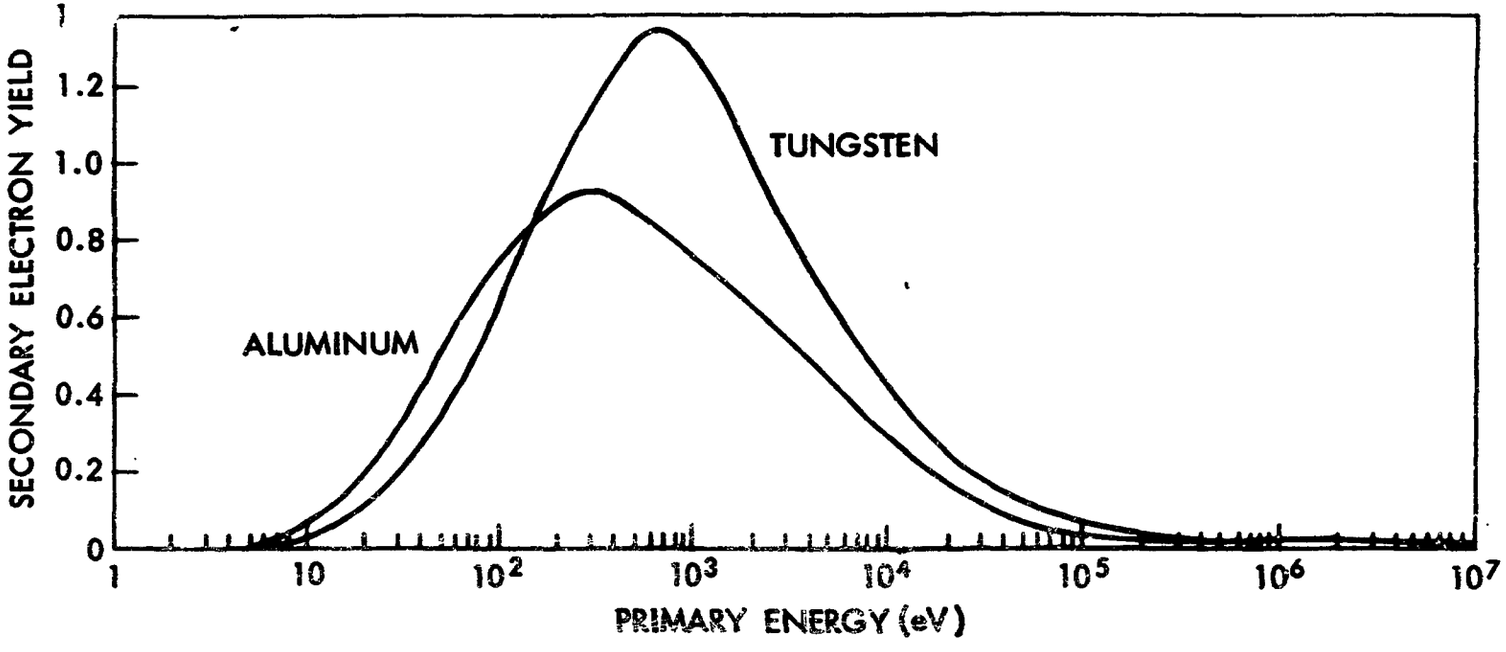

Figure 8. Secondary Electron Yield for Electron Impact on Tungsten and Aluminum

to 1.6 MeV that the energy loss rate is in agreement with Bethe's stopping-power formula:

$$\delta_p = k \frac{dE}{dx} = \frac{C_1}{E} \ln (E/C_2) \tag{4.4}$$

The reflection coefficient, r, is significant only at low primary energies below about 10 eV. In general, r is of the order of 0.05 at zero primary energy and decreases with increasing energy according to the relation

$$r = \frac{W^4}{16 (E + W)^3 + W^3} \tag{4.5}$$

where W is the sum of the Fermi energy and work function of the metal, and E the primary energy, both measured in Rydberg units (13.54 eV).[68] Guth and Mullin[69] have found r to be 0.05 for tungsten near zero volts. The use of Equation (4.5) with a work function of 3.5 eV and a Fermi energy of 5.6 eV yields a reflection coefficient of 0.04 for Al at zero volts.

Figure 9 shows the back-diffusion coefficient η for Al and W as a function of primary energy.[61,70] The curves have been extrapolated to zero at 100 eV because the average energy, $\bar{E}/E$ of back-diffused electrons is 0.50 for Al and 0.60 for W in terms of the primary energy, whereas 50 eV is usually taken to be the energy distinguishing back-diffused electrons from true secondaries.

Figure 10 shows the total yield δ for Al and W as a function of primary energy, obtained by combining the appropriate values for the various coefficients in accordance with Equation (4.3).

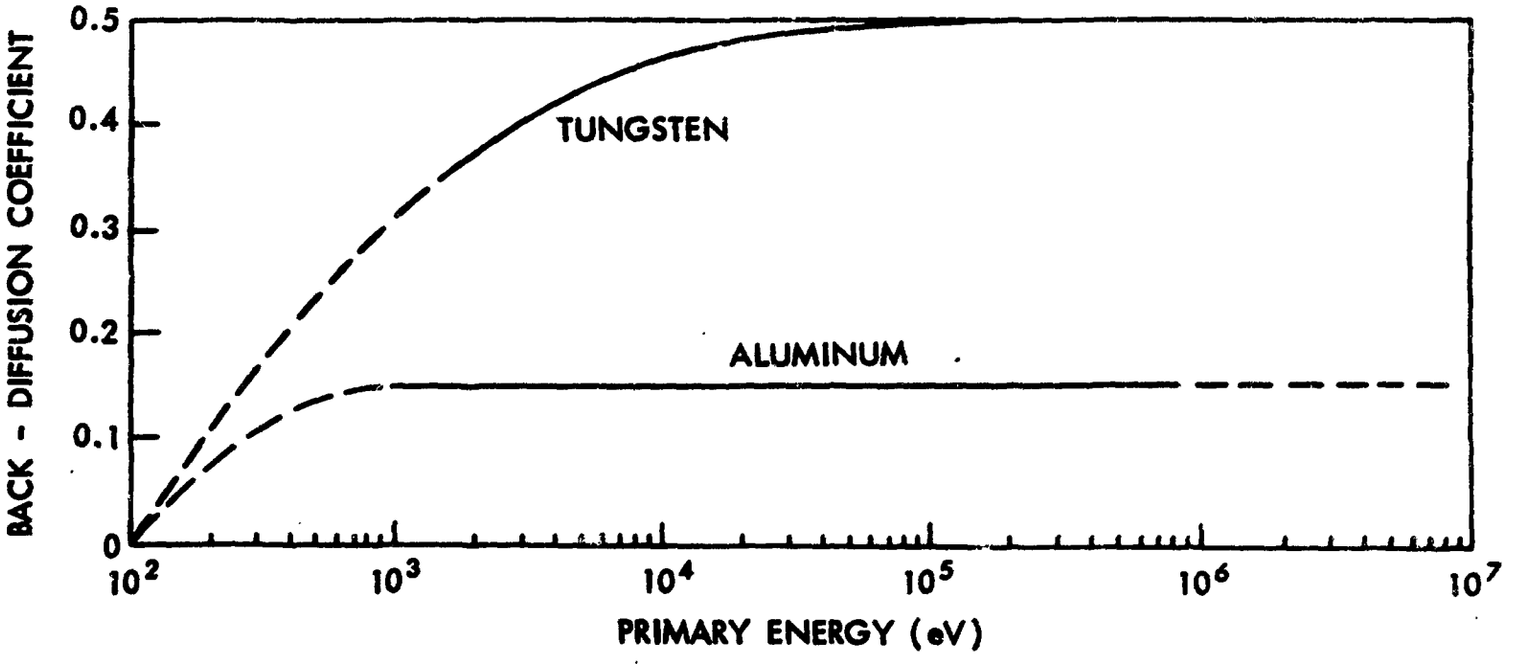

Figure 9. Back-Diffusion Coefficient for Tungsten and Aluminum

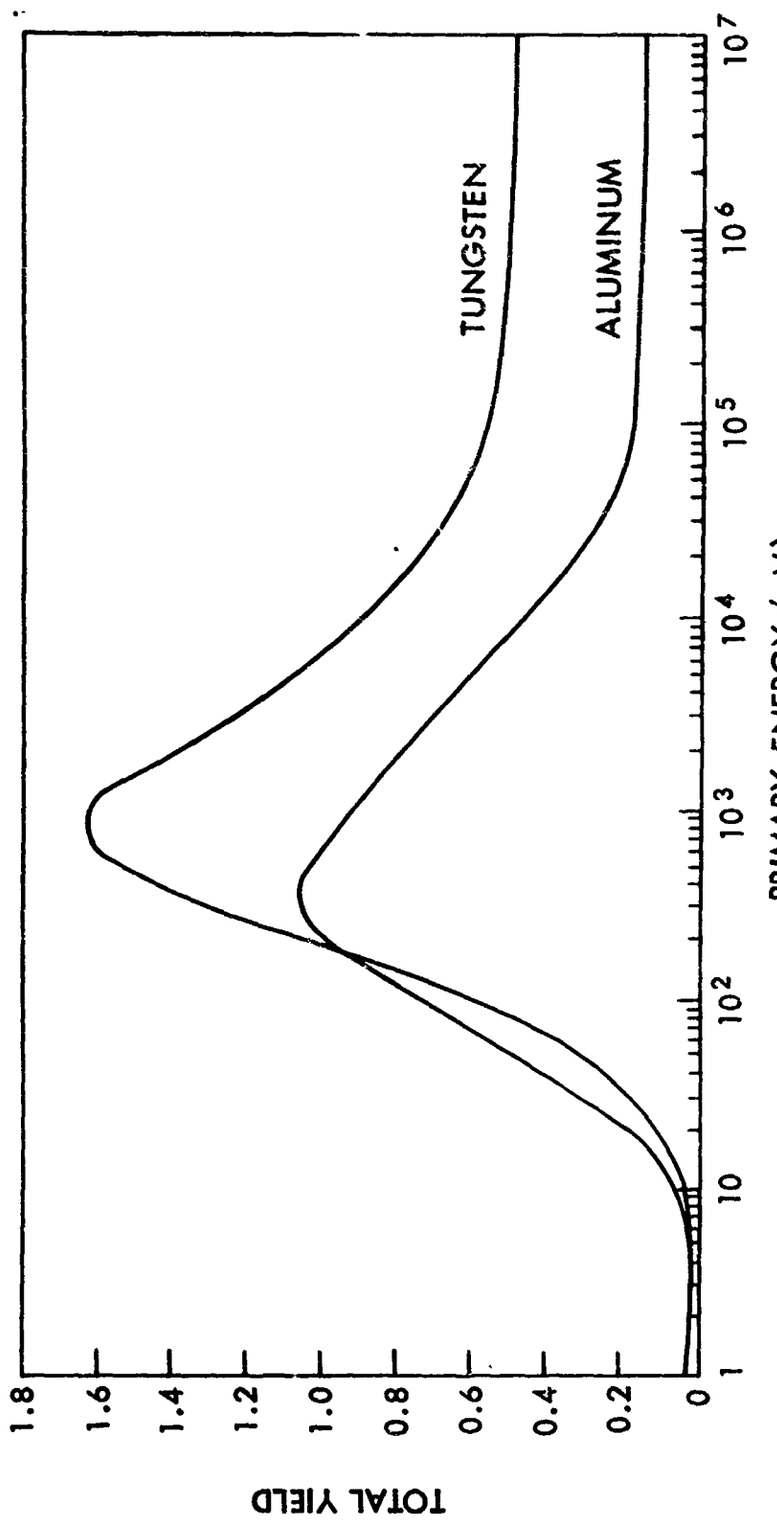

Figure 10. Total Secondary Electron Yield for Tungsten and Aluminum

It should be added that above δ_p max the yield is dependent upon the angle of incidence of the primaries. At energies near the maximum yield it is given by

$$\ln (\delta/\delta_0) = C (1 - \cos \theta) \tag{4.6}$$

where C depends on the energy of the primaries.[62] At higher energies the yield is proportional to sec θ.[63] An effective yield for an isotropic flux of primaries may be defined by

$$\delta_{eff} = \int_0^{\pi/2} \delta(\theta) \sin \theta \cos \theta \, d\theta \tag{4.7}$$

This reduces to $\delta_{eff} = \delta_0$ for the $\delta = \delta_0 \sec \theta$ law.

All the secondary electrons emitted from a spherical body in space will escape if the satellite potential is negative. For positive potentials it is necessary to know the energy distribution of the secondaries; however, for reasonable potentials—i.e. less than +50 volts—only the energy distribution of the true secondaries is needed since the back-diffused primaries will still escape.

Schultz and Pomerantz state that "the energy spectra of secondary electrons emitted from metals bombarded by relativistic electrons are practically identical with those measured at very much lower primary energies by Kollath."[67] Figure 11 gives this differential energy spectrum. There is abundant evidence that the angular distribution of the secondaries follows a cosine law, hence it is a straightforward procedure to compute the number that escape from a body with the use of Equation (4.1).

3. Secondary Emission of Electrons Upon Ion Impact. The predominant positive ions in the upper ionosphere are 0+ from 150 km to approximately

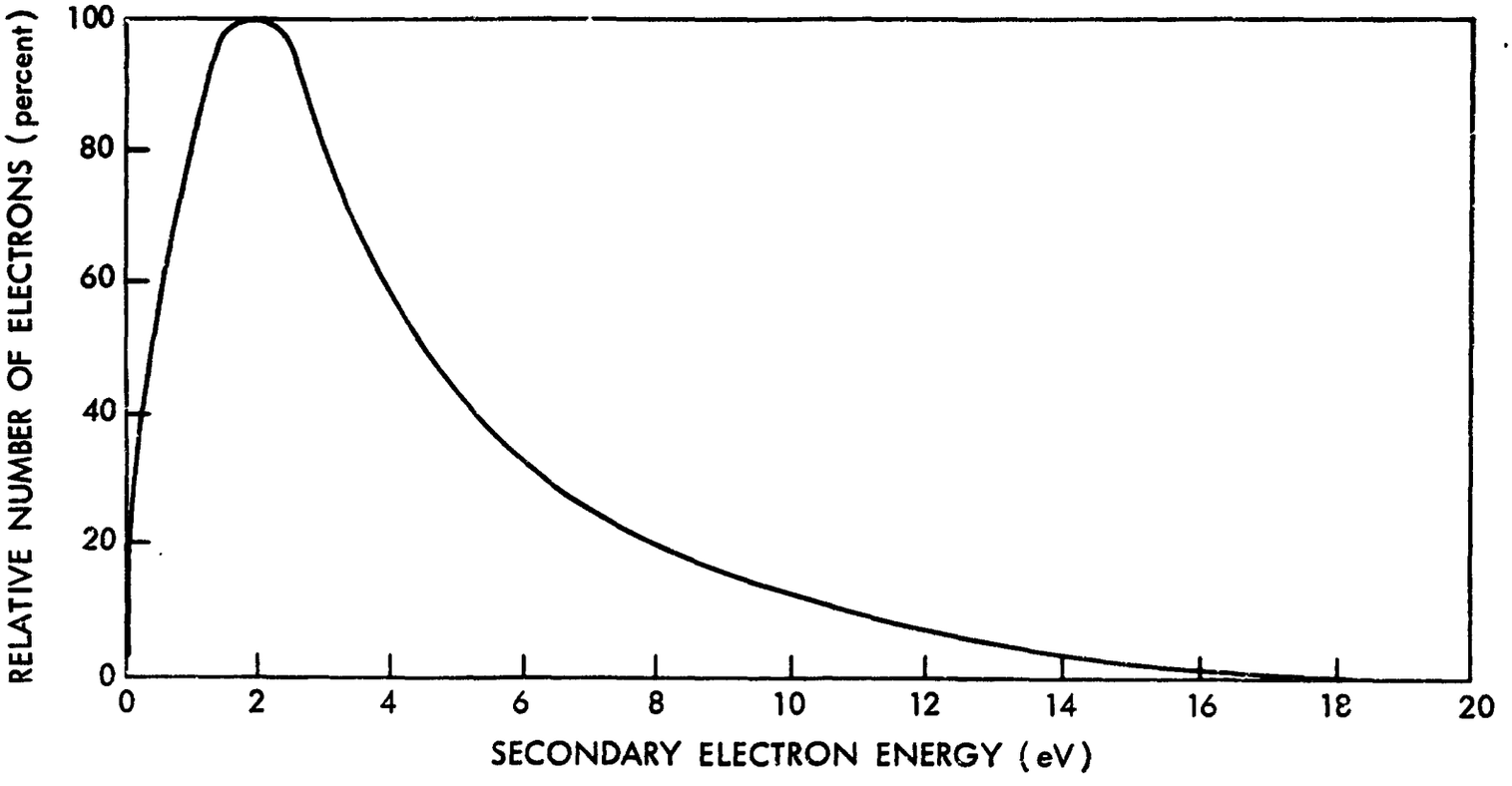

Figure 11. Energy Spectrum for Secondary Electrons

10^3 km and H^+ at higher altitudes with a more or less thin belt of He^+ between. These are thermal ions, with energies on the order of a fraction of an eV. In addition, there are belts of energetic protons, with energies up into the 100 MeV range in the radiation belts.

Below about one keV the yield for secondary electron emission from ion impact is very nearly independent of the ion's kinetic energy. This is because the ion is neutralized directly to the ground state as it approaches very near to the metal surface. The number of excited electrons depends on the available potential energy after neutralization which is determined by the ionization potential, ϕ_i, of the incident atom and the work function of the target metal ϕ_w, as illustrated in Figure 12.

When a conduction electron is captured by the incident ion, it makes available a maximum energy of $\phi_i - \phi_w$. At least ϕ_w of this must be used to free another electron from the metal so that the condition for secondary emission by this mechanism is that $\phi_i > 2\,\phi_w$. It is apparent from the figure that the yields for various ions incident on several metals depend primarily on the difference $\phi_i - 2\,\phi_w$. This relationship is used to estimate the yields in the following table with the exception of He^+ on W which has been measured by Hagstrum.

Table II

	Al, ϕ_w = 3.5 eV	W, ϕ_w = 4.6 eV
H^+, ϕ_i = 13.5 eV	0.086	0.041
He^+, ϕ_i = 24.6 eV	0.38	0.295
0^+, ϕ_i = 13.6 eV	0.088	0.045

It should be added that the yield is quite dependent on the condition of the metal surface. Hagstrum's data is for atomically clean surfaces, whereas the platinum in Parker's measurement may have had some

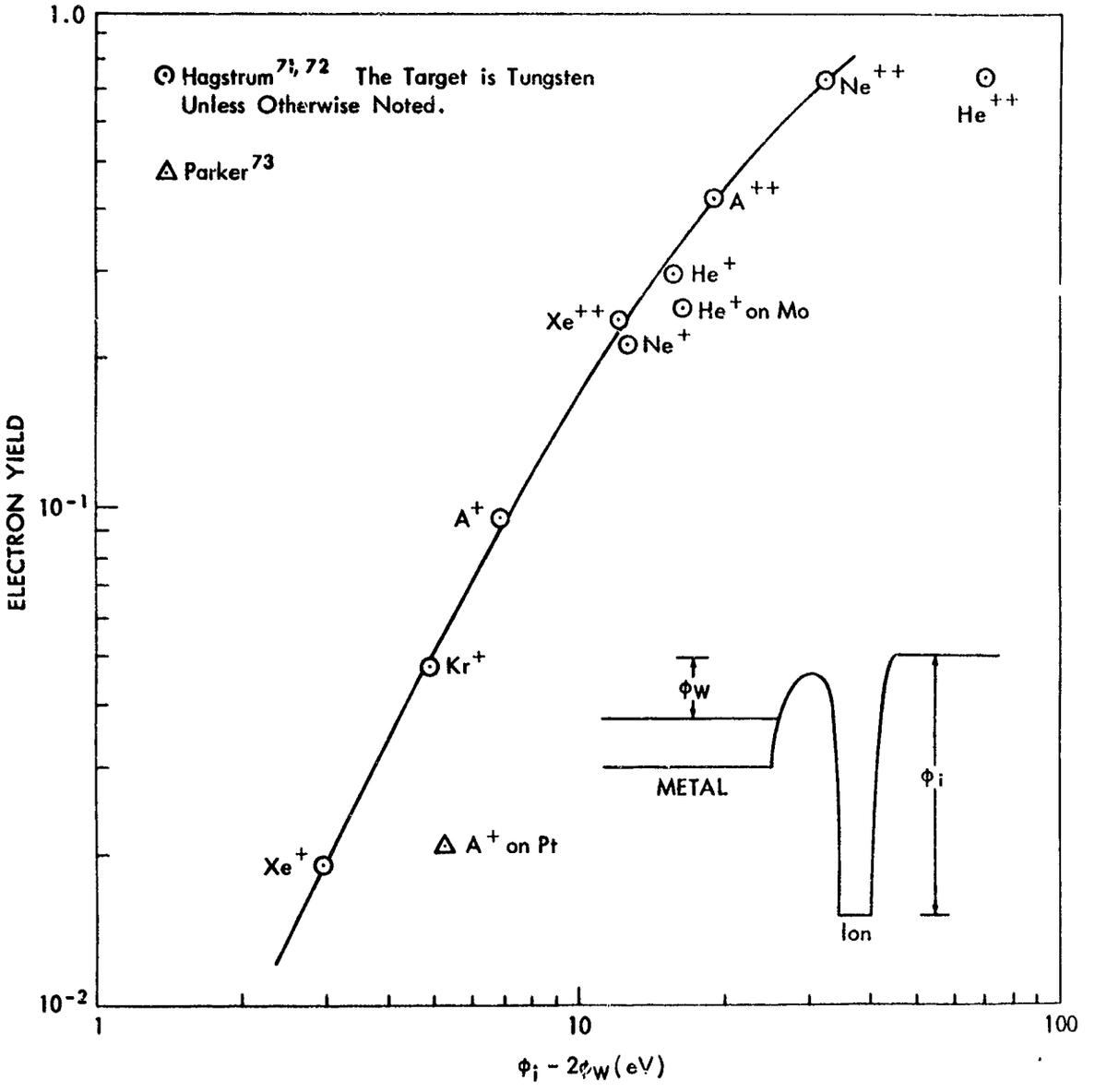

Figure 12. Secondary Electron Emission from Ion Impact at Low Kinetic Energies

residual impurity even though the measurement was made only 25 second after flashing the surface. The He^{++} ion probably liberates electrons through the two-step resonance capture process rather than by the Auger process.[74]

Figure 13 shows the yields for H^+ on Al and W from 1 keV up to about 10 MeV. The curves have been extrapolated to the value of Table II at 1 keV. They show a broad maximum at about 100 keV converging to a single curve independent of the target material at higher energies.

The variation of the ion yield as a function of angle of incidence of the primaries has been measured by Oliphant[82] and by Allen.[83] Their results show that the yield is proportional to sec θ. Thus the effective yield for an isotropic flux of monoenergetic ions incident on a surface will be unchanged if the flux is given in units of no/cm^2-sec-steradian.

Reflection coefficients for He^+ incident on clean and contaminated tungsten have been measured by Hagstrum to be 0.0017 and 0.00043 respectively and were found to be fairly insensitive to the ion energy.[84] Although reflection coefficients for H^+ and 0^+ on tungsten or aluminum are not available, they are probably somewhat larger but still less than 0.02.[85] Hagstrum suggests that these values are representative of the reflection of ions whose ionization energy is large compared to twice the work function of the solid. It is concluded that ion reflection is unimportant as far as charging effects on a body in space are concerned.

The energy distributions of secondary electrons are quite dependent on the state of the surface but in general peak near 2 eV with a Maxwellian shape. For practical reasons Figure 11 will be used when needed to compute the escaping electron current for positive satellite potentials. It will be assumed that the angular distribution of the secondary electrons is a cosine function.

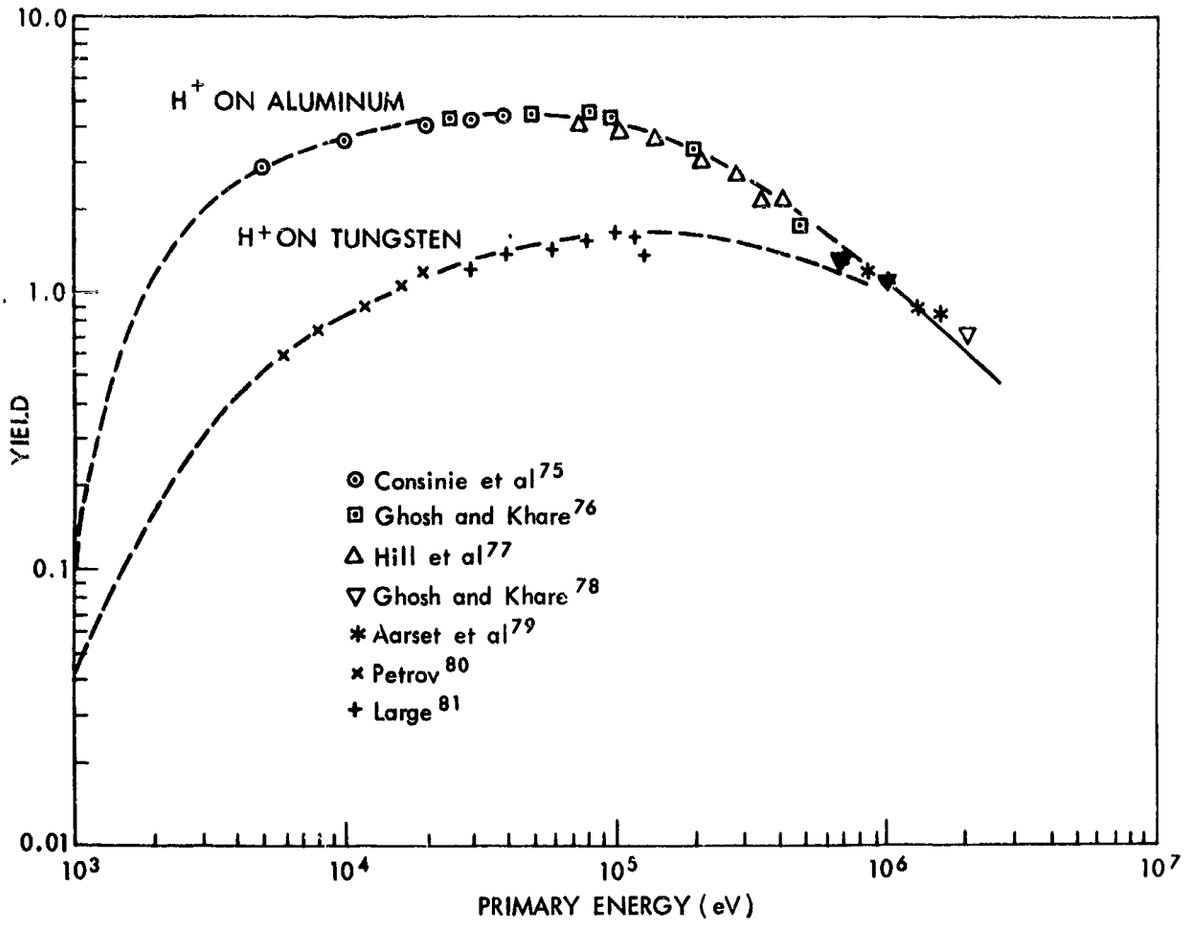

Figure 13. Secondary Yield of Electrons for Proton Impact at Energies Above 1 Kev

BLANK PAGE

CHAPTER V

OTHER CHARGING MECHANISMS

1. Discharge Time for a Body in a Plasma. It was stated in Chapter III that the most important mechanisms for charging a body are the collection of environmental electrons and ions and the secondary processes treated in Chapter IV. It is necessary to consider other possible mechanisms to see under what conditions this assumption is justified.

The concept of the discharge time τ for a body in a plasma is useful in assessing the relative importance of a proposed charging mechanism in comparison with ion and electron collection. Suppose that a body at an equilibrium potential determined by a balance between ion and electron accretion from the environmental plasma suddenly acquires an additional amount of charge by some other mechanism which acts only momentarily. The body will return to its previous potential in a time on the order of τ seconds. If the frequency of occurrence of this other mechanism is small compared with the quantity τ^{-1}, then its effect on the average equilibrium potential may be ignored.

As an example, consider a small body at a negative potential where the ion and electron currents are given by Equations (3.2) and (3.3) respectively. The change in the charging current to the body due to a sudden small change in potential is on the order of

$$\Delta I \cong \frac{n e a_+ A}{2\sqrt{\pi}} \frac{e}{kT} \Delta\phi \tag{5.1}$$

Hence, we may write

$$\frac{dQ}{dt} \cong \frac{-n e \alpha_+ A}{2\sqrt{\pi}} \frac{eQ}{CkT} = -\frac{Q}{\tau} \tag{5.2}$$

where Q is the excess charge over that at equilibrium and C is the body's capacitance. Thus we find that the discharge time τ for a small sphere of radius r is given by

$$\tau = \frac{2\sqrt{\pi}\, CkT}{n e^2 \alpha_+ A} = \frac{\epsilon_0 \sqrt{2\pi\, kT\, m_+}}{n e^2 r} = \frac{\tau_p^2}{\tau_B} \tag{5.3}$$

where τ_p^{-1} is the ion plasma frequency, $1/2\pi \sqrt{n e^2/\epsilon_0 m_+}$, and τ_B is a characteristic time describing how long it takes an ion to travel a distance comparable to the dimensions of the body. Representative values for τ for a 10 micron radius body are 2×10^{-3} sec in the ionosphere and $2 \times 10^{+3}$ sec in interplanetary space. Discharge times for larger bodies will be proportionately smaller although sheath effects will then complicate the definition of τ.

2. Cosmic Rays. Spitzer[17] has shown that cosmic rays have a negligible influence on the rate of charging of small dust grains in interstellar space. The flux of primary cosmic rays outside the earth's atmosphere is about 1 cm^{-2} sec^{-1} , whereas the flux of ions from the plasma in interplanetary space is at least 10^5 cm^{-2} sec^{-1} . The ionization produced in a particle along the path of the cosmic ray will be on the order of or less than 10^6 electrons/cm, and only those produced within a depth of 10^{-7} cm from the surface will be able to escape. Hence, a cosmic ray particle is no more effective than a single low energy environmental electron in charging a small particle.

In large bodies the effects of showers in increasing the charging efficiency must be considered. If the body dimensions are large compared to the interaction length for star production, then both the primary and the products of the stars will come to rest in the body. One would expect a maximum in the charging efficiency at a body dimension on the order of a few interaction lengths. There is an analogy between this picture and the situation in the earth's atmosphere where the flux of cosmic ray particles reaches a maximum at a depth of about 60 gm/cm^2, or one interaction length. The corresponding distance is on the order of 0.1 to 1 meter for appropriate densities. However, the flux in the atmosphere at the Pfotzer maximum is only double that outside the atmosphere; hence it may safely be concluded that the increase in charging efficiency is less than an order of magnitude, and the charging effect of cosmic rays may be disregarded.

3. Radioactivity. Radioactive material in a body in space constitutes a charging mechanism both through the escape of emitted charged primaries from the radioactive nuclei and also through the escape of secondary electrons excited by the primary in its passage to the surface.

To compete with the minimum expected ion flux in interplanetary space of 10^5 cm^{-2} sec^{-1} used in the preceding section, a surface activity of 3 μ-curies/cm^2 is required if only the primaries are taken into account. The efficiency with which secondaries can be produced will be of the same order of magnitude as the yields for secondary electrons discussed in Chapter IV. Thus β radiation has a low efficiency near 1% until it has slowed down to less than one KV, where the efficiency peaks at values somewhat greater than unity. Proton and α-emission efficiencies will have a maximum value near ten at energies near 100 KV.

This line of reasoning is supported by looking at the specific ionization rates for these radiations. Peak ionization rates are less than 10^8 ion-pairs/cm for both protons and α-particles in tungsten and occur near 100 KV, similar to the secondary yields in Figure 13. These specific ionization rates were computed from stopping cross-sections per atom, using 30 eV as the energy required to form an ion pair.[86] The peak in production for electrons occurs at a few hundred eV. Ionization cross-sections for electrons in gases show a maximum less than about 10^{-15} cm^2 at these energies, which, if applied to a solid material such as tungsten, yield a specific ionization somewhat under 10^8 ion-pairs/cm[60]. Since the secondary electrons will have energies below about 20 eV, only those excited within about 20Å of the surface will escape. This yields an upper limit of 20 for the efficiency of a primary in producing secondaries which can escape from the body.

The amount of radioactive material in bodies in space has been studied extensively from the viewpoint of determining the ages of meteorites. Typical values for the induced activity as a result of cosmic ray bombardment are on the order of a few hundred disintegrations per minute (dpm) per kg of material, or 10^{-11} curies/kg.[87] Similar activities have been measured on sections of recovered satellites.[88] It is obvious that the charging effects of such low quantities of radioactive material are entirely negligible.

Satellites sometimes carry quantities of radioactive material in conjunction with certain types of experiments, or as a power source. Such sources are usually well shielded but should still be considered as potential charging mechanisms. Clearly, each such source must be evaluated individually.

4. Thermionic Emission. Shen and Chopra[36] have discussed the effect upon the equilibrium potential of thermionic emission of electrons from bodies in space. They found that the temperature of a metallic body with a work function of 3.8 eV must exceed 700°K before it could have any significant effect. They assumed that the emission current was balanced by electron collection from the surrounding plasma characterized by a density of $10^3/cm^3$ and a temperature of about 1000°K.

If a work function of 3.5 eV is assumed, a surface temperature of about 800°K is required for an electron emission of 10^5 cm^{-2} sec^{-1} to compete with the minimum expected ion flux. Such a high temperature is likely only in special situations, such as when a meteor or space vehicle enters the earth's atmosphere below 100 km at high speeds, or when a body approaches sufficiently close to the sun. A body with a typical albedo for meteors of about 0.4, whose temperature is determined by a balance between solar flux and black-body radiation, will have a temperature of 800°K only when it approaches a distance of 0.19 astronomical units–half the distance of Mercury's orbit from the sun. The effects of thermionic emission will not be pursued further in this investigation.

5. Field Emission. Spitzer and Savedoff[19] have pointed out that for small dust grains field emission of electrons will limit the potential when it is negative. The onset of field emission occurs at surface field values between 10^6 and 10^7 volts/cm, the lower field corresponding to an emission flux of 10^5 cm^{-2} sec^{-1} for a work function of 3.5 eV. Since the surface field of a small spherical particle is ϕ/r, the potential is limited to negative values below approximately $10^6 r$. Thus, field emission is important only for dust grains of radius $\sim 10^{-5}$ cm (0.1 micron) and less.

6. Collisions with Dust Grains. One square cm of satellite surface will be hit by a dust grain with a radius larger than 0.3 microns approximately once every 50 seconds in the vicinity of the earth.[89] This impact frequency decreases rapidly for larger grains; it probably also decreases by at least three orders of magnitude as one proceeds from the vicinity of the earth into interplanetary space. The value of 0.3 micron was chosen because smaller particles cannot remain at the earth's distance from the sun on account of the solar radiation pressure.

In spite of the fact that one impact will produce many free electrons, the time between impacts is so large compared with the discharge time due to the plasma that the charging effects of such encounters may be completely disregarded.

7. The Effect of Radio Frequency Fields. Early speculations[11,90] that the rf fields around telemetry and other antennas on satellites might influence the satellite potential by a rectifying effect on currents from the plasma have been put on a quantitative basis by a group of Japanese investigators working on radio frequency probes.[91,92] (See also recent articles by Crawford and Harp[93,94] on the theory of the rf resonance probe.)

At rf frequencies below the plasma frequency the electron current density to a negative body is given by

$$j = j_0 I_0 (v/V_-) \tag{5.4}$$

Here j_0 is the current density to the probe with no rf field, I_0 is the modified Bessel function of the first kind, v the amplitude of the rf voltage and V_- the equivalent electron temperature. The current density is independent of frequency until close to the plasma frequency where it rises to a maximum and then falls to the value j_0 at higher frequencies.

The Bessel function in (5.4) was obtained by integrating Equation (3.2) over one period of the rf voltage. Thus one would expect (5.4) to hold only at frequencies low enough that the electron's transit time from outside the sheath to the probe is small compared to the rf period. At positive potentials the effect would also be computed for low frequencies by averaging the appropriate equation from Table 1 over a period.

The maximum in the current occurs close to but generally at a lower frequency than the plasma frequency. The resonant frequency depends primarily on the geometry of the probe. The height of the current maximum depends both upon the geometry and upon the effects of damping by the plasma. Collisional damping predominates if the neutral density is high enough; otherwise there is an "rf phase-mixing technique akin to Landau damping."[94] The former mechanism has been studied to some extent, but very little is known about the latter, which would be the prevailing mechanism in the upper atmosphere. The effect will be discussed further when the Explorer VIII data is presented.

BLANK PAGE

CHAPTER VI

MAGNETIC FIELD EFFECTS

1. The Induced $\vec{V}\times\vec{B}$ Potential Gradient. Beard and Johnson[8] pointed out that a satellite moving across the magnetic field of the earth would experience an induced potential gradient of as much as 0.2 volts/meter. This effect was observed on Explorer VIII through its effect on the electron current to a plasma probe.[40] The phenomenon may be described as follows: a conducting body moving across the magnetic field is polarized so that in a coordinate system moving with the body the electric field due to the induced polarization charge exactly cancels the induction field in the interior of the body. The polarization charge, in turn, is the source of a real field external to and carried along with the body which depends on the geometry of the body (and the environmental plasma), but whose effect on the plasma (i.e. on particle collection or on the sheath) may be described by saying that the potential of the surface of the body varies linearly with distance in the $\vec{V}\times\vec{B}$ direction.

The best way to see this is to make a Lorentz transformation of the magnetic field to the moving satellite reference frame. A uniform electric field is obtained given by $\vec{V}\times\vec{B}$ in MKS units. The effect of this uniform electric field on a conducting body can then be calculated by the usual methods of electrostatics. For example, a sphere in a uniform field gives rise to a potential distribution described by a dipole term plus the uniform field term. The effective external electric field is then obtained by subtracting the uniform field since the effect of the

magnetic field on the charged particles in the plasma can best be described by using the Lorentz force. Hence, the effective potential on the conducting surface is a linearly increasing function in the $\vec{V} \times \vec{B}$ direction.

This effect is important primarily for the collection of electrons which depends exponentially on the satellite potential if it is negative. Beard and Johnson computed the effect on electron collection to a rectangular parallelepiped satellite.[8] The electron current to a negative sphere moving in a magnetic field may be computed as follows: in a spherical coordinate system centered in the sphere the surface potential is given by

$$\phi = \phi_0 + |\vec{V} \times \vec{B}| \, R \cos\theta < 0 \tag{6.1}$$

where the z-axis is taken in the $\vec{V} \times \vec{B}$ direction. An element of area given by $2\pi R^2 \sin\theta \, d\theta$ is at the potential given by (6.1), so that the current to the satellite is, from Equation (3.2),

$$I_- = \frac{n_- e \alpha_-}{2\sqrt{\pi}} \int_0^{\pi} e^{(\phi_0 + |\vec{V} \times \vec{B}| R \cos\theta)\,(e/kT)} \, 2\pi R^2 \sin\theta \, d\theta \tag{6.2}$$

We obtain

$$I_- = \frac{I_0 \sinh (e\,|\vec{V} \times \vec{B}|\, R/kT)}{(e\,|\vec{V} \times \vec{B}|\, R/kT)} \tag{6.3}$$

where I_0 is the electron current that would be collected by the sphere if it were at the uniform potential ϕ_0.

The practical consequence of this induction effect is that for large spacecraft one end of the structure is "pinned" close to zero volts or slightly positive, with the other end becoming relatively more negative.

This is because the positive current to the body is limited, whereas the negative electron current increases more strongly. Thus, in Equation (6.3), as the $\vec{V} \times \vec{B}$ term increases, the potential ϕ_0 contained in I_0 must become more negative to maintain I_- relatively constant and equal to I_+.

2. Effect of a Magnetic Field on the Direct Collection of Particles. In addition to the induction effect caused by the motion of a body, a magnetic field can also affect the collection of charged particles by restricting their direction of incidence. Consider, for example, a cylinder with its axis parallel to the magnetic field. Electrons approach the cylinder by spiralling along the magnetic field with a certain radius of gyration, ρ. For an electron to be collected at a given point on the side of the cylinder at least two conditions must be met: first, the distance of the magnetic field line about which the electron moves from the cylinder axis must be less than $R + \rho$, but greater than the absolute value $|R - \rho|$, where R is the radius of the cylinder; and second, the distance of the point from the end of the cylinder must be less than the "wavelength" of the spiral. It is apparent that the current to the side of such a cylinder must decrease as the distance from either end increases.

This effect is important whenever ρ is small compared to the size of a body, and consequently is important for electron collection by rockets and satellites, since ρ is on the order of cm in the ionosphere. Because of the fact that this effect on electron collection in the upper atmosphere has not been treated quantitatively in the literature, a calculation is made here for both cylindrical and spherical bodies with the assumption of zero potential difference between the body and the plasma. The results for a cylinder will be applicable to probes mounted on the side of a rocket; indeed, there is evidence for anomalously low electron

currents to such probes on rockets flown at Fort Churchill, Canada, where the rocket axis was within a few degrees of the magnetic field direction.

A Maxwell-Boltzmann velocity distribution for electrons may be written as follows, using cylindrical coordinates in velocity space:

$$f(v_z, v_T) = n_- \left(\frac{m_-}{2\pi kT}\right)^{3/2} e^{-\frac{m_-}{2kT}(v_z^2 + v_T^2)} \tag{6.4}$$

where v_z is the component of velocity along the field line, and v_T is the transverse component. The radius of gyration is given by

$$\rho = m_- v_T / Be \tag{6.5}$$

and the wavelength by

$$\lambda = 2\pi m_- v_z / Be \tag{6.6}$$

At the plane $z = 0$ defining the front face of the cylinder, the current density of incident electrons is given by

$$J_z = \iint e\, v_z\, f(v_z, v_T)\, 2\pi\, v_T\, dv_T\, dv_z \tag{6.7}$$

where $2\pi\, v_T dv_T dv_z$ is the volume element in velocity space. The geometry of the problem is described in Figure 14, where r is the distance of the guiding center field-line from the cylinder axis, and ϕ is the phase angle of the electron in its circular motion defined with respect to the $\phi = 0$ line as shown in the figure. All electrons with $r < R - \rho$, where $\rho < R$, will be collected on the front face independent of its phase angle ϕ at the plane $z = 0$. To be collected on the side of the cylinder the condition $R - \rho < r < R + \rho$ must be met, and the phase angle must be

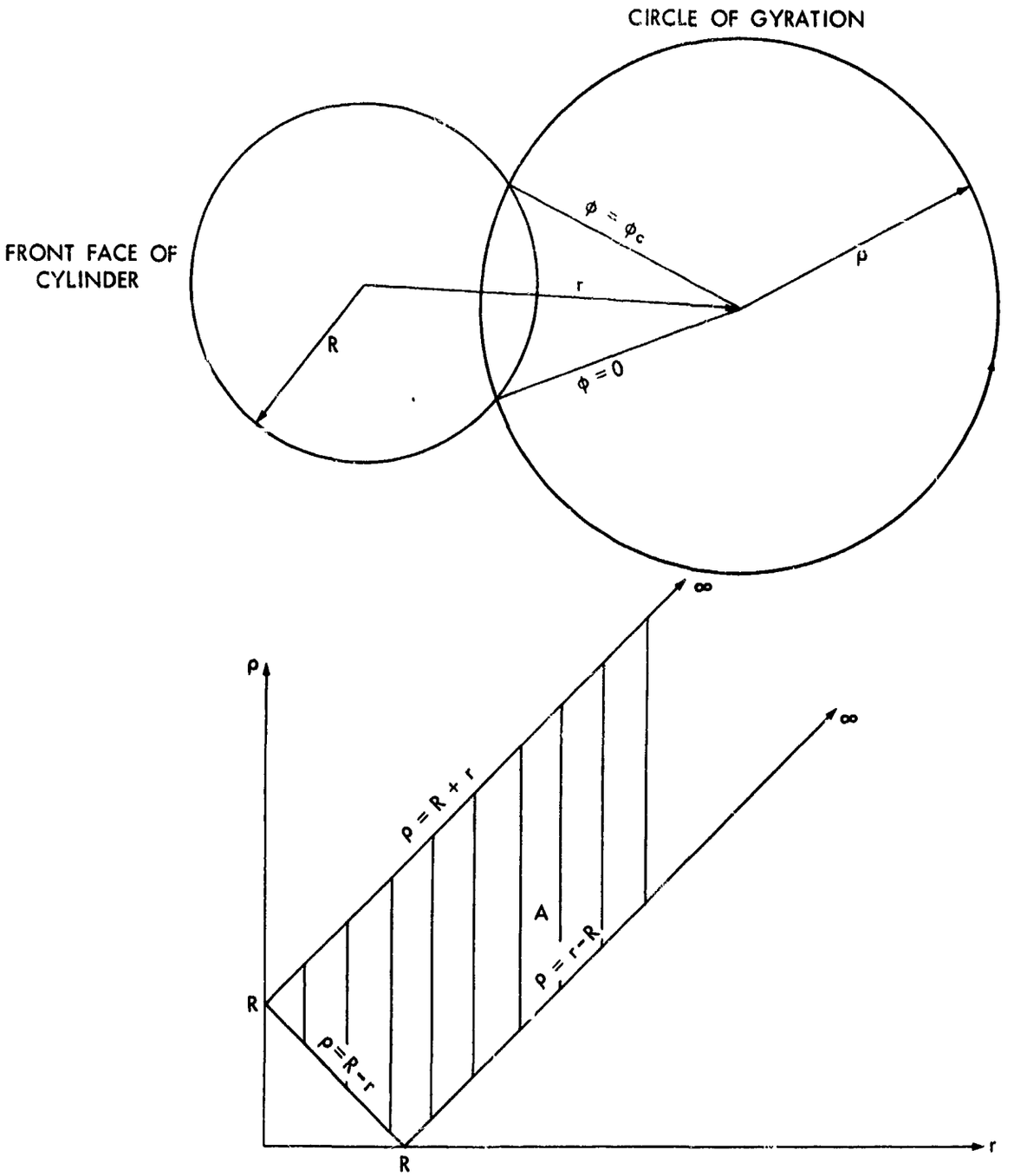

Figure 14. The Effect of a Magnetic Field on Electron Collection by a Cylinder; a) The Geometry of Collection. b) Integration Area in the r-ρ Plane

between 0 and ϕ_c as it reaches the plane $z = 0$. The particle impacts the cylinder when ϕ reaches ϕ_c at a distance z along the cylinder that is proportional to the phase angle $(\phi_c - \phi)$ and the velocity v_z:

$$z = \frac{v_z\,(\phi_c - \phi)}{\text{angular velocity}} = \frac{\lambda}{2\pi}\,(\phi_c - \phi) \tag{6.8}$$

where

$$\phi_c = 2\pi - 2 \arccos\left(\frac{r^2 + \rho^2 - R^2}{2r\rho}\right) \tag{6.9}$$

Obviously, if this value of z exceeds the cylinder length L, the particle will miss the cylinder completely. It follows that if the above conditions are satisfied for a given r, ρ and λ, that all the particles with an initial phase angle ϕ and with wavelengths between λ and $\lambda + d\lambda$ will be collected in the surface element $2\pi R dz$, where

$$dz = \frac{1}{2\pi}\,(\phi_c - \phi)\,d\lambda \tag{6.10}$$

The current per unit length to the cylinder will then be given by

$$\frac{dI}{dz} = \int \frac{J\,2\pi r\,dr}{dz}\left(\frac{d\phi}{2\pi}\right)$$

or,

$$\frac{dI}{dz} = \frac{2n_- e a_- z}{\sqrt{\pi}\,\rho^{*4}} \iint_A \int_{\phi=0}^{\phi=\phi_c} \rho e^{-\left[\left(\frac{\rho}{\rho^*}\right)^2 + \frac{r^2}{\rho^{*2}(\phi_c - \phi)^2}\right]} d\rho\,dr\,d\phi \tag{6.11}$$

where α_- has been defined previously in Chapter III, and where $\rho^* = m_- \alpha_- / Be$. The area of integration for the variables ρ and r is the shaded area in Figure 14, bounded by the lines $\rho = R + r$, $\rho = R - r$ and $\rho = r - R$. This may be integrated with respect to r to obtain

$$\frac{dI}{dz} = \frac{n_- e \alpha_-}{\rho^{*3}} \iint_A \rho r e^{-(\rho/\rho^*)^2} \left[1 - \operatorname{erf}\left(\frac{z}{\rho^* \phi_c}\right)\right] d\rho \, dr \qquad (6.12)$$

So far we have been considering electrons incident at one end of the cylinder only. Electrons arriving from the opposite end will constitute a current of the same form but with z replaced by (L - z). Hence the total current will be given by

$$\frac{dI}{dz} = \frac{n_- e \alpha}{\rho^{*3}} \iint_A \rho r e^{-(\rho/\rho^*)^2} \left[2 - \operatorname{erf}\left(\frac{z}{\rho^* \phi_c}\right) - \operatorname{erf}\left(\frac{L - z}{\rho^* \phi_c}\right)\right] d\rho \, dr \qquad (6.13)$$

The first term may be integrated with the result

$$\left(\frac{dI}{dz}\right)_1 = \frac{n_- e \alpha_-}{2\sqrt{\pi}} (2\pi R) \qquad (6.14)$$

which is just the current per unit length for the case of no magnetic field. The other terms have been integrated numerically for a choice of values for R and ρ^* characteristic of a Nike-Apache rocket in the ionosphere. The resulting currents normalized to the current of (6.14) are shown in Figure 15.

It is apparent from the figure how for a typical Nike-Apache payload length of 60" the current per unit length at the mid-point of the rocket has decreased by two orders of magnitude. In fact, the curve for L = 60" is essentially identical to the current per unit length due to electrons arriving from one direction only. This effect probably explains

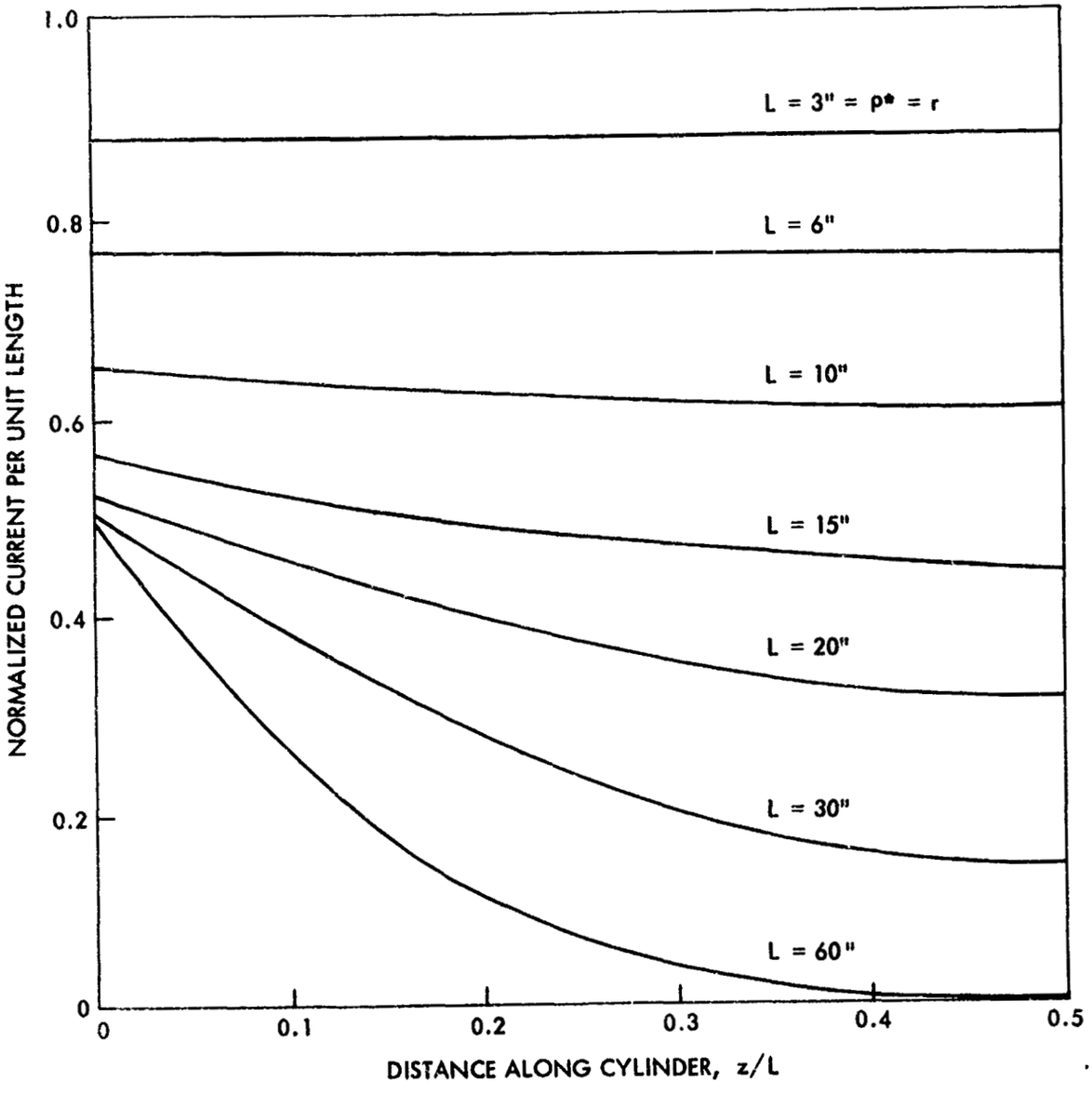

Figure 15. The Electron Current to a Cylinder in a Magnetic Field

why measured electron currents to probes on the nose-tips of Nike-Apache rockets have been observed to be low by a factor of two when compared with normal diffusion theory.[95]

A similar procedure has been followed to compute the electron current to a sphere as a function of the ratio of the sphere's radius to the most probable radius of gyration, ρ^*. The geometry is illustrated in Figure 16, where the magnetic field is parallel to the z-axis. The equations for the spiral described by the electron are

$$\left.\begin{aligned} x &= x_1 + \rho \cos\left(\frac{\omega z}{v_z} + \phi\right) \\ \text{and} \\ y &= y_1 + \rho \sin\left(\frac{\omega z}{v_z} + \phi\right) \end{aligned}\right\} \qquad (6.15)$$

where (x_1, y_1) are the co-ordinates of the guiding center. When this is combined with the equation for the sphere, $r = R$, the following equation is obtained for the value of z where the particle is incident on the sphere:

$$R^2 - z^2 = r_1^2 + \rho^2 + 2r_1 \rho \cos\left(\frac{\omega z}{v_z} + \phi\right) \qquad (6.16)$$

The left-hand and right-hand sides of this equation are also shown in Figure 16 as a function of z. It is apparent that all particles with $(r_1 - \rho)^2 > R^2$ cannot be collected, while all particles with $(r_1 + \rho) < R$ will be collected. Those with $(r_1 - \rho)^2 < R^2 < (r_1 + \rho)^2$ may or may not be collected depending upon the particle's phase angle ϕ and its wavelength. The critical phase angle, ϕ_c, is defined as the phase angle necessary so that the particle merely grazes the sphere. It is found

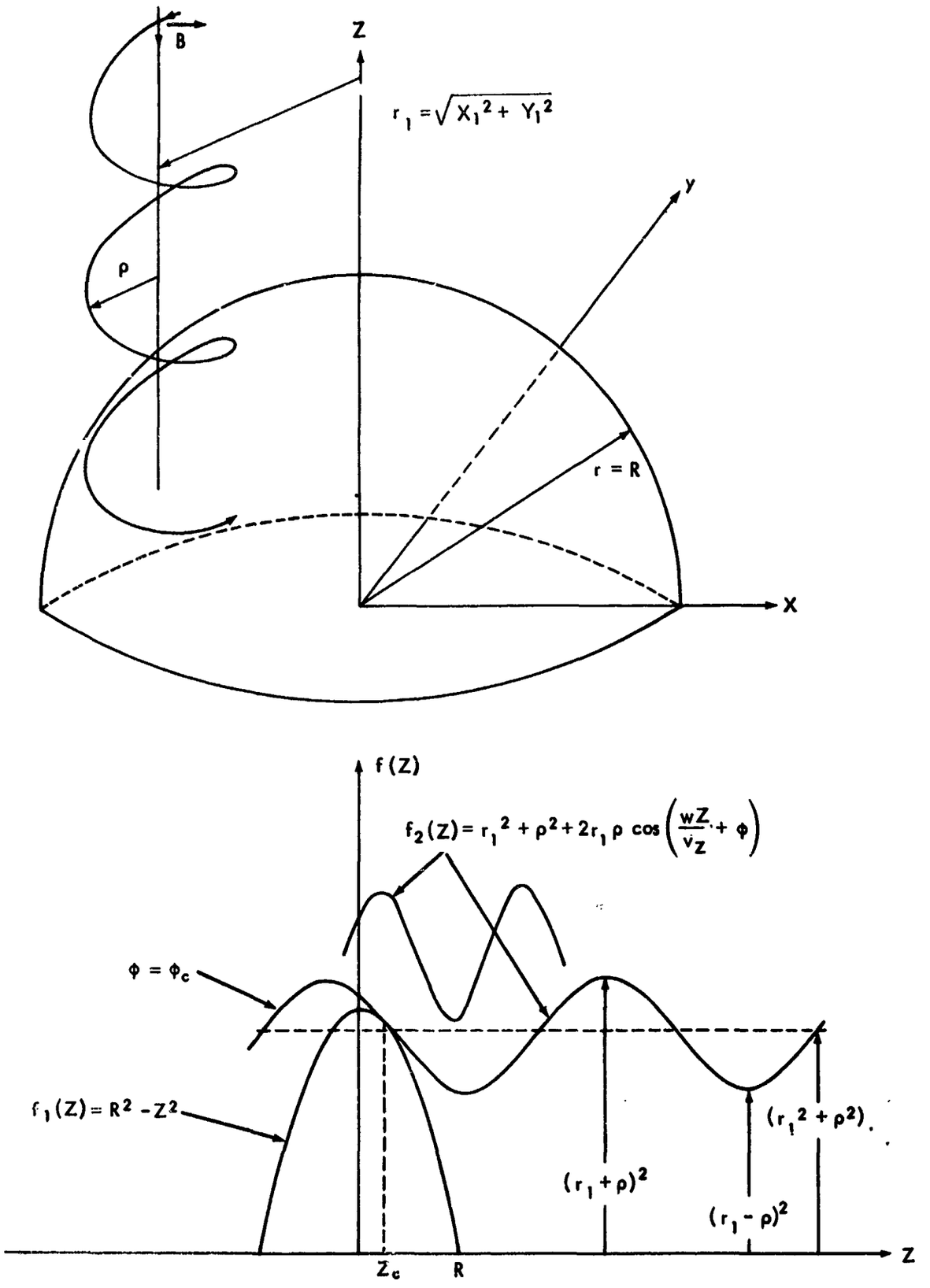

Figure 16. The Geometry of Electron Collection by a Sphere in a Magnetic Field

by combining Equation (6.16) with the equation obtained by differentiating (6.16) with respect to z. We find

$$\phi_c = \arccos\left[\frac{R^2 - z_c^2 - r_1^2 - \rho^2}{2r_1\rho}\right] - \frac{\omega z_c}{v_z} \tag{6.17}$$

where

$$z_c^2 = R^2 - 2\left(\frac{v_z}{\omega}\right)^2 - r_1^2 - \rho^2 + 2\sqrt{\left(\frac{v_z}{\omega}\right)^2\left[\left(\frac{v_z}{\omega}\right)^2 - R^2 + r_1^2 + \rho^2\right] + r_1^2\rho^2} \tag{6.18}$$

All particles with $-\phi_c < \phi < +\phi_c$ will <u>not</u> be collected.

The case when $\phi_c = 0$ occurs when the particle trajectory grazes the sphere twice, once when approaching and once when leaving. This defines a minimum wavelength, $\lambda_m = 2\pi m_- / Be\,(v_z)_m$, for a given r_1 and ρ, such that all particles with shorter wavelengths will be collected regardless of their phase angle. We obtain for the total current:

$$I = \frac{4n_- e\alpha_-}{\sqrt{\pi}\,\rho^{*2}}\left\{\int_{r_1=0}^{R}\int_{\rho=0}^{R-r_1}\int_{u=0}^{\infty}\int_{\phi=0}^{2\pi} Q(r_1, \rho, u, \phi)\,d\phi\,du\,d\rho\,dr_1\right.$$

$$\left. + \iint_A\left[\int_{u=0}^{u_m}\int_{\phi=0}^{2\pi} Q\,d\phi\,du + 2\int_{u=u_m}^{\infty}\int_{\phi_c}^{\pi} Q\,d\phi\,du\right]d\rho\,dr_1\right\} \tag{6.19}$$

where $u = v_z / \alpha_-$, and where

$$Q(r_1, \rho, u, \phi) = r_1\,u\,\rho\,e^{-u^2}\,e^{-(\rho/\rho^*)^2} \tag{6.20}$$

The area A is the same as shown in Figure 14. All the integrations may be carried out in a closed form except for the term containing ϕ_c.

The total current to the sphere in terms of the current with no magnetic field is

$$\frac{I}{I_0} = \frac{1}{2}\left[1 + \frac{\sqrt{\pi}}{(R/\rho^*)}\ (2\text{-erf}\ R/\rho^*) + \frac{1}{(R/\rho^*)^2}\left(1 - e^{-(R/\rho^*)^2} + \frac{8F(R/\rho^*)}{\pi}\right)\right] \quad (6.21)$$

where $F(R/\rho^*)$ is the result of a computer integration of the term in (6.19) containing ϕ_c. This current is plotted in Figure 17, verifying the effect of a magnetic field in reducing the electron current to a large sphere by a factor of two.

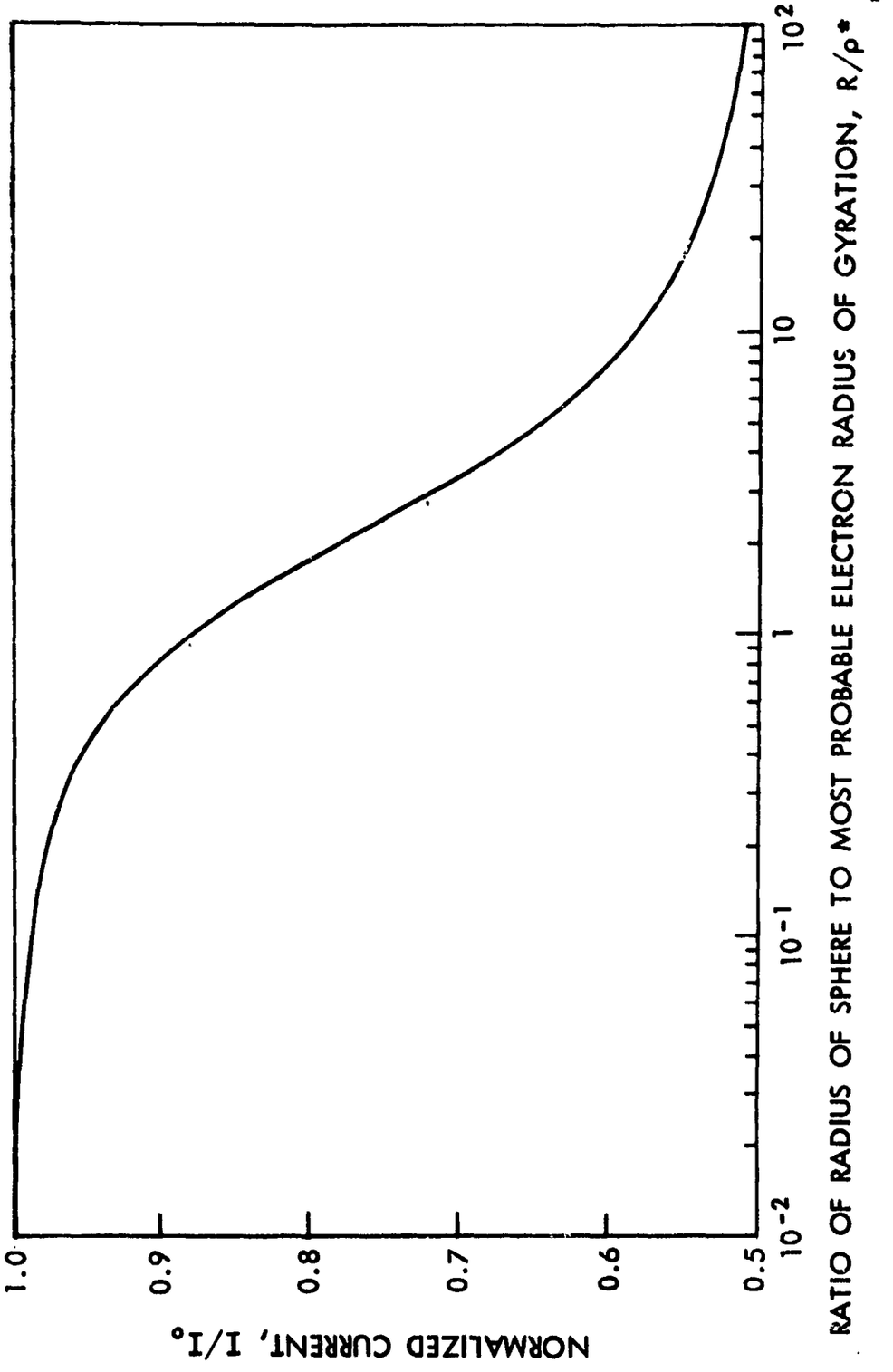

Figure 17. The Electron Current to a Sphere in a Magnetic Field

BLANK PAGE

CHAPTER VII

EQUILIBRIUM POTENTIALS FOR VARIOUS ENVIRONMENTS

1. General Equations and Computational Procedure. The general procedure for finding the equilibrium potential of a body is to set the total current to the body equal to zero. The corresponding potential is the equilibrium potential, in accordance with the discussion in Chapter I. In this section some general results are presented in the form of equations and graphs showing expected equilibrium potentials as a function of various parameters such as temperature, body size, body velocity, etc. In the following sections equilibrium potentials will be computed for representative conditions in the upper atmosphere of the earth and in interplanetary space.

For a small spherical body at rest we use (see Table 1) Equation (3.3) for ions and Equation (3.2) for electrons and find

$$\left(\frac{m_+ T_-}{m_- T_+}\right)^{1/2} e^{\phi e/kT_-} = 1 - \frac{\phi e}{kT_+} + Q \tag{7.1}$$

as long as the body is negative. Here Q is the normalized current density

$$Q = \frac{\sqrt{\pi}\, J}{2n\, e\, \alpha_+} \tag{7.2}$$

where J is the sum of both photoemission current density and current densities of energetic particle fluxes and their secondaries. This is a transcendental equation which must be solved numerically. Solutions for Q = 0 are shown in Figure 18 as a function of the temperature ratio

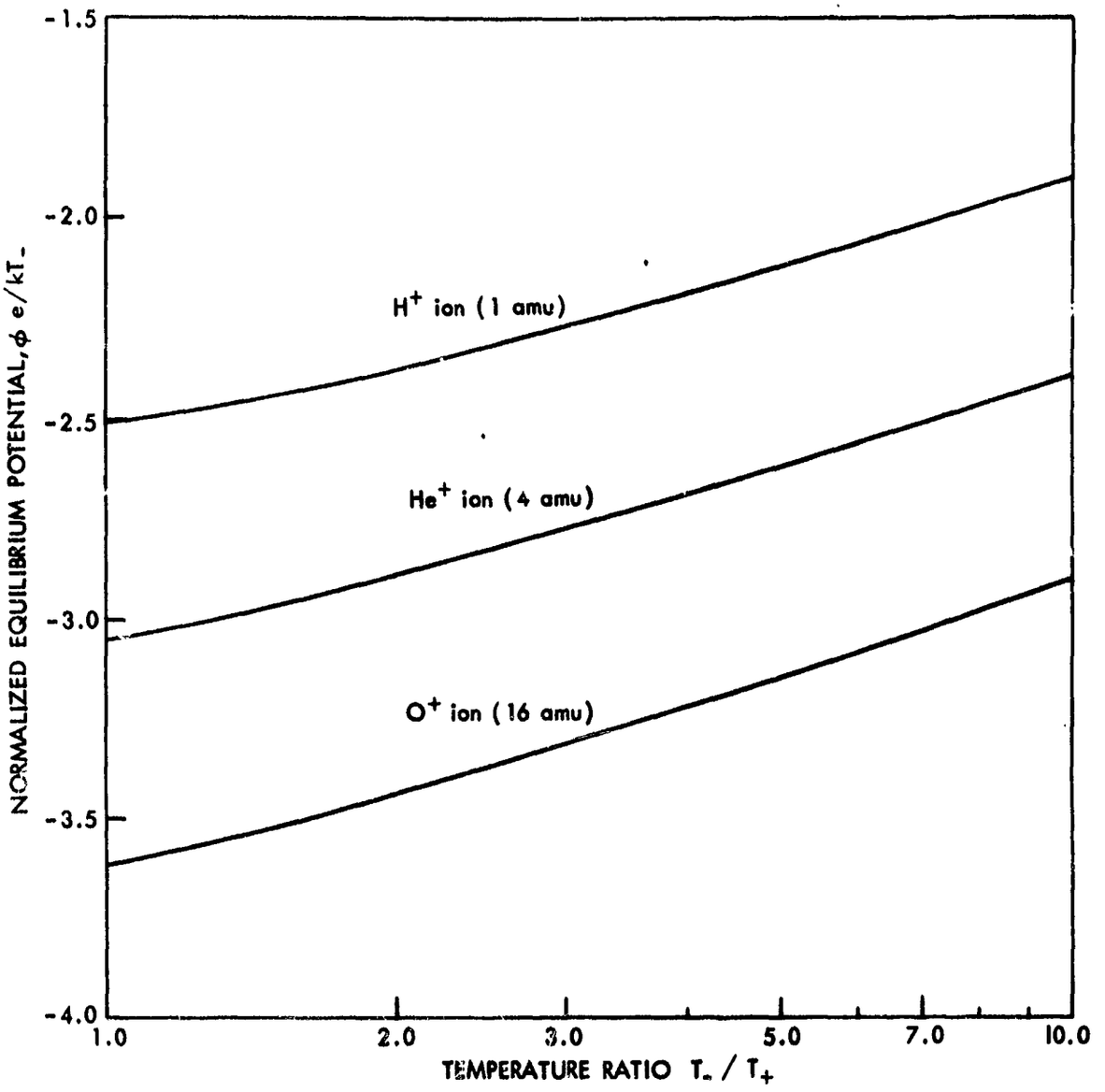

Figure 18. Equilibrium Potentials for a Small Body at Rest without Photoemission or Secondary Emission

T_- / T_+ for ion environments of 0^+, He^+ and H^+. As one would expect, a body is more negative when the atmospheric ion is heavier because of the lower thermal velocity. Although the normalized potential becomes less negative for an increasing temperature ratio, the potential itself becomes more negative. In other words, if T_+ were constant but T_- were increased, the potential of the body would become more negative even through the quantity $\phi e/kT_-$ becomes smaller in magnitude. There are both theoretical and experimental reasons for believing that thermal equilibrium is not always present in the atmosphere.[96]

Equilibrium potentials as a function of Q are shown in Figure 19 for 0^+ and H^+ environments and for three temperature ratios. At large values of Q the curves become quite flat. This is because the ion current is becoming unimportant in comparison with the (positive) photo- and/or energetic particle currents. When the ion current is negligible we find

$$\frac{\phi e}{kT_-} \cong \ln\left(\frac{\sqrt{\pi}\, J}{2n\, e\, \alpha_-}\right) \tag{7.3}$$

as long as

$$\left(1 - \frac{\phi e}{kT_+}\right) << Q < \left(\frac{m_+ T_-}{m_- T_+}\right)^{1/2} \tag{7.4}$$

When Q exceeds the right-hand side of this inequality the body becomes positive. When this is true Q is at least $\sqrt{m_H/m_-} = 42.87$. Hence the positive ion current may be disregarded, and we find

$$\phi e/kT_- = Q_p f_1(\phi) + Q_+ [1 + Y_+ f_2(\phi)] + Q_- [1 - Y_1 f_2(\phi)] - 1 \tag{7.5}$$

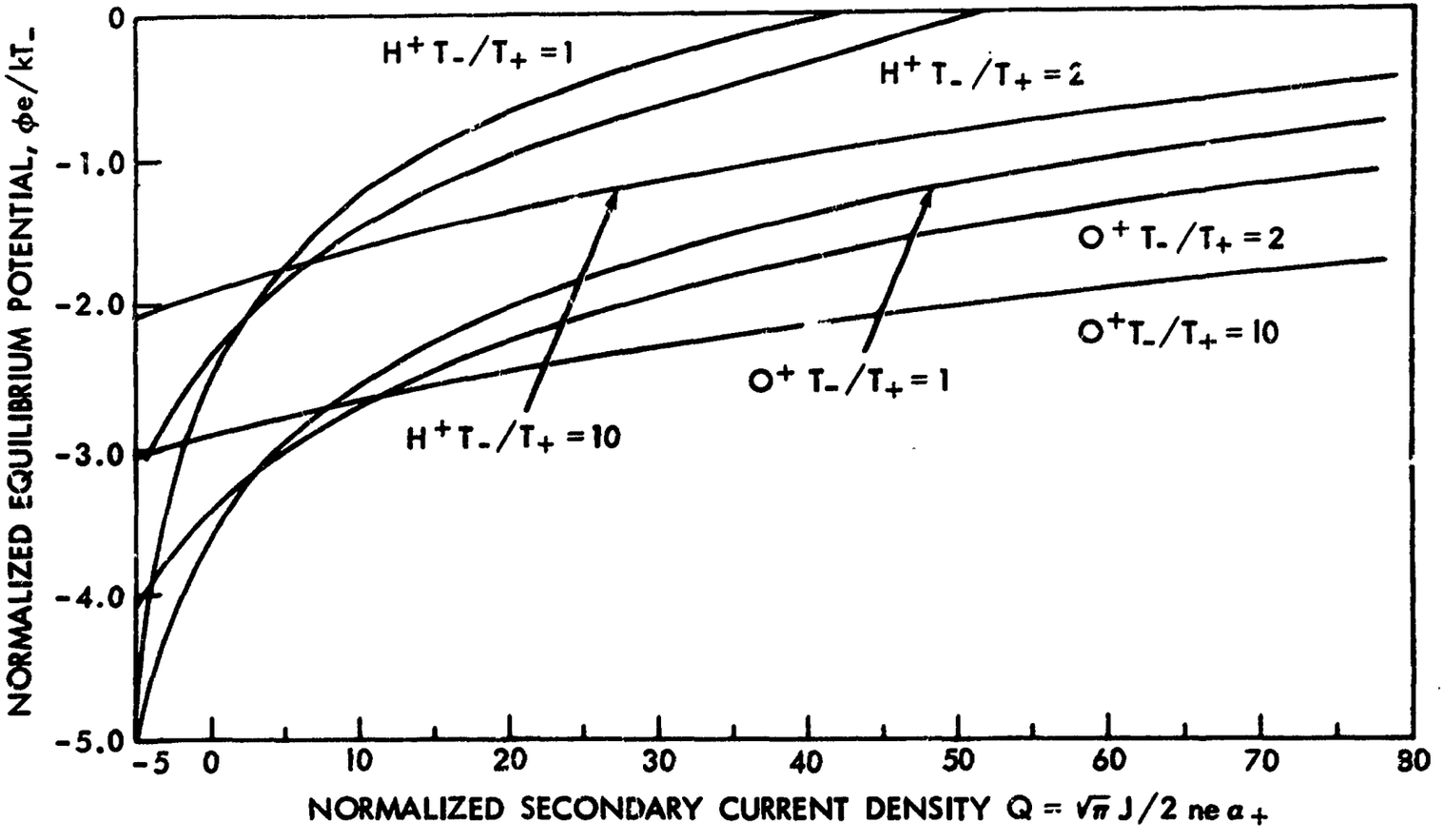

Figure 19. Equilibrium Potentials for a Small Body at Rest as a Function of Photoemission and/or Secondary Emission

where Q_p, Q_+, Q_- are the normalized photoemission and energetic particle current densities. $Y_\pm$ is the effective secondary electron yield for the energetic particles; and $f_1(\phi)$ and $f_2(\phi)$ are curves of current versus voltage obtained for a small body from Figures 7 and 11 respectively, and normalized to unity at $\phi = 0$.

Although a "small body at rest" may not at first glance seem to apply to many real situations, this is not the case. Micrometeorites or other dust particles have been shown to be important in and below the D-region of the ionosphere in providing a sink for atmospheric ions and electrons. Their potential which must be known to estimate the magnitude of this effect may be calculated from the preceeding equations and graphs. The equilibrium potential of small particles in interplanetary space where the positive currents to particles are due to photoemission and solar wind protons may also be computed from Equations (7.3) or (7.5).

For larger bodies sheath effects must be taken into account. As long as $Q = 0$ the equilibrium potential of the body will be negative. The appropriate equations are (3.2), (3.4), (3.5) and (3.6). Solutions for the equilibrium potential have been obtained numerically and are shown in Figure 20 as a function of the ratio of the body radius to the Debye length. Magnetic effects have not been included. When the ratio r/L is large, Equation (3.7) may be used with the result:

$$\frac{\phi e}{kT_-} \cong -1/2 \ln\left(\frac{T_- m_+}{T_+ m_-}\right) \tag{7.6}$$

The magnetic effect of Chapter VI, Section 2, may easily be included in this equation by subtracting from the right hand side the quantity $\ln(I/I_0)$ of Figure 17.

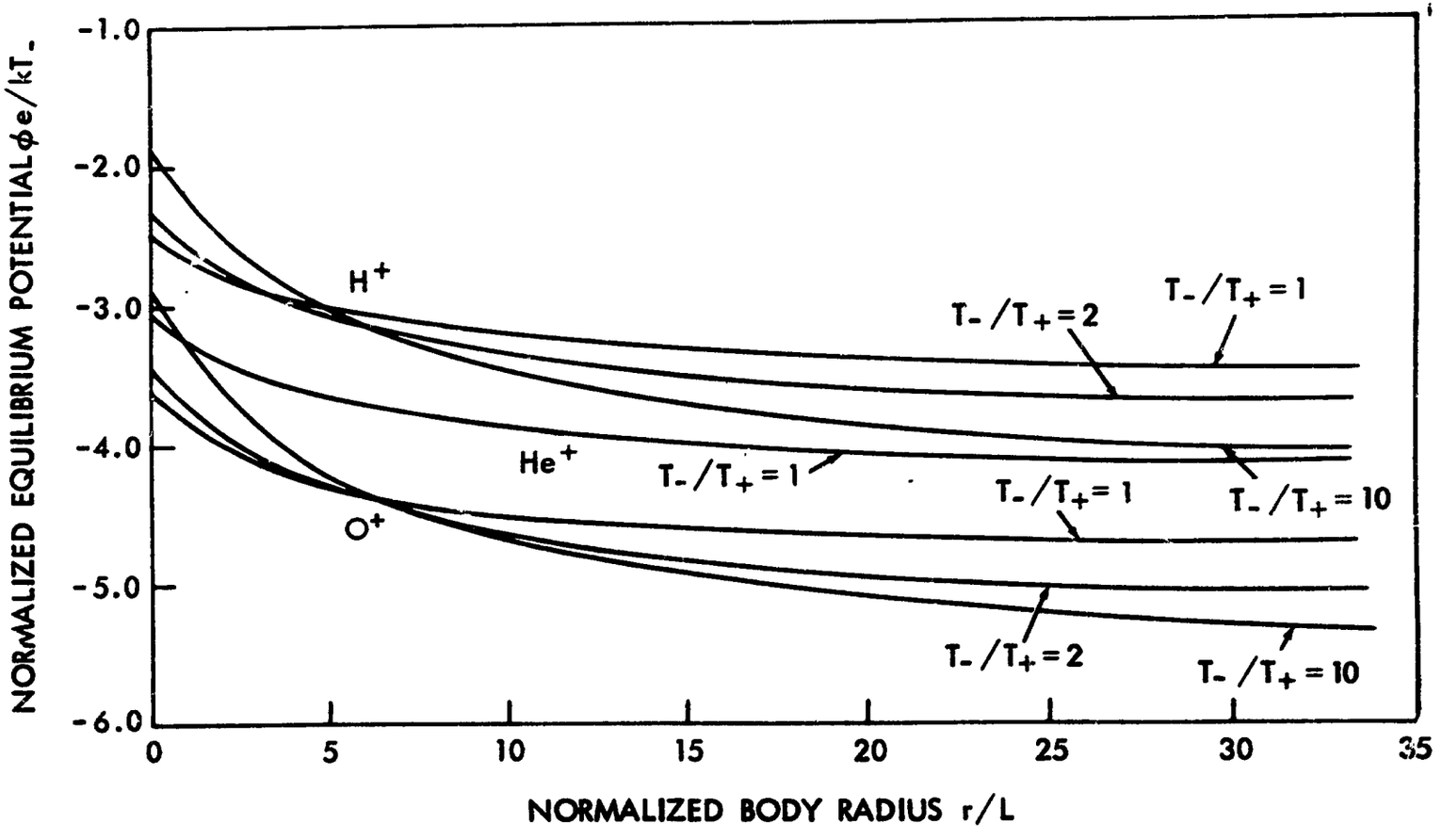

Figure 20. Equilibrium Potentials for a Body at Rest and without Photoemission as a Function of its Size

Figure 21 shows solutions for the equilibrium potential of a small moving body as a function of its Mach number, M, for the case when Q = 0. The appropriate equations are (3.14) for ions and 3.2 for electrons as long as the potential is negative. We find

$$\left(\frac{m_+ T_-}{m_- T_+}\right)^{1/2} e^{\phi e/kT_-} = \frac{\sqrt{\pi}}{2M}(\mathrm{erf}\, M)\left(M^2 - \frac{\phi e}{kT_+} + \frac{1}{2}\right) + \frac{1}{2}e^{-M^2} + Q \qquad (7.7)$$

As the velocity initially increases the ion current first decreases, as ions cannot catch up to the satellite from behind, and then increases as more and more are swept up in front. As a result, the equilibrium potential first becomes more negative, reaches a maximum, and thereafter becomes more positive.

The effects of photoemission on a small moving body are shown in Figure 22. Note the change from a linear to a logarithmic scale for the abscissa at Q = 10. Equation (7.7) was used for negative potentials and the following equation (from (3.9) and (3.3)) for positive potentials when Q is large:

$$\frac{1}{f_1(\phi)}\left\{\left(\frac{m_+ T_-}{m_- T_+}\right)^{1/2}\left(1 + \frac{\phi e}{kT_-}\right) - \frac{\sqrt{\pi}}{4} M\, G(M, \phi)\right\} = Q \qquad (7.8)$$

where $G(M, \phi)$ is the curly bracket of Equation (3.9). The equation has been written in this form because it has been found that the easiest computational procedure is to compute Q for a series of choices for ϕ.

When ϕ is positive the Mach number becomes relatively unimportant. This again is because the ion current is small compared with the large positive photocurrent. The equilibrium potentials are almost independent of the nature of the ion. This can be verified by noting that the curves for O^+ are displaced to the right by a factor of four from those for H^+, which is the ratio of the corresponding thermal velocities

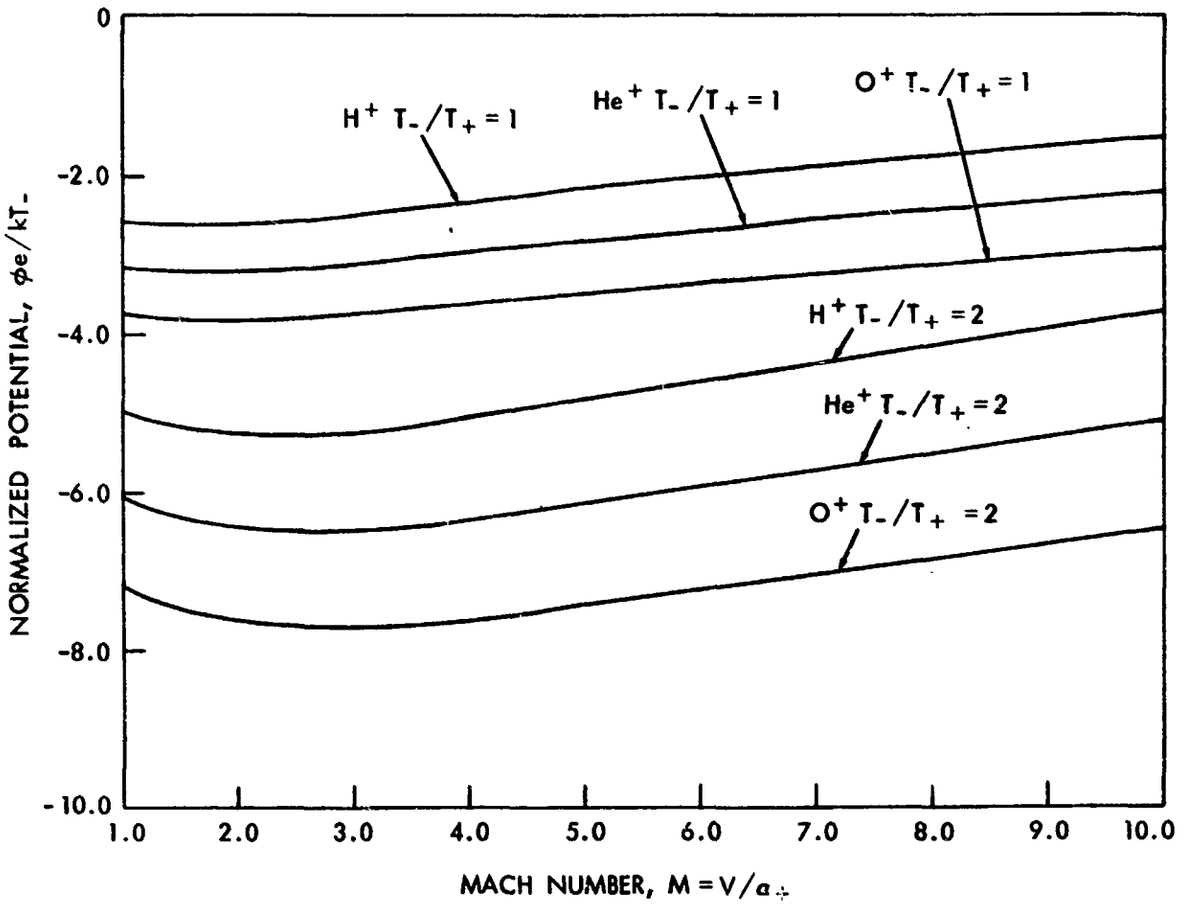

Figure 21. Equilibrium Potentials for a Small Moving Body without Photoemission

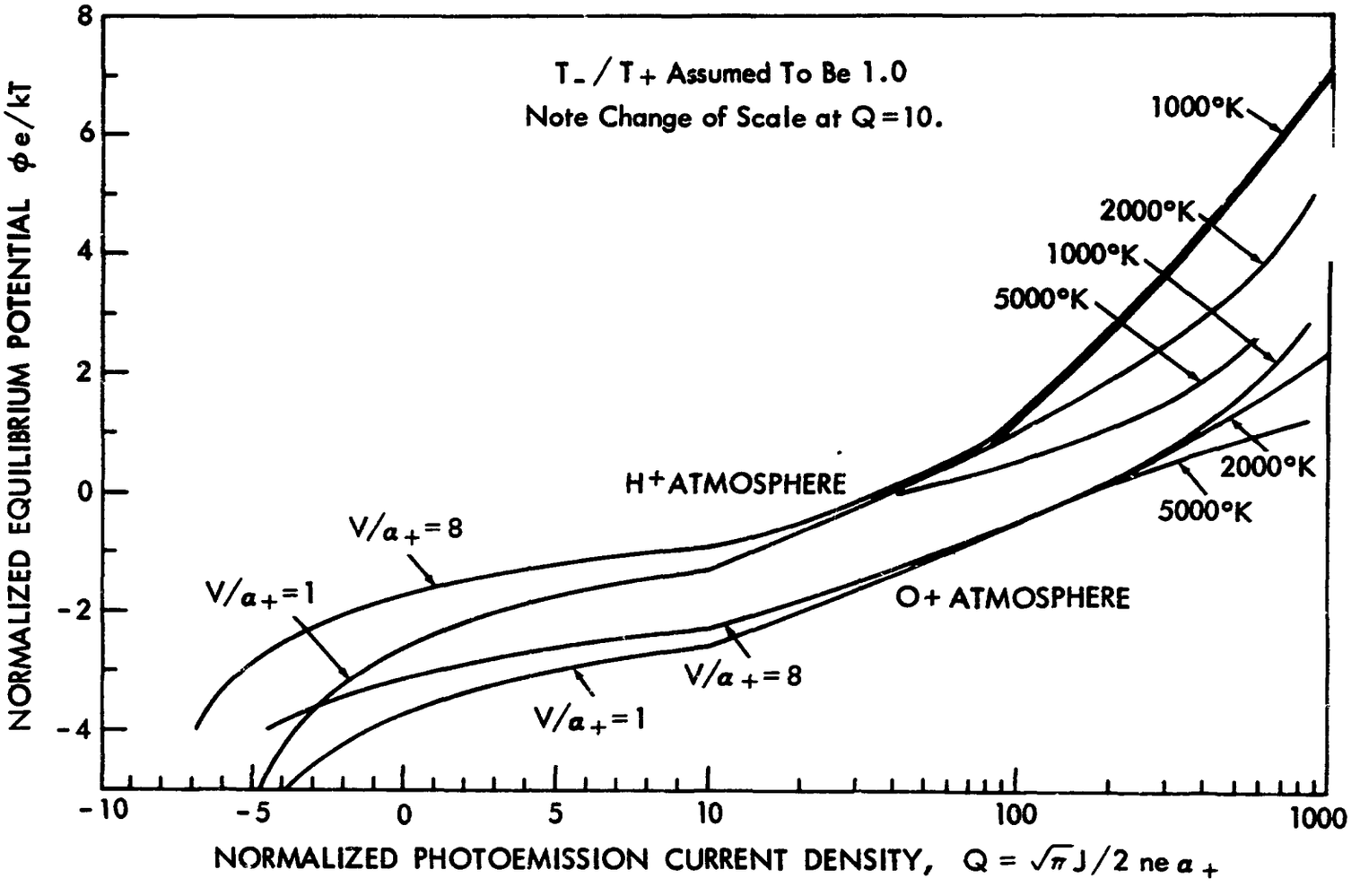

Figure 22. Equilibrium Potentials for a Small Moving Body as a Function of Photoemission

and hence also the ratio of the corresponding definitions for Q. Since the electron current to a small body is unaffected by the body's motion, the equation for large ϕ reduces to (7.5). The reason that the plasma temperature must appear explicitly is that the function $f_1(\phi)$ giving the relative number of photoelectrons that escape is independent of T.

Turning now to the case of a large body in motion, we must take into account the effect of the wake on the electron current as discussed in Section 3.4. Figure 23 shows computed equilibrium potentials as a function of Mach number for two bodies whose radii are 5 and 10 Debye lengths. In this figure Q is zero and no magnetic effects have been included. The ion current was computed according to the method described in the appendix. In addition, results are shown when the ion current was computed from the sheath approximation of Equation (A13) together with Equation (3.13). It is apparent that the two methods agree very well for Mach numbers greater than about three.

Figure 24 shows the effect of photoemission in driving a large body to positive potentials. The radius has been taken to be 33.3 Debye lengths. That the equilibrium potential does not depend strongly on size once r/L exceeds 10 can be seen by comparing the potentials at Q = 0 with the corresponding solutions in Figure 23. The effect of the induced potential gradient due to the magnetic field in driving the body more negative is shown by the dashed curve for a Mach number of unity and an oxygen ion atmosphere. In Figure 24 the sheath approximation for the ion current of Equation (A13) in the appendix was used with Equation (3.13) for negative potentials and Eq. (3.9) for positive potentials.

2. Expected Equilibrium Potentials in the Ionosphere for Large and Small Bodies. To illustrate the range of equilibrium potentials expected in the earth's ionosphere, two model atmospheres have been chosen

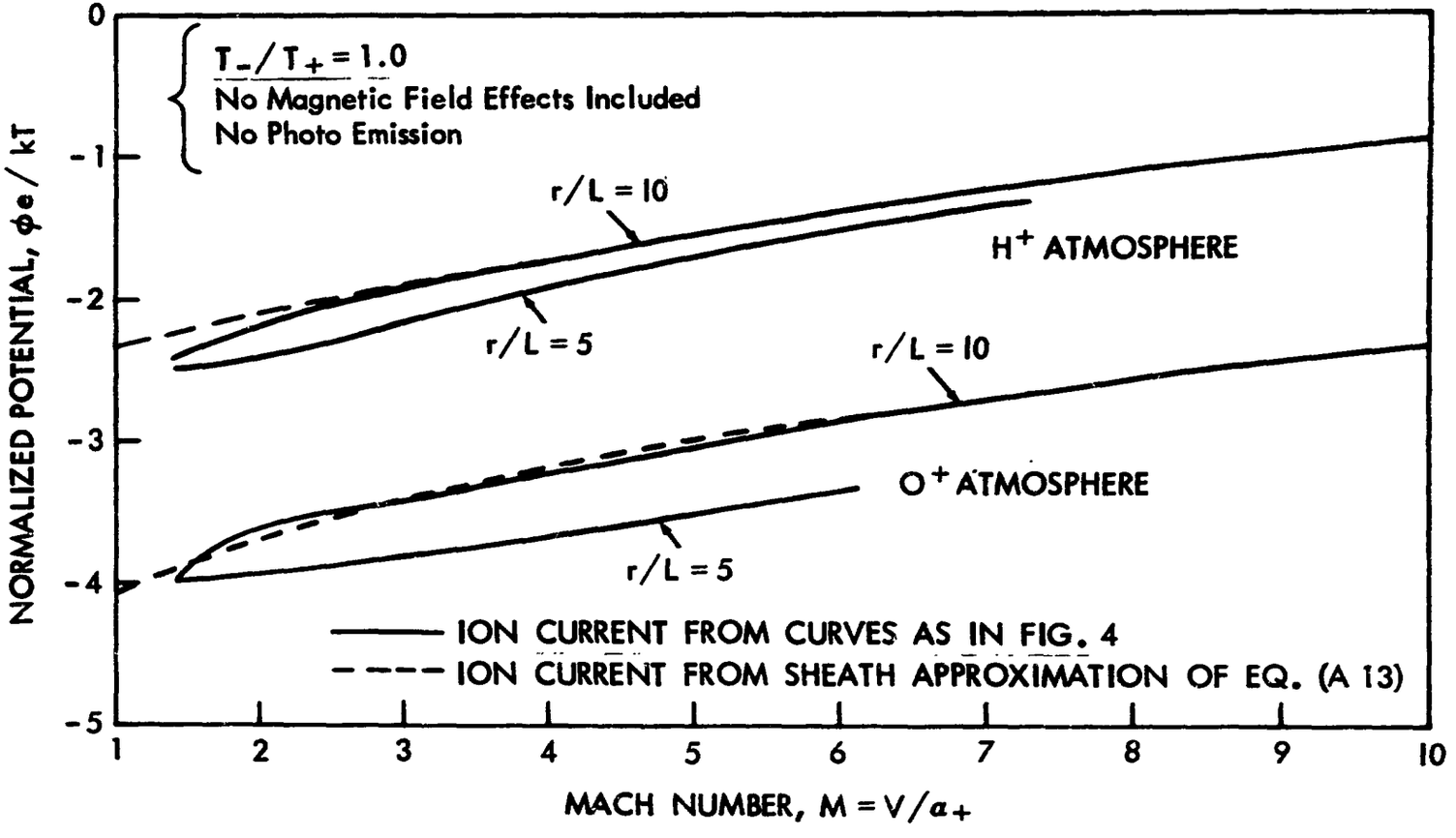

Figure 23. The Effect of size on the Equilibrium Potentials of a Moving Body

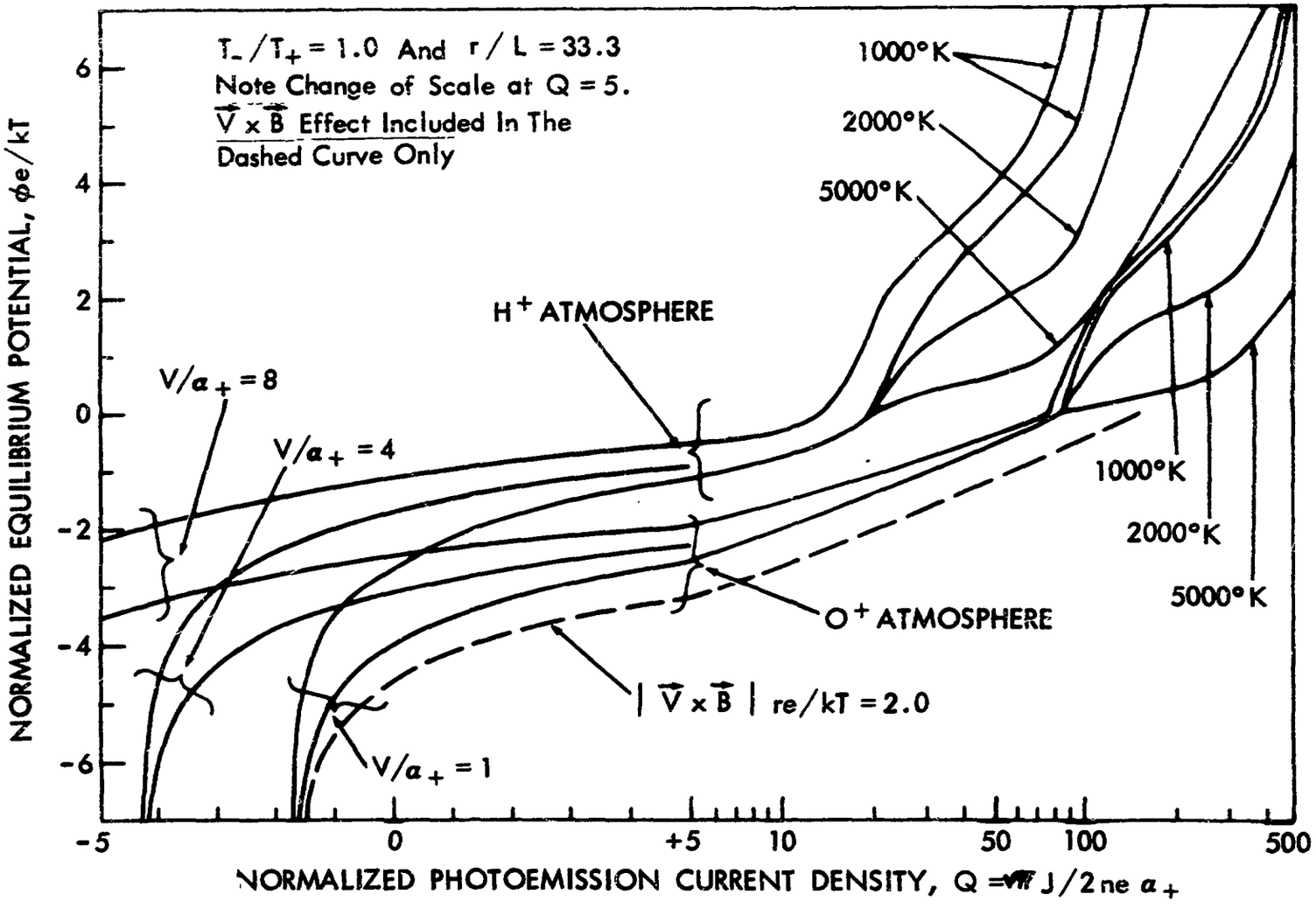

Figure 24. Equilibrium Potentials for a Large Moving Body as a Function of Photoemission

corresponding to low and medium temperatures. The data in Chapter VIII will describe equilibrium potentials for high temperatures. Figure 25 shows the ion densities and temperatures chosen for the cold model, and Figure 26 the corresponding quantities for the warm model. The procedure in constructing each model was as follows: A temperature for the isothermal region above 500 km was first chosen. The peak electron density was then chosen to be 2×10^6 cm^{-3} at 280 km for the warm model and 2×10^5 at 350 km for the cold model, in accordance with typical diurnal maximum and minimum densities.[96] Chandra's expressions for electron density in the upper F region were then used to compute densities from 200 km to 425 km.[97] Below 500 km T_- was set equal to T_+ for the cold model and normalized to the neutral gas temperature variation as published by the US Committee on Extension to the Standard Atmosphere.[98] For the hot model the ion temperature was set equal to the standard atmosphere neutral gas temperature, but the electron temperature measured on NASA rocket 6.04 was used. This rocket experiment flown on March 26, 1961, found an electron temperature at 360 km of 1600°K. The ion densities above 400 km geopotential altitude (425 km true altitude) were computed from Bauer's ternary ionosphere model, which uses that altitude as a reference level.[100,101]

Bauer's model was used up to 6000 km altitude. Temperatures in the cold model were kept at 700° all the way out to 20,000 km altitude (4.14 earth radii), whereas for the warm model the temperature was increased in accordance with recent measurements by Serbu.[102] Serbu's observation that the electron density beyond 2.2 earth radii may be approximated by a power law with an exponent of -3.4 was used to compute the total electron density out to 20,000 km.

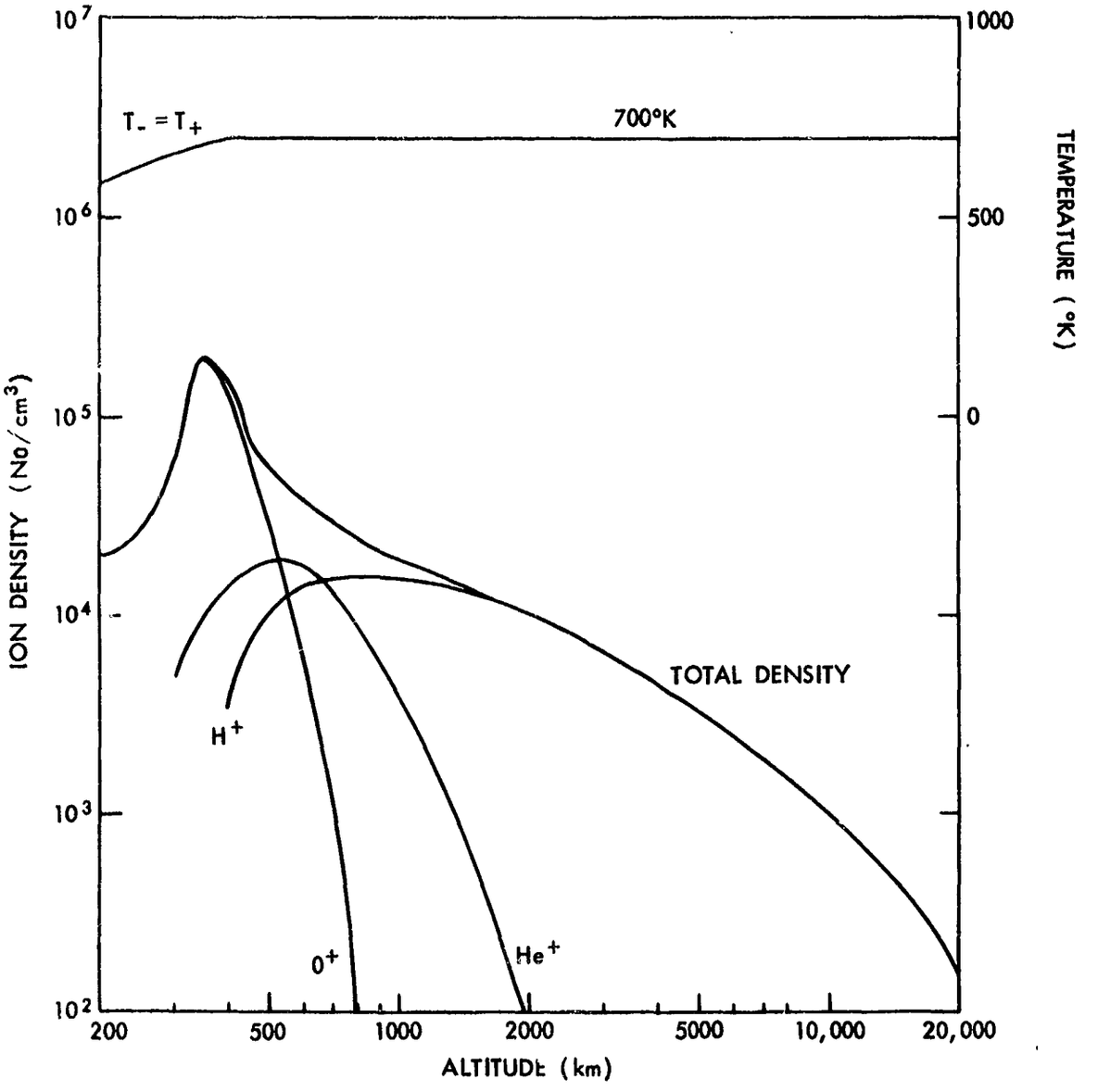

Figure 25. Cold Model Ionosphere

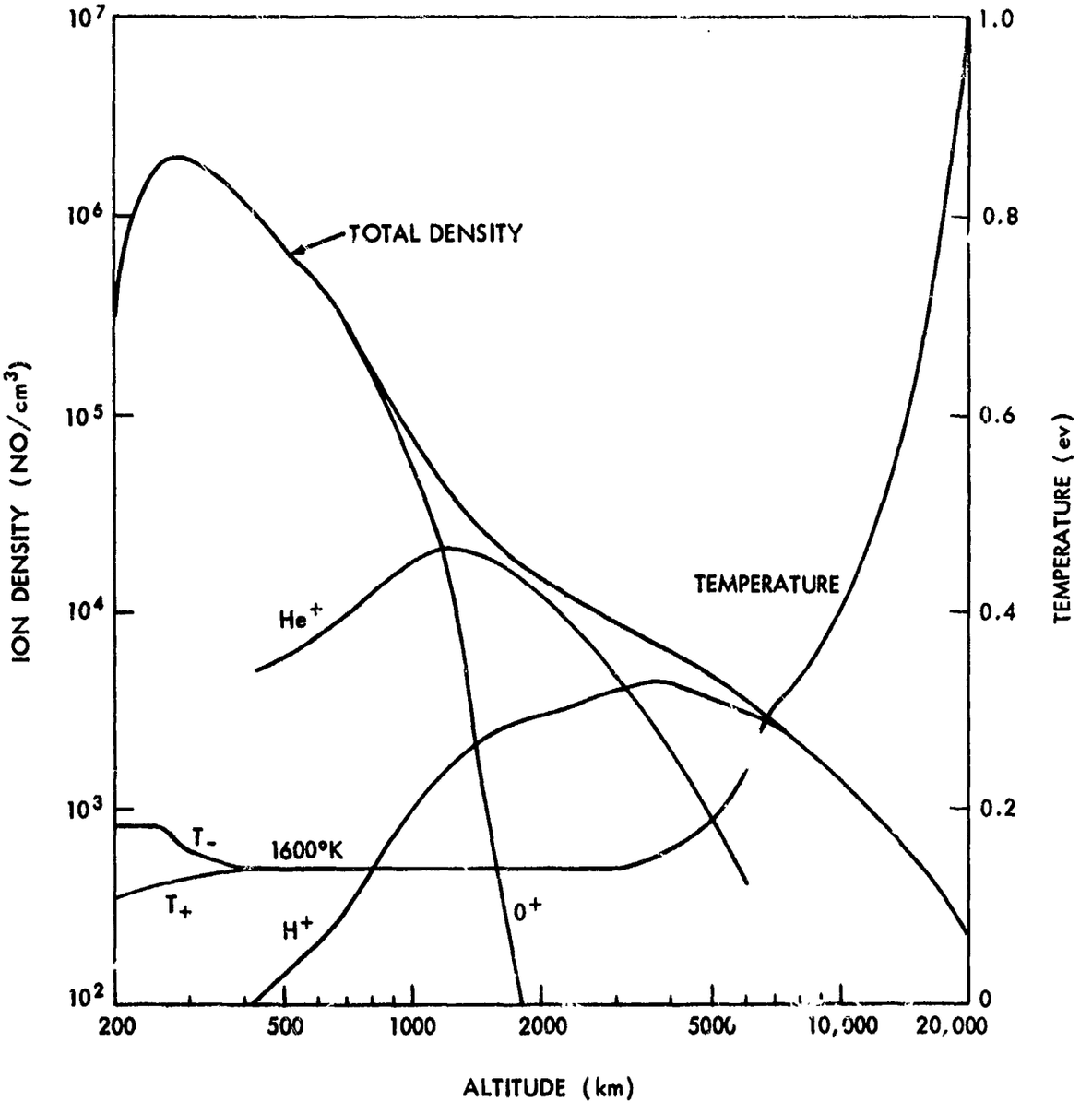

Figure 26. Warm Model Ionosphere

The equilibrium potential of both a small and a large body have been computed for both model atmospheres under conditions of darkness and sunlight. The body was assumed to have a velocity equal to that necessary for a circular orbit at the corresponding altitude. The magnetic induction effect was included for the large body by assuming that it was moving perpendicularly to the earth's magnetic field. This would be true for a body moving in the earth's geomagnetic equatorial plane. Finally, the secondary emission yields for the three kinds of ions encountered as well as for electrons (incident on Al) were included in the calculation.

The equations used in the calculations will not be given here. They are similar to those given in the preceding section but more complicated in that the ion current in general involves a summation over the three ion constituents. The photoemission current density was taken to be 4×10^{-9} amp/cm^2, and the radius of the large body to be 1.0 meters.

The results of the calculations are shown in Figures 27 and 28. Several general observations may be made. First, the potentials for the large and the small bodies are very similar, lying in the range from -0.1 to -0.6 volts, until the effect of photoemission begins to predominate. Photoemission begins to have a significant effect at about 1000 km altitude, but positive potentials are not obtained until about 5000 km in a cold atmosphere and 10,000 km or above in a warm atmosphere. In darkness the satellite potential is mainly a function of the temperature alone, as can be seen from the constancy of each solid curve in the isothermal region of the atmosphere. At higher altitudes – above 10,000 km – there is a much greater range in the possible values for the potential.

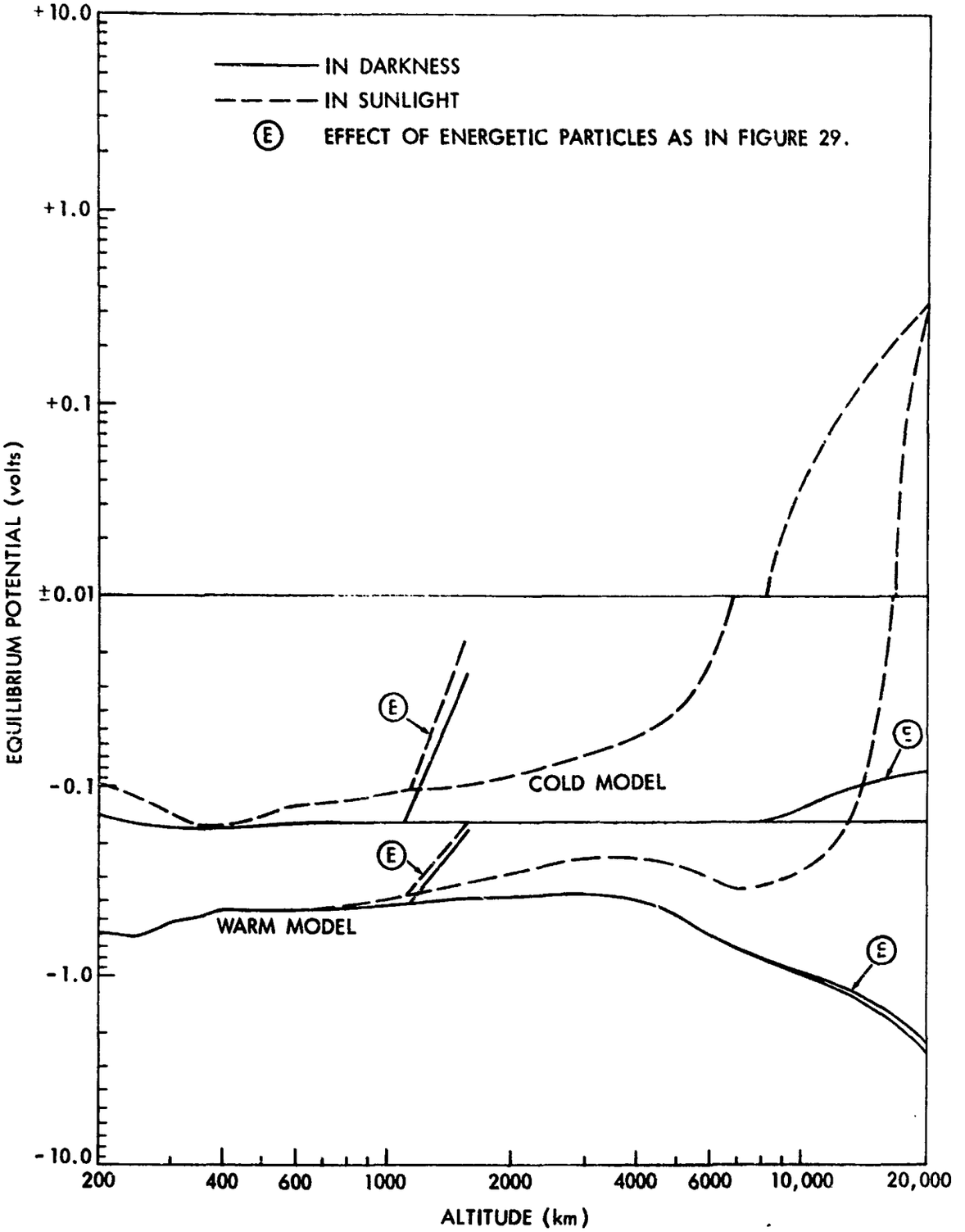

Figure 27. Equilibrium Potentials for a Small Body in Cold and Warm Model Ionospheres

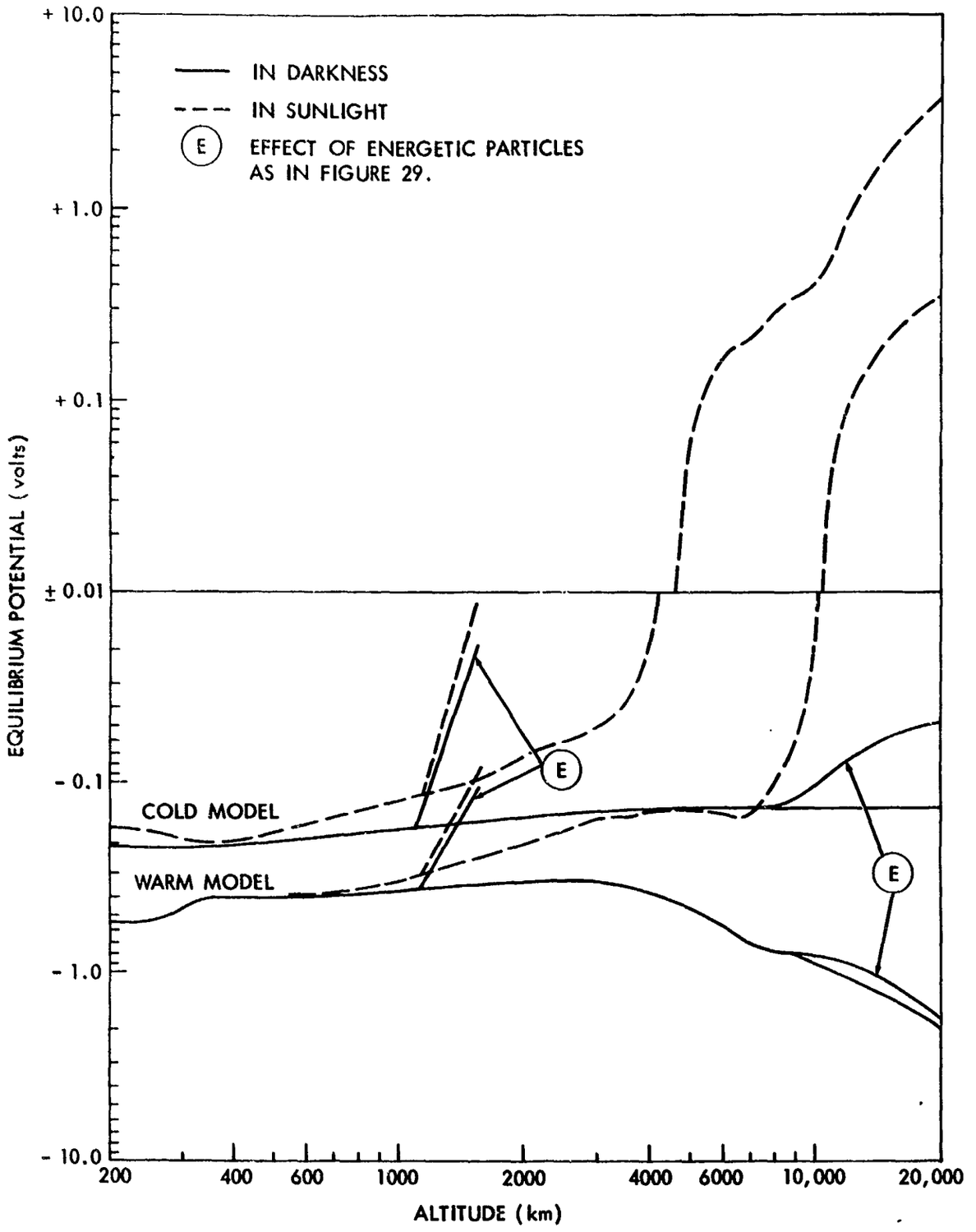

Figure 28. Equilibrium Potentials for a Large Body in Cold and Warm Model Ionospheres

The effect on the equilibrium potential of energetic particles trapped in the earth's magnetic field has not been investigated in detail, except for some estimates made recently by Kurt and Moroz.[103] Figure 29 exhibits typical energetic particle fluxes in the earth's magnetic equatorial plane. Not shown is the inner zone proton belt between approximately 1000 and 10,000 km consisting of 10 Mev and higher energy particles.[104] The maximum omnidirectional flux of these protons is about 5×10^4 cm^{-2} sr^{-1} at about 4000 km, which is much too small a flux to be a significant charging current. Much more significant is the belt of low energy (5KeV) protons found by Freeman[105] and also described by Hilton et al.[106] Extremely large fluxes were observed; but the spacial extent and altitude of maximum flux of these protons is not known. These protons would have a significant effect on the equilibrium potential, as is shown by the curves marked with an "E" between 1100 and 1550 km. The effectiveness of these protons is enhanced by the production of secondary electrons with a yield of 2.8, corresponding to an aluminum surface.

In the same region of space as the high energy proton belt there are known to be large fluxes of energetic electrons. There are apparently large fluctuations in these fluxes with time, but the variation and extent of these fluxes are not well known. A typical observation of electrons with energies above 20 KeV is shown.[107] At these energies the total secondary emission coefficient is 0.3 or less on aluminum. The effect of these fluxes on the equilibrium potentials shown in Figures 27 and 28 was computed and found to be either insignificant or just barely distinguishable.

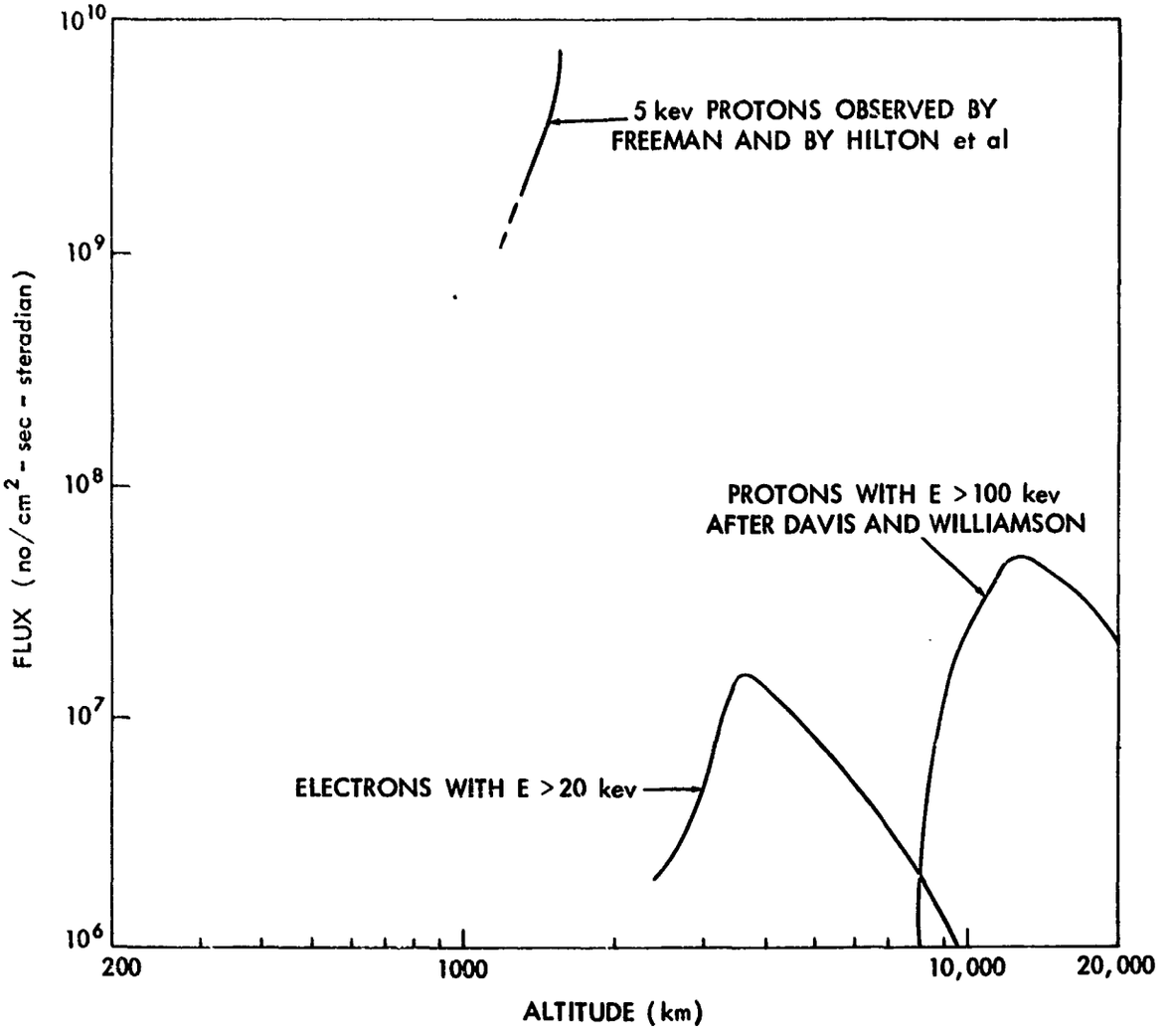

Figure 29. Typical Energetic Particle Fluxes in the Earth's Magnetic Equatorial Plane

More significant are the outer zone protons with energies above 100 KeV described by Davis and Williamson.[108] They found an exponential energy spectrum with a scale factor of 400 KeV at the altitudes shown. An integration of the secondary electron yields of Figure 13 over this energy spectrum results in an effective yield of 2.25 for these protons incident on aluminum, and 1.34 for incidence on tungsten. The effect of these protons on the equilibrium potential is shown above 10,000 km for the case of an aluminum surface in darkness. A body with a tungsten surface would have a potential between the two curves. In the sunlight the effective "Q_+" due to these protons is at most less than 4% of the value of Q due to photoemission.

It is emphasized that these choices of fluxes of energetic particles are illustrative only. In reality the fluxes vary widely not only in time but also as one moves away from the magnetic equator. This discussion is primarily for the purpose of demonstrating that the energetic particles trapped in the earth's magnetic field can have a significant effect on the equilibrium potential of a body.

3. Expected Equilibrium Potentials in the Earth's Magnetosphere and in Interplanetary Space. The earth's magnetosphere may be defined as that region of space where the motion of charged particles is controlled by the earth's magnetic field. It is characterized by a relatively hot ionized gas with a temperature from a few thousand to 50,000°K, and by large fluxes of energetic electrons.[109,110] There is a well defined outer boundary to the magnetosphere which is quite analogous to the hydrodynamic description of the supersonic flow at a fluid around a blunt object. In this case the blunt object is the magnetic field and the fluid is the expanding ion and electron gas coming from the solar corona,

aptly called the solar wind. At the magnetosphere boundary (magnetopau e) there is a sharp drop in the magnetic field, a narrow transition region, and then a shock-front caused by the solar wind impact. Interplanetary space is characterized by the solar wind streaming radially outwards from the sun at velocities from 300 to 10^3 km/sec, and with densities of 5 to 20 ions/cm^3.[111,112]

The calculation of equilibrium potentials in both these regions is considerably simplified by the fact that the effect of low energy ions may be usually disregarded. Within the magnetosphere the flux of energetic (> 30eV) electrons is apparently usually larger than the total positive ion flux – at least at distances beyond about six earth radii from the earth's center. Consequently, the equilibrium potential of a body in the magnetosphere will be determined by a balance between the effects of photoemission and incident electrons only.

Another simplification is the fact that the low particle densities and high temperatures result in a large value for the Debye length – typically 2 meters or larger. Therefore, it is not a bad approximation to use the small body equations for bodies as large, even, as typical spacecraft. Finally, because of both the negligible effect of low energy ions and the relatively low velocities of bodies in these regions with respect to the electron thermal velocity, the body may be regarded to be at rest.

The equilibrium potential in the magnetosphere is very sensitive to the ratio of energetic electron flux to photoemission flux. For a negative body we find

$$\phi = \frac{kT_-}{e} \ln \left\{ \left[\frac{\sqrt{\pi}\, J_p}{2n\, e\alpha_-} \right] \left[1 - \frac{J_-}{J_p} (1 - Y_-) \right] \right\} \qquad (7.9)$$

as long as

$$\frac{J_-}{J_p}(1 - Y_-) < 1 < \frac{J_-}{J_p}(1 - Y_-) + \frac{2n e \alpha_-}{\sqrt{\pi}\, J_p}$$

When the energetic electron flux dominates photoemission the potential may rise to a very high negative value – to a potential characteristic of the energetic electrons. In this case the low energy positive ions should be included in the calculation. However, this is not a very likely possibility for bodies with metallic surfaces. Maximum observed energetic electron fluxes are on the order of $10^9/cm^2$-sec, yielding a current of $\sim 10^{-10}$ amp/cm^2, which is smaller than expected photoemission currents.[110] In addition, these large fluxes were for electrons in the 200 eV to 40 KeV energy range, so that secondary emission is likely to be significant in reducing the efficiency of those electrons.

When the right hand side of this inequality is violated the body will become positive:

$$\frac{\phi e}{kT_-} = \frac{\sqrt{\pi}\, J_p}{2n e \alpha_-} \left\{ f_1(\phi) - \sum_i \frac{J_i}{J_p} [1 - Y_i f_2(\phi)] \right\} - 1 \qquad (7.10)$$

Solutions to (7.10) are shown in Figure 30 for an electron energy spectrum with two peaks: One at an energy ($\sim$500 eV) such that the secondary yield is unity, and one at a higher energy where the yield is 0.3. The potential is limited to a few volts positive as the photo- and secondary electrons are returned to the body. It was found that when the ratio J_0/J_p, corresponding to the higher energy flux, exceeded 0.14, the potential did not exceed +1 volt for the values of J_1/J_p shown in the figure.

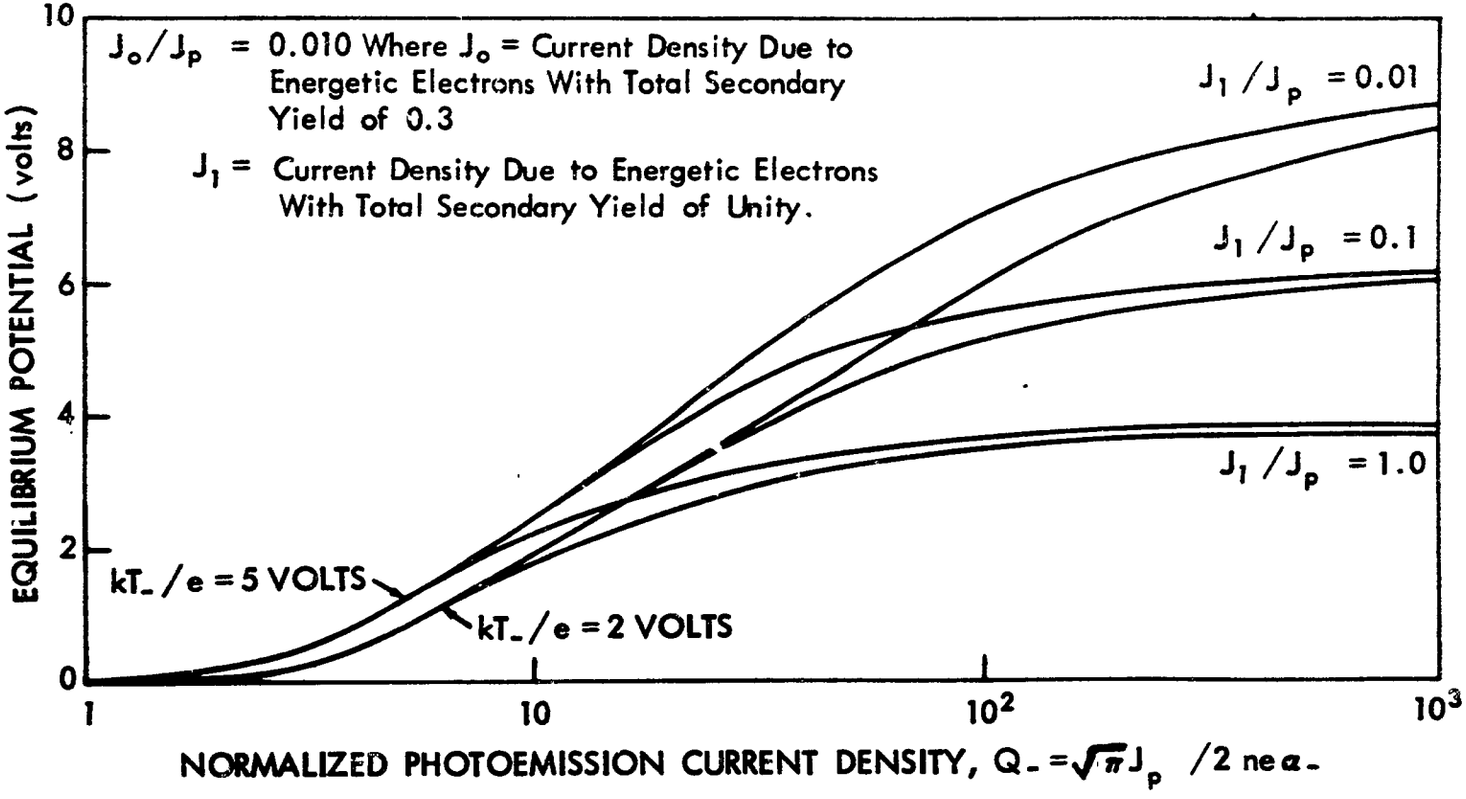

Figure 30. Positive Equilibrium Potentials for a Body in the Magnetosphere

In interplanetary space the protons in the solar wind should be taken into account, although they contribute only about 10^{-10} amp/cm^2, a factor of 10 less than photoemission. However, their effectiveness is not reduced much at positive potentials as is the case for photoemission. Electrons in the solar wind apparently have two distinct energies – one from 3-5eV with densities equal to the proton density, and a higher temperature group (20-50eV) with an order of magnitude smaller density.[113] The equilibrium negative potential is

$$\phi = \frac{kT_-}{e} \ln \left\{ \frac{\sqrt{\pi}}{2n e \alpha_-} \left[J_+ (1 + Y_+) + J_p \right] \right\} \qquad (7.4)$$

The low temperature values for T_-, n_-, α_- should be used as long as the potential is not so negative that the flux of low temperature electrons has been reduced to a value less than that of the more energetic group. When this does occur the values for T_-, n_-, α_- should be that of the more energetic electrons.

In general one would expect a positive equilibrium potential in interplanetary space unless the material of the body is such that photoemission is unimportant. Solutions of the following equation:

$$\frac{\phi e}{kT_-} = \frac{\sqrt{\pi}\, J_p}{2n_- e \alpha_-} \left\{ f_1(\phi) + \frac{J_+}{J_p} \left[1 + Y_+ f_2(\phi) \right] \right\} - 1 \qquad (7.12)$$

are shown in Figure 31 for values of potential between 0 and +20 volts. The secondary yield has been neglected for proton energies less than 1 KeV, and has been taken to be 2.0 for the 3KeV protons. The latter energy is expected only occasionally, as after large solar flares. Typical values for Q_- and J_+/J_p are 10 to 100 and 10^{-1} to 1 respectively.

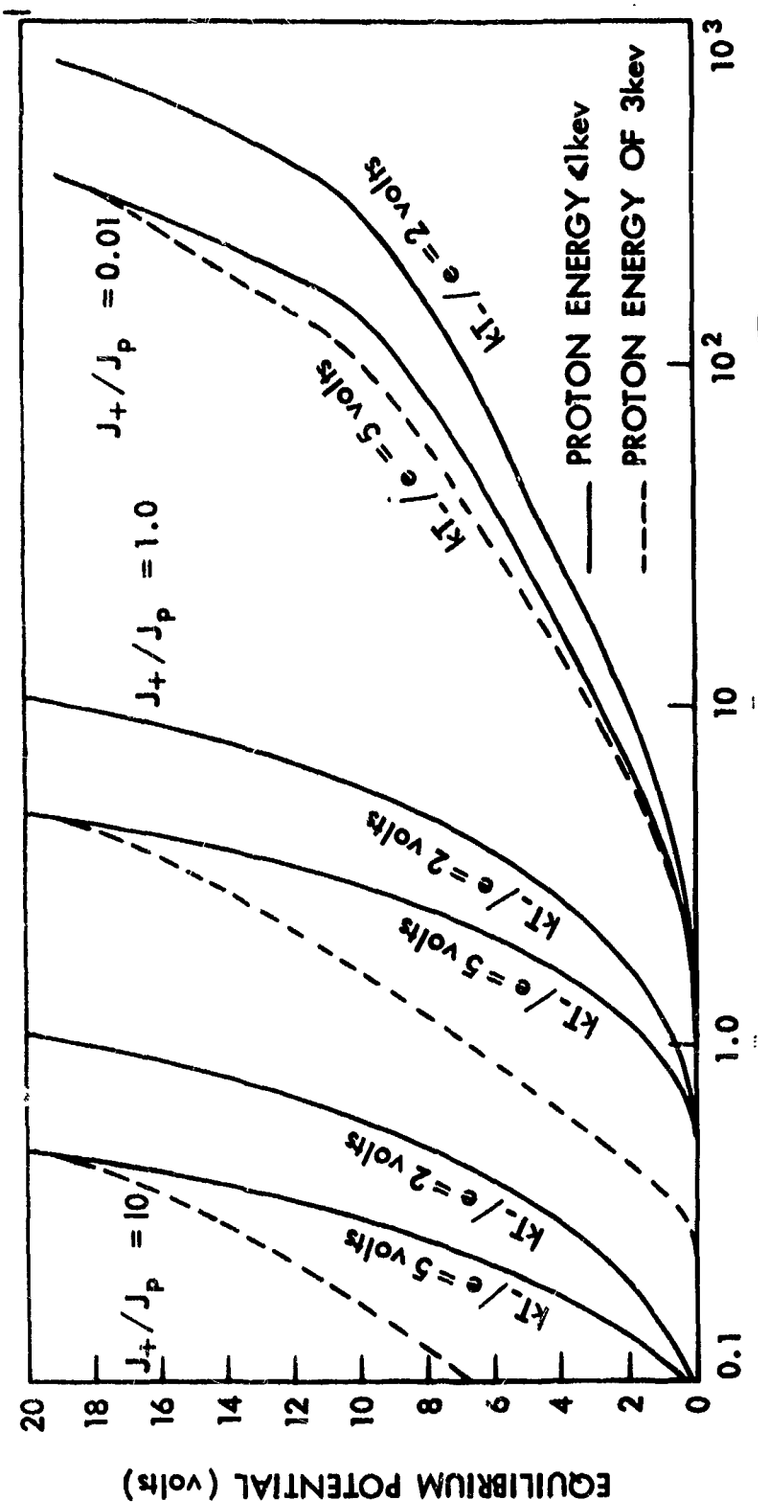

Figure 31. Positive Equilibrium Potentials for a Body in Interplanetary Space

It is apparent that a considerable positive potential could develop. Once +20 volts is exceeded the secondary electrons cannot escape, and the equilibrium potential is simply

$$\frac{\phi e}{kT_-} = \frac{\sqrt{\pi}\, J_+}{2n\, e\, \alpha_-} - 1. \qquad (7.13)$$

BLANK PAGE

CHAPTER VIII

EQUILIBRIUM POTENTIALS MEASURED ON THE EXPLORER VIII SATELLITE

1. Description of Experiment. The Explorer VIII Satellite was launched on November 3, 1960, from Cape Canaveral, Florida, into an orbit with an inclination to the equator of 50°, a perigee of 420 km and an apogee of 2300 km. Its primary mission was the direct measurements of electron density and temperature, positive ion concentration and mass, and the interaction between the vehicle and the ionized atmosphere. To accomplish this mission the following experiments were flown: three current monitors were situated on the satellite equator, two consisting of single-grid charged particle traps appropriately biased to measure positive ion and electron current densities, and one consisting of an exposed plate to monitor the total net current. Two electron traps to measure electron density and temperature were mounted on the top cone of the satellite (see Figure 32); and one ion trap to measure positive ion density, temperature and mass was also mounted on the equator. In addition, there was an electric field meter mounted on the top surface and a radio-frequency plasma impedance probe consisting of two 10 foot wires extending outward from the equator along opposite radii. In addition to the preceding experiments, there were also two micrometeorite experiments and an attitude sensing system consisting of a solar cell and a horizon sensor, both mounted on the equator.

The data from the experiments were sent by a 108 Mc telemetry system to any of the eleven NASA ground stations within range when

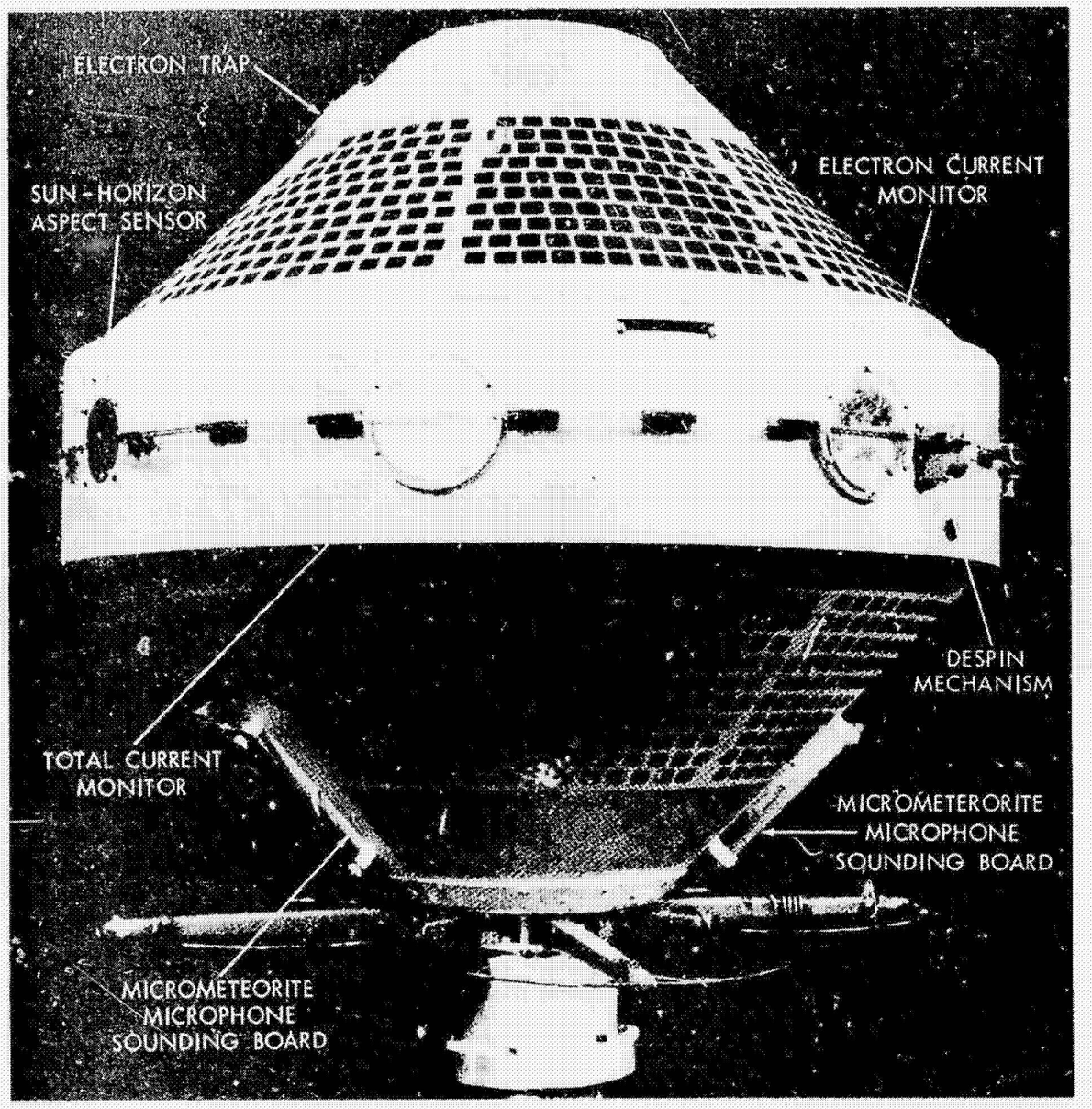

Figure 32. Explorer VIII Satellite, Showing Component Locations

the data were obtained. All the instrumentation operated continously except the electric field meter which was turned on for two minute periods by radio command from the ground.

The shell of the satellite was made of aluminum and consisted of two truncated cones joined at the equator by a short cylinder 30 inches in diameter and 6-1/8 inches high. The axis of the satellite was also 30 inches long, including the 3-inch cylinder at the bottom used for connection to the booster. The total exposed surface area was 2750 in^2, which yields an effective radius for an equivalent sphere of 14.8 inches.

Shortly after launch the satellite was "de-spun" to a spin-rate of approximately 20 rpm. The celestial co-ordinates of the positive spin-axis remained in the region of zero degrees declination and 180° right ascension during the satellite's useful life of five weeks. The data from the horizon sensor proved to be difficult to analyze, with the result that there was an uncertainty of about ±15° in the spin-axis co-ordinates. The angle between the spin axis and the sun was known to remain close to 60°.

A more detailed description of the satellite and the instrumentation is available elsewhere.[114] Some of the results of the experiments which have been reported are measurements of the sheath currents, including the first experimental verification of the induced potential gradient due to the satellite's motion in the earth's magnetic field;[40] the first direct detection of helium ions in the earth's upper atmosphere;[115] and the diurnal variation of temperature in the upper atmosphere.[116]

This investigation is concerned only with the results obtained from the single-grid electron trap. A block diagram of the experiment is shown in Figure 33. The sensor consists of a grid flush with the satellite skin with a sweep potential varying from -1.2 to +8 volts and back in 0.4

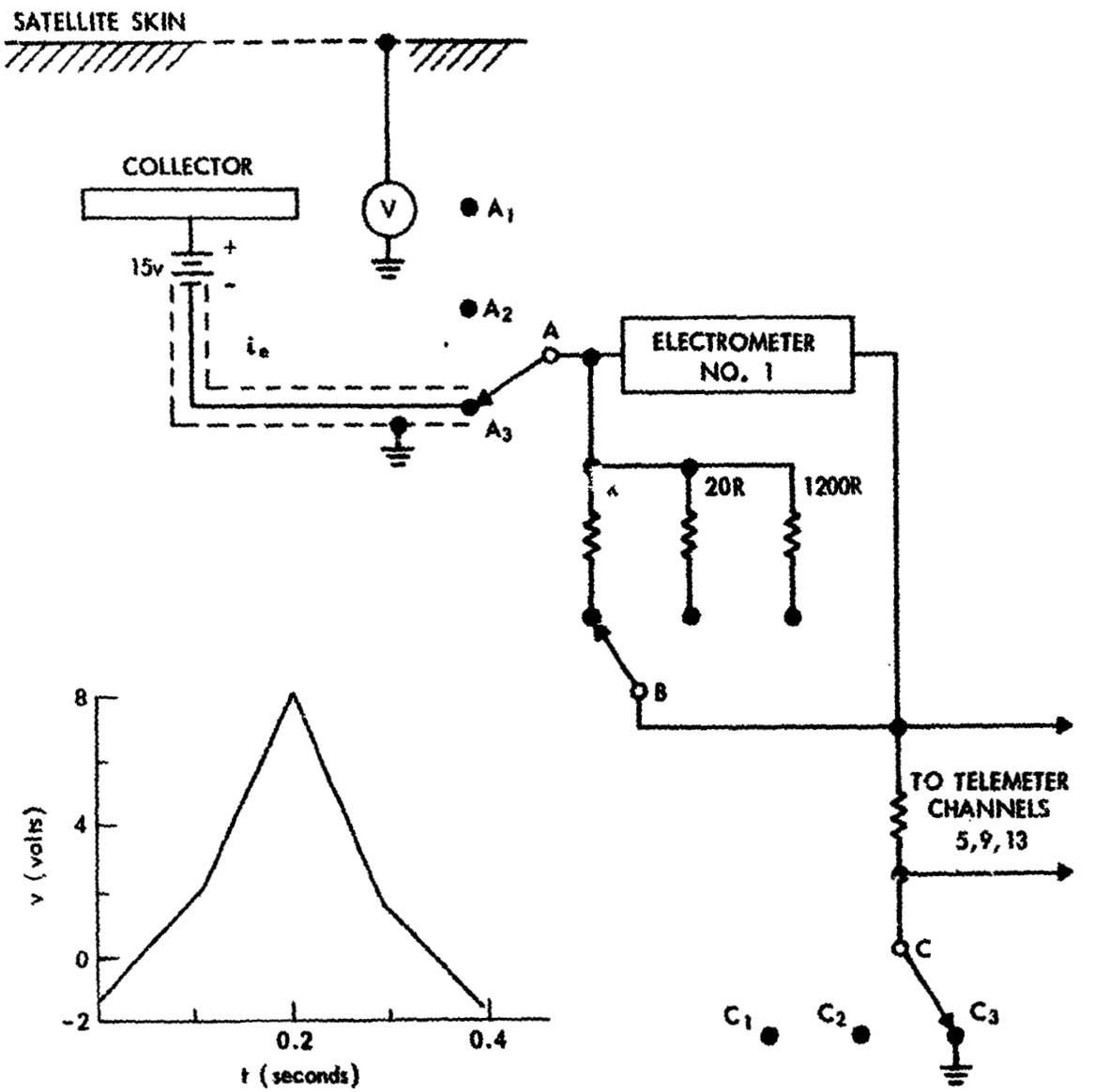

Figure 33. Block Diagram of the Electron Trap on Explorer VIII

sec as shown in the figure inset. Behind this grid is a collector biased at +15 volts to remove photoemission and incoming ion current from the measured collector current. The electrometer employed 100% negative feedback to maintain stability against drift and to keep the collector at a constant potential independent of the measured current. It was time-shared with the ion current monitor and the ion trap, each experiment being connected for a 30 second period consisting of three 10-second intervals on each of three electrometer ranges. Currents from 10^{-9} amp to 5×10^{-5} amp could be measured.

The principle of the experiment is as follows: as long as the grid is negative with respect to the plasma, the current decreases exponentially with voltage in accordance with Equation (3.2). The slope of the straight line obtained when the logarithm of the current is plotted against potential is determined by the electron temperature:

$$\frac{d(\ln I)}{dV} = \frac{e}{kT} \tag{8.1}$$

When the grid is positive with respect to the plasma, electrons are attracted and the current increases at a slower rate which depends on the geometry as well as the electron temperature. The potential V_s at which this change in character of the electron current occurs identifies the time when the grid was at the same potential as the plasma. Since the measured potential is with respect to the satellite, we identify ϕ_s, the satellite potential with respect to the plasma, as $-V_s$. The electron density may be simply computed from the current at that point by the relation

$$(I)_{V=V_s} = neAt \left(\frac{kT_-}{2\pi m}\right)^{1/2} \tag{8.2}$$

where t is the electrical transparency of the grid (53%), and A is the aperture area of 13.0 cm .

Theoretically it should also be possible to obtain the satellite potential from the shape of the current versus voltage curve obtained from the ion trap.[117] Actually, this proved to be quite difficult because of the strong dependence of the current on the angle between the normal to the trap and the satellite velocity vector.

2. Experimental Results. Figure 34 shows a typical current-voltage curve obtained with the electron trap. The circled points were obtained with the electrometer in the medium sensitivity range and the crosses with the high sensitivity range. In this case the data from the two ranges was obtained 1.5 seconds or one half of a spin period apart. In general, the data was chosen to be either a full period apart or very close together on either side of the range switching, although this was not always possible. Successive points are separated in time by about 0.010 seconds. The currents below about 2×10^{-8} amp were corrected for a displacement current effect due to the changing voltage on the grid.

The characteristically linear portion of the curve on this semi-log plot with a distinct change in slope at 5.2×10^{-7} amp is plainly apparent. The following procedure was used to compute the temperature, density and satellite potential: All currents greater than 1% of full scale on the low and medium sensitivity ranges and 10% of full scale on the high sensitivity ranges, but less than the apparent break-point in the slope, were fitted to a straight line by a least-squares calculation. This line was plotted and the fit to the data was examined at and above the break-point to see if points there should be added or subtracted. Then a new least-squares calculation was made with the new set of points. This process was repeated until there was no question that the best possible

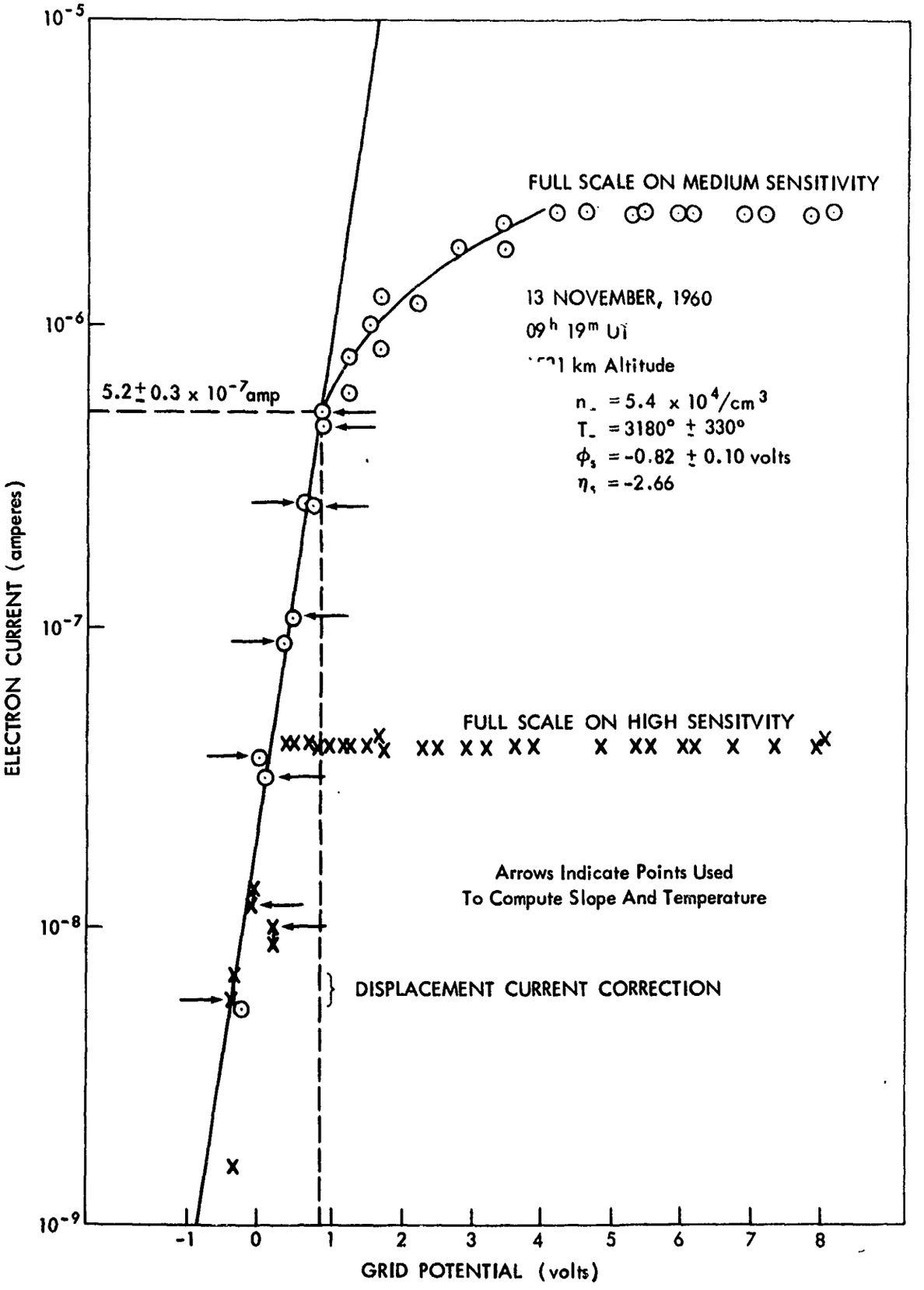

Figure 34. Typical Current-Voltage Curve Obtained with the Electron Trap

estimate of slope and break-point had been obtained. The density, satellite potential and electron temperature with its standard deviation were then computed from Equations (8.1) and (8.2).

This procedure was used to compute densities, temperatures and satellite potentials from some 250 current-voltage curves. The temperatures and densities obtained on magnetically quiet days (according to the Committee on Characterization of Magnetic Disturbances[118,119]) are presented in Figures 35 and 36. The satellite potentials are presented in Figures 37 through 39. The data has been separated according to magnetic activity because there was a significant difference in the results between magnetically quiet, medium or disturbed conditions. During a given condition, however, there was no significant difference between results on different days that was not obscured by the experimental scatter.

It is reasonable to expect atmospheric conditions to stay reasonably stable from day to day over the Explorer VIII orbit for a given condition, because of the fact that the local mean time was practically a fixed function of position in the orbit. Thus, diurnal variations would not appear explicitly but would be folded into the variation with altitude in the same way from orbit to orbit. This feature of the orbit is of course due to the fact that the plane of the orbit is fixed in inertial space and consequently rotates quite slowly (one degree per day) with respect to the sun. The local mean time shown in Figures 35-39 is for November 20, and is good to within about ±1 hour over the active life of approximately one month.

For these reasons, plus a consideration of the sources of error in the measurements, if is felt that the scatter in the data is primarily experimental rather than a reflection of real geophysical

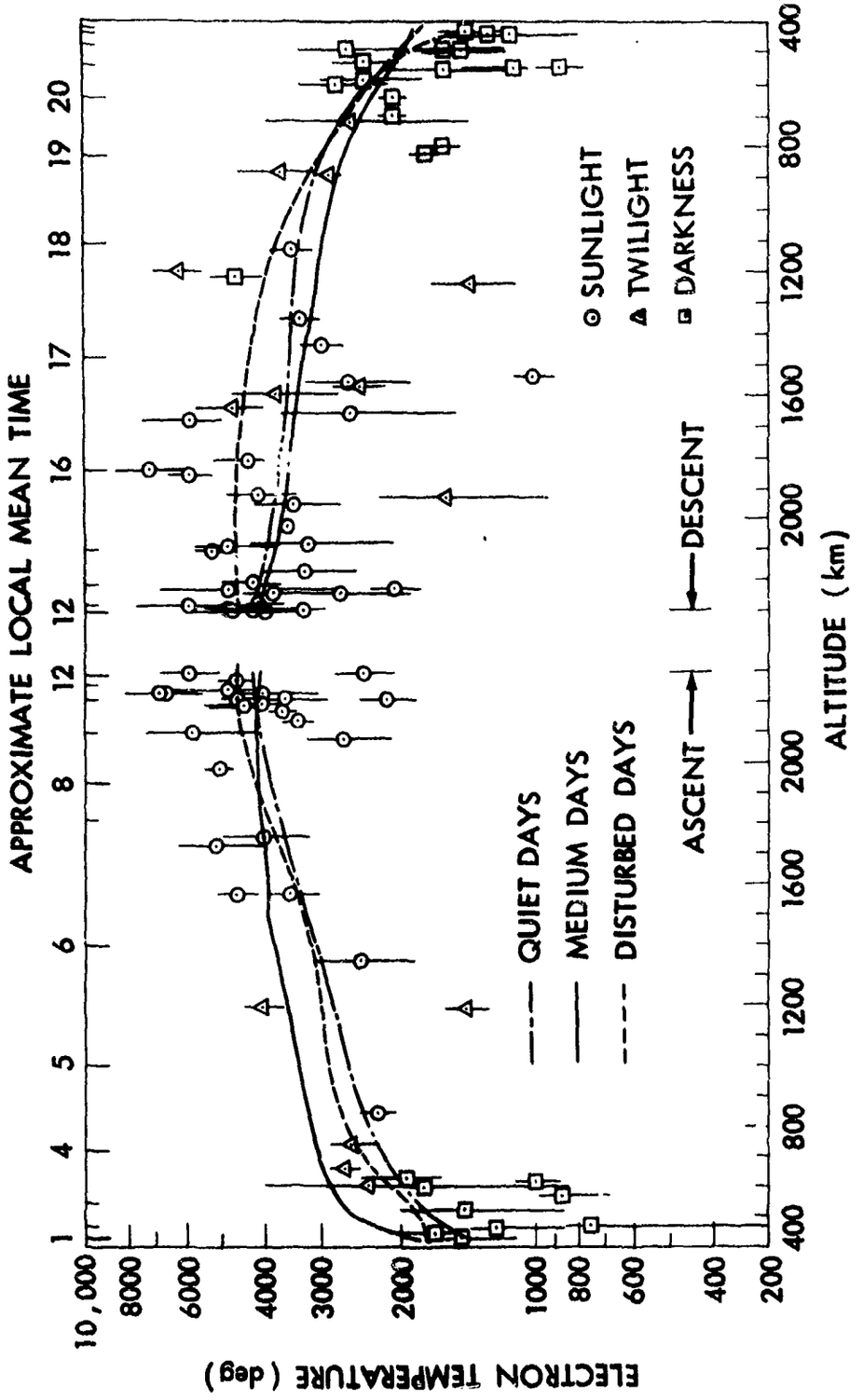

Figure 35. Measured Electron Temperatures for Magnetically Quiet Days; Lines Indicate Mean Values Used in Calculations

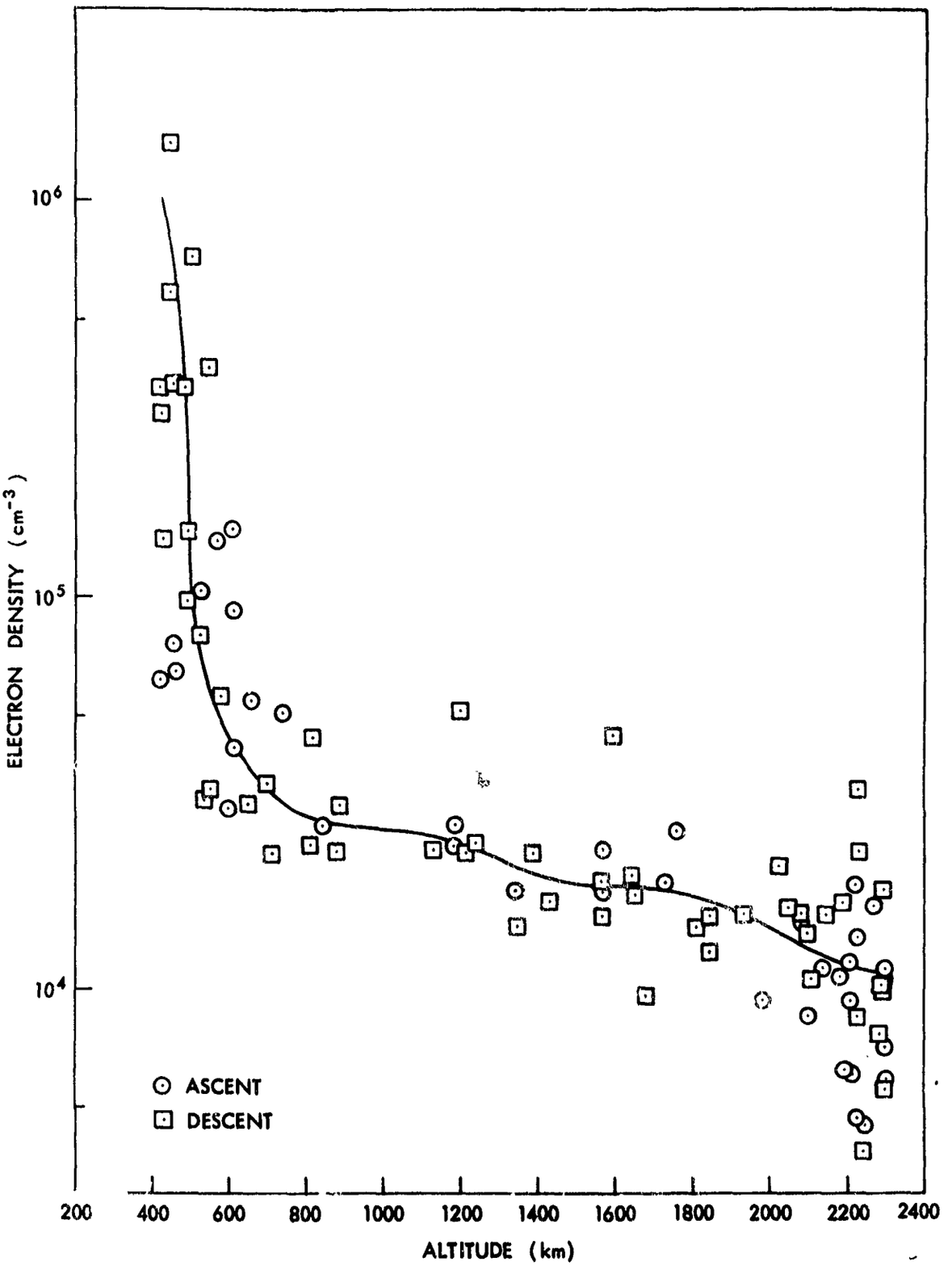

Figure 36. Measured Electron Densities for Magnetically Quiet Days; Line Indicates Values Used in Calculations

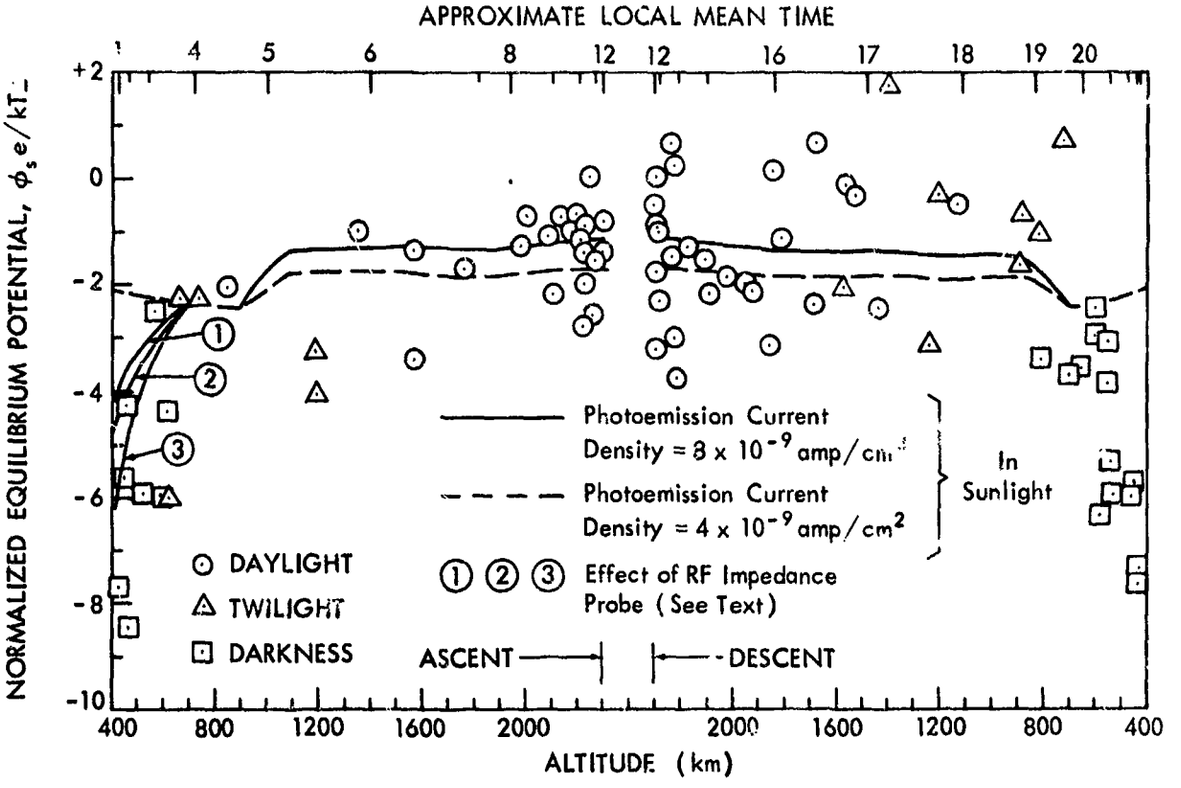

Figure 37. Measured and Calculated Equilibrium Potentials for Explorer VIII on Magnetically Quiet Days

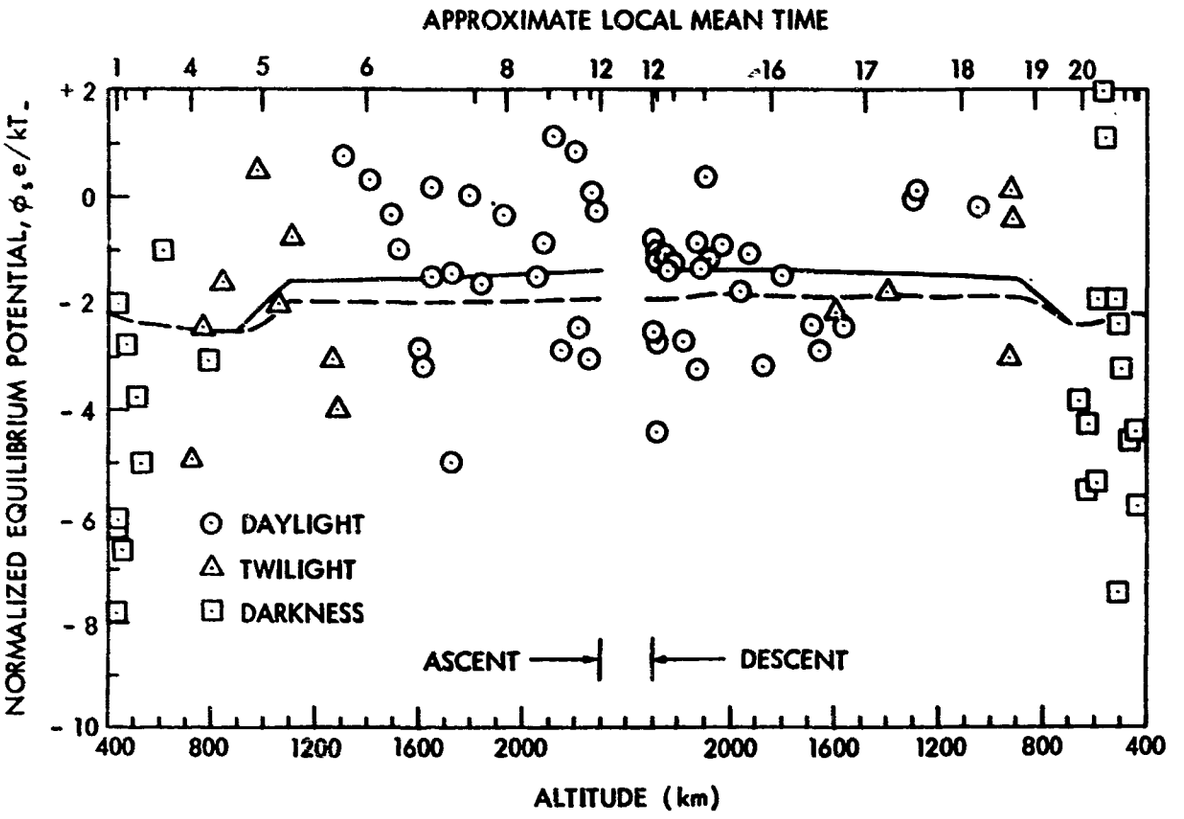

Figure 38. Measured and Calculated Equilibrium Potentials for Explorer VIII on Moderately Magnetically Active Days

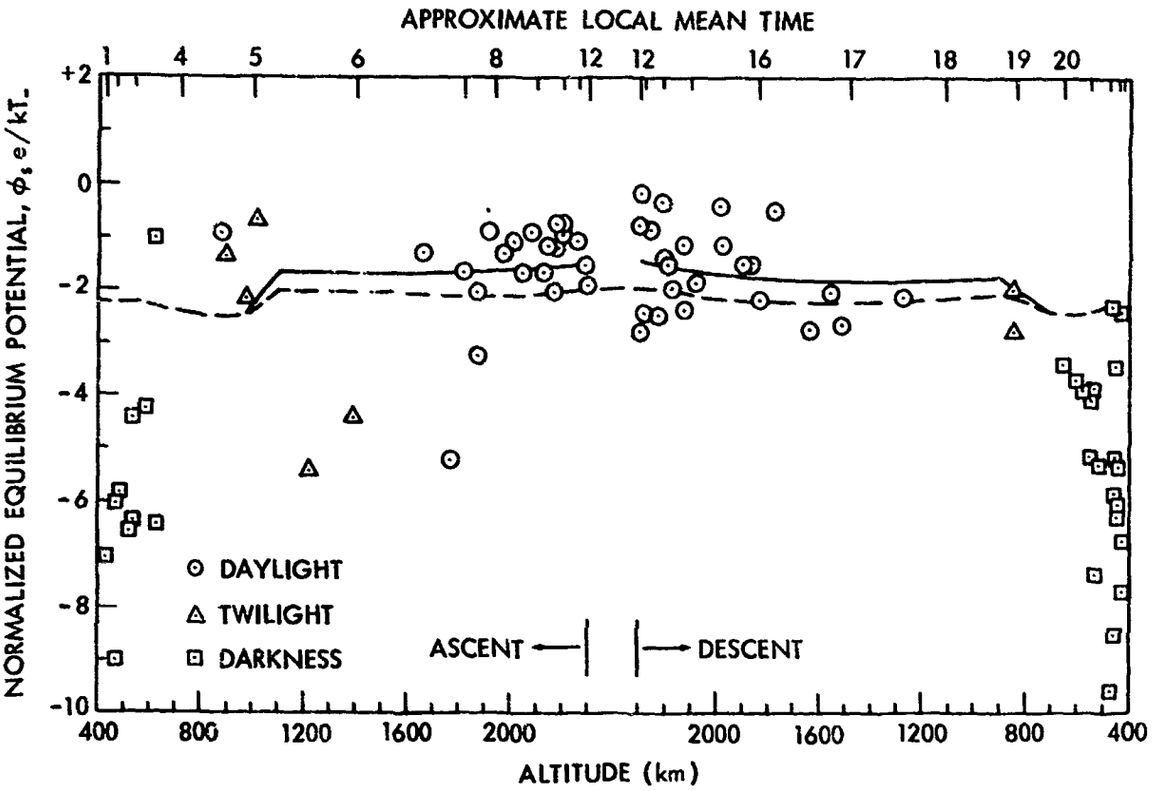

Figure 39. Measured and Calculated Equilibrium Potentials for Explorer VIII on Magnetically Disturbed Days

variations. The typical standard deviation for the measured temperature was about 25% rather than the 11% of Figure 34. The measured satellite potential is in turn very sensitive to the measured slope of the current-voltage curve which determines the position of the break. The absolute value of the grid voltage is known within an uncertainty of about ±0.08 volts. This uncertainty affects the determination of ϕ_s more strongly than it affects the determination of the temperature where only the relative voltage is needed.

The uncertainty in the measured currents is about 1% of full scale for the low and medium sensitivity ranges and 10% for the high sensitivity ranges, as indicated previously. The computed density reflects not only this uncertainty but also the uncertainties in the temperature and in the determination of the break-point.

Before the measured satellite potentials can be compared with theoretical values, the dimensionless potential $\eta_s = \phi_s e/kT$ must be computed. The relative error in η_s is the sum of the relative errors in ϕ_s and T. Consequently, it was decided that a useful comparison of the measured satellite potentials with theoretical values could best be done by using a smooth curve of temperature and density over the orbit to compute the expected potentials. This way the non-systematic discrepancies between the measured and predicted values reflect primarily the scatter in the measured ϕ_s alone. The smoothed temperatures representing a running mean for the three magnetic conditions are shown in Figure 35. These were used both in the theoretical calculation of η and in the normalization of the measured ϕ_s. Only the electron density data for the magnetically quiet days is shown in Figure 36.

The following expression was used to compute the expected values for η :

$$\frac{(1-\delta)}{8}\sqrt{\frac{m_+}{m_-}}\left[e^{\eta}+\left\{\begin{matrix}(L/R)^2\\ \text{or}\\ e^{\eta}\end{matrix}\right\}\right]\left(\frac{\sinh p}{p}\right)\ F(R/\rho^*)$$

$$-\frac{A_v}{A_T}\frac{\sqrt{\pi}}{2}M(1+Y)\left(1+\frac{2t(\eta)}{R}\right)\left[\left(1+\frac{1}{2M^2}\right)\text{erf}\,M+\frac{e^{-M^2}}{\sqrt{\pi}M}\right]=\frac{A_s\sqrt{\pi}\ Jp}{A_T 2n\ e\alpha_+} \qquad (8.3)$$

In this expression δ and Y are the reflection coefficient and secondary yield for electrons and oxygen ions respectively. Bauer has shown that for the high temperatures found here, oxygen ions will be predominant over the whole orbit.[101] L is the Debye length and R the effective radius of the satellite of 0.37 meters. The quantity $(L/R)^2$ is used in accordance with the discussion in Section 3.4 on the effect of the wake. The term containing p represents the magnetic induction effect of Equation (6.3), and $F(R/\rho^*)$ is the ordinate of Figure 17. The cross product of $\vec{V}$ and $\vec{B}$ is a fixed function of position in the orbit if it is assumed that the earth's magnetic field is a dipole with an axis along the earth's geographic axis. M is the Mach number, V/α_+ ; $t(\eta)$ the sheath thickness after Equation (A13) of the appendix; and A_T , A_s , A_v , are the total area and the projected areas in the direction of the sun and velocity vector respectively. It has been assumed that the ion temperature is equal to the electron temperature.

The results of the computations are shown by the lines in Figures 37 through 39. The dashed curve is for a photoemission current density, Jp, of 4×10^{-9} amp/cm^2 and the solid curve for 8×10^{-9} amp/cm^2.

There is reasonable agreement at the higher altitudes between the curves and the data points, particularly with the higher photoemission current value. A systematic overestimate of the electron density has the same effect on the predicted potential as an underestimate of photoemission. This is a more likely explanation of the better fit of the solid than the dashed line. For the disturbed days an even higher values for (J_p/n) is indicated.

Below 700 km the measured values of η are much more negative than is expected. The change in potential due to passage from sunlight to darkness is reflected by the change in the curves between 900 and 1100 km on ascent and 900 and 700 km on descent, and is not of sufficient magnitude to be an explanation.

It is suggested that the more negative potentials at low altitudes are caused by the rf impedance probe experiment on the satellite. This probe, consisting of the two 10-foot wires described previously, was operated continuously at a frequency of 6.5 Mc. The amplitude of the rf voltage was about 0.3 volts. At high altitudes where the electron density is low, the local plasma frequency is much lower than 6.5 Mc. Consequently, the additional current to the probe due to the rf is negligible, as is discussed in Section 5.7. As the satellite descends in altitude, the plasma frequency increases;

$$f_p = \frac{1}{2\pi}\sqrt{\frac{Ne^2}{m_- \epsilon_0}} \qquad (8.4)$$

and as the satellite approaches perigee, the plasma frequency will in general go through the probe frequency. For example, the electron density of $10^6/cm^3$ occurring at 425 km in Figure 36 corresponds to a plasma frequency of 9 Mc. Therefore, a very large increase in electron

current to the probe results as the probe frequency goes through the resonant frequency, which drives the whole satellite to a more negative potential.

To put this suggestion on a quantitative basis, it is necessary to know the value of the current at the resonant peak and the resonant frequency, which is generally somewhat lower than the plasma frequency. Whale has shown that resonance occurs for a cylindrical dipole antenna at $f_p/\sqrt{2}$, which yields a resonant frequency of 6.34 Mc for the density of 10^6 electrons/cm^3 at 425 km.[120] At these altitudes the resonant peak height is determined by a phase-mixing damping rather than collisional damping.

This mechanism has not yet been studied extensively, but Crawford has suggested that the ratio $(\Delta i/i_0)_{peak}$ to $(\Delta i/i_0)_{f<<f_p}$ is probably between 5 and 100 under these conditions in the ionosphere.[121] Figure 40 illustrates the additional current to a probe as a function of f/f_p. This curve was computed from Equation (19) of Harp and Crawford[94] with an assumed collision frequency to give a peak current ratio of 20. The resonant frequency here is at 0.68 f_p.

At 425 km for the quiet model, where $n_e = 1 \times 10^6$ /cm^3, the increased current to the probe at f/f_p = (6.5/9.0) Mc = 0.72 is $\Delta i = 39\, i_0$, where i_0 is the current to the probe with no rf. When this added electron current is taken into account in the left-hand side of (8.3), the new equilibrium potential, $(\phi_e e/kT)$, is -4.16 rather than -2.1. This potential is indicated by the curve marked (1) in Figure 37. The value of $\Delta i/i_0$ necessary at 500 km to give the indicated potential of -3.3 is 11.9 where f/f_p is approximately 1.6.

It should be emphasized again that the shape of the resonance curve in Figure 40 is based on the collisional damping model, which does not

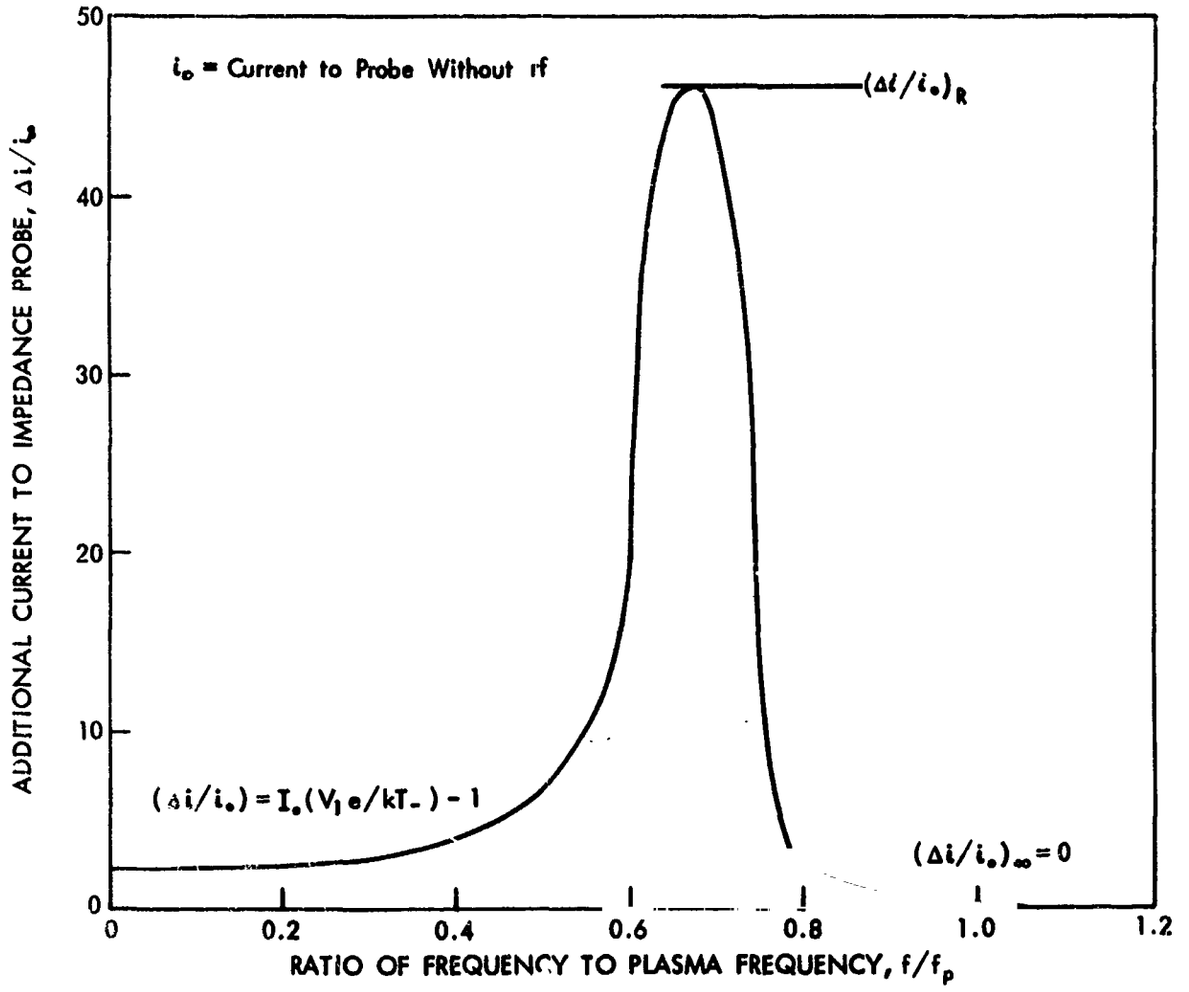

Figure 40. The Response of a Radio-Frequency Probe in a Plasma

apply at these altitudes in the ionosphere. There is evidence from some resonance probes flown by Japanese experimenters that the resonance peak in the ionosphere is much broader.[122] This is also indicated by the Explorer VIII potential data. In general, the potential begins to go more negative between 500 and 600 km where the electron density is near 10^5 /cm^3 rather than 10^6 /cm^3, and hence $f/f_p \cong 2.3$. However, the fact that this effect depends so strongly upon the electron density means that the smoothed model for the density in the computations will not reproduce the measured potentials closely.

The curves marked (2) and (3) have been computed by assuming that at 425 km the probe frequency is at the resonant frequency. The ratios of $(\Delta i/i_0)_{pk}$ to $(\Delta i/i_0)_0$ have been assumed to be 28.5 and 144 respectively, giving values for $(\phi_s e/kT)$ of -4.59 and -6.12. The corresponding values for the current ratio at 500 km are 13 and 27.

These calculations show that the current resonance effect as the plasma frequency approaches the probe frequency can quantitatively account for the negative potentials observed near Explorer VIII perigee. It is necessary that the resonant peak be broader than what has been observed in laboratory work; but following the indications of the Japanese experiments, it is suggested that the resonant effect is broader at low neutral particle densities where collisional damping does not occur.

3. Conclusions. Two major conclusions may be drawn from these results. The first is that there is general agreement between the predicted values of equilibrium potential and the measured values. Therefore, the various mechanism of charge collection that have been discussed have been evaluated correctly as far as their importance for Explorer VIII is concerned. Further, no important mechanisms have been omitted.

The second conclusion is that much more experimental work remains to be done. An order of magnitude improvement in the accuracy of satellite potential measurement is required. And to evaluate the several charge collection mechanisms, precise measurements of the environmental plasma properties are required simultaneously. If further experimental study of satellite potential is warranted, it should preferably be a satellite designed primarily to that end. This way both the surface characteristics and the geometry of the satellite may be designed with their effect on equilibrium potential in mind. Any feasible experiments that will contribute to an understanding of the potential should be included, and they should be carefully designed so that any effects they might have on the potential themselves can be controlled.

Several areas of further laboratory investigation are also indicated by this study. Much work needs to be done on photoemission yields of materials in the ultra-violet wavelengths. The yields of aluminum especially need to be verified for various surface conditions. Magnesium should be investigated, and also dielectric materials such as mylar that are often used on satellite surfaces. Work is also needed on the secondary yields for ion impacts, especially in the energy range from 1 to 10 KeV.

The theory presented in Chapter VI on the effect of a magnetic field on the collection of electrons is a subject that could easily be pursued in the laboratory, although the extension to the case where electric fields are present will undoubtedly be very difficult.

Finally, the radio-frequency resonance phenomenon at low pressures needs study both experimentally and theoretically. It may be that the best place to pursue this experimentally would be from a satellite where wall-effects can be avoided, and where probes large compared to the Debye length can be employed.

APPENDIX A

ION CURRENT TO A NEGATIVELY-CHARGED MOVING SPHERE

Poisson's equation in spherical coordinates with the space charge given by Equation (3.15) may be written

$$\frac{d^2y}{dx^2} + \frac{2}{x}\frac{dy}{dx} = 1 - e^{-y} \tag{A1}$$

where y is the normalized potential,

$$y = -\frac{\phi e}{kT_-} \tag{A2}$$

and x the radial distance normalized to the Debye length.

Solutions to this equation subject to the boundary condition that $y \to 0$ as $x \to \infty$ are plotted in Figure A1. It should be noted that the solution corresponding to any interior boundary condition defined by the pair of values (x_0, y_0), the potential o the sphere of radius r_0, is described external to x_0 by the single curve on which x_0, y_0 lie.

The approximation made in assuming Equation (3.15) for the space charge is that the ion density is undisturbed, and only the electrons respond to the field in accordance with the Boltzmann factor. Thus, this equation applies to the case where the body's speed is much larger than the ion thermal velocity. In the satellite coordinate system the ions are approaching with uniform speed from one direction. All those with impact parameters less than a certain value will be collected. Walker in his thesis[38] has shown that is is possible to compute this impact parameter from consideration of the conservation of energy and angular momentum without actually obtaining the particle trajectories.

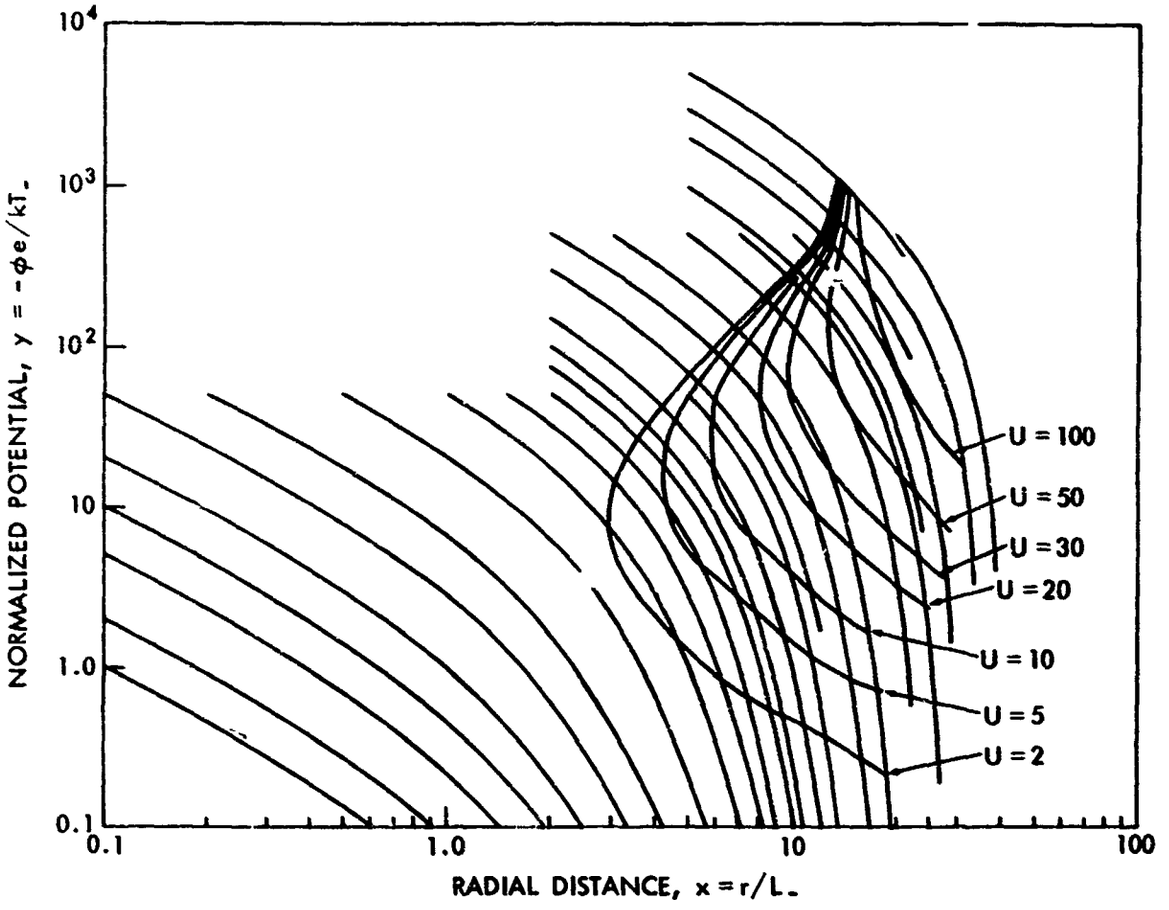

Figure A1. The Potential in Front of a Negatively-Charged Moving Sphere; Contours of the Minimum Distance of Closest Approach are also Shown for Various Ion Energies

Following his discussion, but generalizing to any functional form for the potential (as long as it decreases monotonically), rather than restricting ourselves to a power law as he does, we define the pitch angle α as the angle between the particle velocity vector and the radius vector. The pitch angle at any point for a particle with impact parameter b and initial velocity V is given by

$$\sin \alpha = \frac{b}{r\sqrt{1 - \frac{2\phi e}{mV^2}}} \tag{A3}$$

where ϕ is the value of the potential at the point r.

We divide all trajectories into two classes: periastron trajectories are followed by particles which would have (if there were no absorbing surface) a distance of closest approach, r_{min}, corresponding to the value of r where $\alpha = \pi/2$. Pericritical trajectories are orbits which spiral in towards the origin with α never reaching $\pi/2$. Such trajectories can only exist if the potential falls off more strongly than r^{-2}. This can be seen from Equation (A3) where sin α always increases as r decreases along a trajectory unless ϕ falls off faster than r^{-2}. In this case sin α may have a maximum value less than $\pi/2$.

For a given initial kinetic energy, ions with large b will always describe periastron orbits. If pericritical orbits exist then there will be some minimum impact parameter for which α may equal $\pi/2$. Alternately, there is some <u>minimum</u> distance of closest approach, r_e, at which a particle may arrive and still escape. To find this we differentiate

$$b = r_{min}\sqrt{1 - \frac{2\phi(r_{min})\, e}{mV^2}} \tag{A4}$$

with respect to r_{min}, and find that r_c is defined by the point where

$$\phi(r) + \frac{r}{2}\left(\frac{d\phi}{dr}\right) = + \frac{mV^2}{2e} \qquad (A5)$$

Since $1/2\ mV^2 = 1/2\ mv^2 + \phi e$, this equation describes the surface where the centripetal acceleration is equal to the centrifugal force per unit mass, and it is clear why particles that cross the surface r_c will be accelerated towards the origin.

The corresponding critical impact parameter, b_c, which divides periastron from pericritical trajectories is given by

$$b_c = r_c\sqrt{1 - \frac{2\phi(r_c)e}{mV^2}} = r_c\sqrt{\frac{r_c e}{mV^2}\left(\frac{d\phi}{dr}\right)_c}$$

or

$$x_{bc} = x_c\sqrt{-\frac{x_c}{2u}\left(\frac{dy}{dx}\right)_c} \qquad (A6)$$

in terms of normalized quantities, where $u = mV^2/2kT$.

The program which computed solutions to Equation (A1) also tabulated along with each solution the value of u for a series of values of x_c in accordance with Equation (A5). The corresponding values of x_{bc} were also tabulated. Some of these results are also shown in Figure A1 in the form of contours of the distance x_c for a constant initial energy u. It is apparent that in general each solution to (A1) has two points where Equation (A5) is satisfied. What this means physically can be seen from Figures A2 and A3. In these figures the equivalent one-dimensional potential, Y(x), is plotted against x, where Y(x) is given by

$$Y(x) = (x_b/x)^2\ u - y(x) \qquad (A7)$$

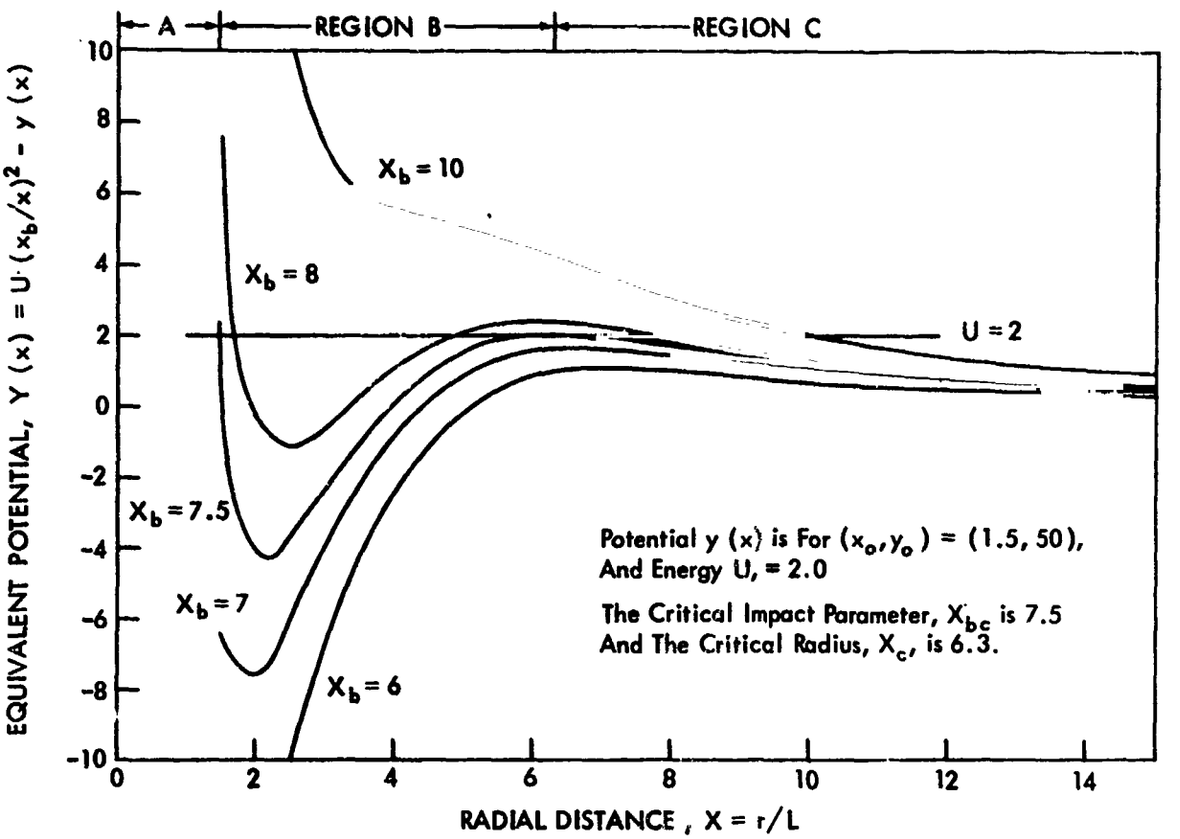

Figure A2. Equivalent Potentials for a Given Potential Distribution and Energy u, but for Various Impact Parameters

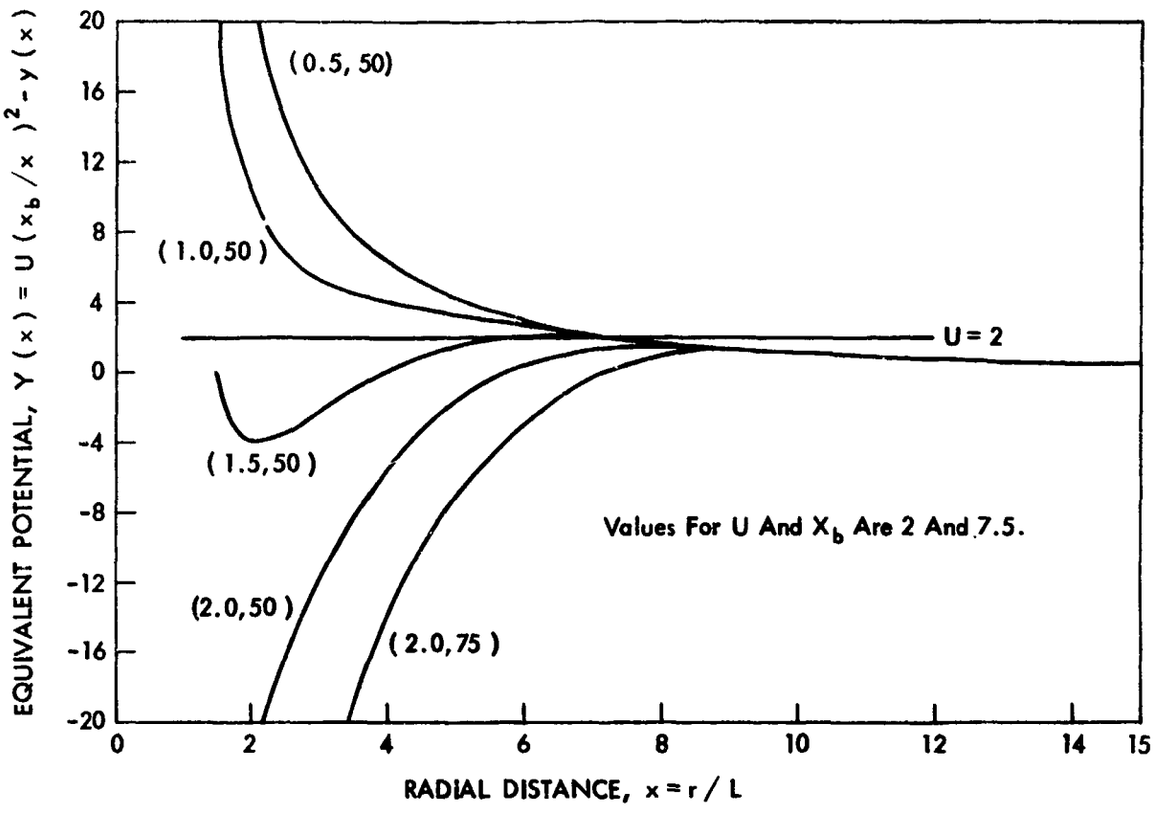

Figure A3. Equivalent Potentials for Various Potential Distributions Denoted by (x_o, y_o), but for a Given Energy and Impact Parameter

(See, for example, Goldstein's discussion of the "fictitious potential" for a two-body central force problem).[123] It is clear from the figures that true pericritical trajectories cannot exist because of the repulsive centrifugal barrier which always dominates the potential at small values of x. It is also generally true that the repulsive centrifugal barrier dominates at large values of x because of the charge on the body by the sheath. However, there may still be a potential well at intermediate values of x. If a particle is to penetrate into this region it must have at least an energy equal to the maximum height of the barrier outside the well.

The distance of closest approach of a particle is the largest value of x in Figure A2 for which the equivalent potential crosses the horizontal straight line corresponding to the particle energy. It is clear, then, that the critical impact parameter, x_{bc}, describes the case when the equivalent potential is just tangent to the particle energy line at the barrier maximum outside the well. The critical radius, x_c, which describes the turning point thus has two values. One is at the position of the barrier maximum and the others is the inner turning point – i.e., the boundaries of region B. Whether or not a particle is collected by the body depends on the relation of the body's radius to the position of the turning point. Particles with impact parameters greater than x_{bc}, the critical impact parameter, will be reflected at the outer centrifugal barrier, while particles with impact parameters less than x_{bc} will come on in to be reflected at the inner barrier.

Three cases may be distinguished corresponding to which of the three regions A, B or C contains the body's radius x_0. If x_0 is in region A, a grazing trajectory exists for an impact parameter x_g less than x_{bc}, and is given by Equation (A4),

$$x_g = x_0 \sqrt{1 + y_0/u} \tag{A8}$$

If x_0 is in region B, a grazing trajectory does not exist (except for trapped particles). All particles with impact parameters less than x_{bc} will spiral in and be collected so that the impact parameter for collection is x_{bc}. In region C grazing orbits again exist and the impact parameter for collection is again x_g of Equation (A8). The rules for collection may be summarized as follows: If $x_0 < x_{bc} < x_g$, use x_{bc} to compute the effective cross-section; otherwise use x_g. The resulting current-voltage curves for various combinations of x_0 and u are shown in Figure 4 of Chapter III.

These rules depend on the fact that the various equivalent potential curves for a given u and (x_0, y_0), but for various values of x_b, do not intersect. This can easily be verified by forming the difference $y_1(x) - y_2(x) = u/x^2 \ (x_{b1}^2 - x_{b2}^2) > 0$ for all x, where $x_{b1} > x_{b2}$.

Figure A3 illustrates how the current to a body changes as the potential is increased. At small potentials corresponding to the uppermost curve the effective cross-section is πx_g^2, which increased linearly with the potential. As the potential increases a well forms which increases in width and depth, so that eventually x_0 moves into and remains in region B. The current is then

$$\frac{I}{I_0} = x_{bc}^2/x_0^2 \tag{A9}$$

which increases more slowly with the potential. Again, it is necessary that the various curves for a given u and x_b but for various solutions to (A1) do not intersect. This may be verified by forming $Y_1(x) - Y_2(x) = y_2(x) - y_1(x)$. Since the solutions y shown in Figure A1 do not intersect this is true of the equivalent potentials as well.

Following Gringauz, we may define x_{bc} as the sheath radius. For large bodies we may make use of this analysis to derive an analytic expression for the sheath radius which may be used in Equations (A9) or (3.13).

For large bodies the second term on the left of Equation (A1) may be neglected, and the right-hand side may be linearized in accordance with the discussion of Section 2 of Chapter I. The solution is then simply

$$y = y_0 e^{-(x-x_0)} \tag{A10}$$

and the condition for x_c is

$$e^{-(x_c - x_0)} (1 - x/2) = - \frac{u}{y_0} \tag{A11}$$

To a first approximation $x_c - x_0$ is given by

$$x_c - x_0 = \ln \left(\frac{y_0 x_0}{2u} \right) \tag{A12}$$

for

$$\left(\frac{y_0 x_0}{2u} \right) > 1$$

and the sheath thickness t by

$$\frac{t}{L} = x_{bc} - x_0 = 1 + \sqrt{1 + \frac{2}{x_0}} \ln \left(\frac{y_0 x_0}{2u} \right) \tag{A13}$$

The error in this approximation increases with increasing ϕ_0 and decreasing x_0. However a comparison with the computer solution for the case where $x_0 = 23$ and $mV^2/2kT = 5$ indicated that the approximate

value for t of (A12) was in error by less than 1%, 10% and 25% for values for $(-\phi_0 e/kT)$ of 1.0, 2.4, and 4.7 respectively. The error in the computed current will be still less, by a factor of about $(2t/r_0)$.

APPENDIX B

SUMMARY

A body in the upper atmosphere or in space will acquire an electric charge through various mechanisms such as impacts by ions and electrons or electron emission. The charge on a body influences its rate of charging with the result that an equilibrium charge, or potential, is reached such that the net current to the body vanishes. Knowledge of the equilibrium potential of a body in space is needed to determine the motion of micrometeorites, the drag on earth satellites, and to assess the behavior of certain experiments on satellites. The various treatments of the problem in the literature have generally been restricted to a consideration of only a few charging mechanisms. Little data has been obtained, and in no case have the measurements been analyzed in terms of the expected potential with an evaluation of all the possible charging mechanisms.

The collection of ions and electrons from the environmental plasma as a function of potential depends upon the body's size, shape, and velocity. The appropriate equations for ion and electron currents to a sphere are available in the literature for bodies small compared to a Debye length. For large bodies, an estimate of the influence of the plasma sheath is required to determine the current in an attractive field. Walker's estimate of sheath thickness is used for bodies with velocities small to the charged particle thermal velocity.[1] Poisson's equation has been solved numerically for high-velocity spheres, and the ion current obtained by an analysis of the ion's distance of closest approach. A negative space charge is formed in the wake behind such a body which reduces the electron current.

Photoemission is an important charging mechanism for bodies in sunlight. Measurements of photoelectric yields in the near and far ultraviolet for aluminum and tungsten are reviewed and compared with photocurrents measured above the atmosphere. A photocurrent density near 4×10^{-9} amp/cm^2 is indicated for both materials. Secondary electron emission upon energetic ion or electron impact may also be an important charging mechanism, especially in the earth's radiation belts. Secondary yields taking into account reflection and primary back-diffusion are presented for electrons and for ions for energies up to 10 MeV.

There are several other charging mechanisms that in general may be neglected except possibly in special circumstances. These include the effects of cosmic rays, radioactivity, thermionic and field emission, collisions with dust grains, and the influence of radio-frequency electric fields. A magnetic field can affect the equilibrium potential of a body in two ways: the motion of the body through the field induces a potential gradient which results in an increased electron current; in addition, the restriction of the electron to a spiralling motion along the field line decreases the effective collection area of the body. Expressions describing this latter effect are derived for both cylinders and spheres.

These charging mechanisms are evaluated for conditions in the upper atmosphere and in interplanetary space, and are combined into expressions from which the equilibrium potential may be determined. In the ionosphere where electron densities are relatively high, the equilibrium potential is typically a few tenths of a volt negative. The important mechanisms are environmental ion and electron collection. The energetic particles in the earth's radiation belts have a negligible effect

except for the large fluxes of 5 KeV protons observed by Freeman[2] and the 100 KeV protons beyond 2 earth radio observed by Davis and Williamson.[3] At higher altitudes the equilibrium potential may become positive in the sunlight as photoemission predominates over positive ion collection.

In the earth's magnetosphere where electron densities are low, large energetic particle fluxes may occur. The potential is sensitive to the ratio of electron flux to photoemission, and may vary widely. Positive values, which are more likely, are limited to a few volts, but large negative values are possible for large energetic electron fluxes. In interplanetary space positive potentials due to both photoemission and the solar wind protons are expected, unless the material is such that photoemission is unimportant.

The equilibrium potential of the satellite Explorer VIII has been measured between the altitudes of 420 and 2300 km in both darkness and sunlight by means of an electron trap experiment. The results are compared with expected values calculated from the expressions derived earlier for equilibrium potential. The calculations include magnetic field effects and photoemission, and make use of simultaneous measurements of the plasma density and temperature. Although there is considerable scatter to the experimental potentials, there is general agreement at higher altitudes with perhaps a larger photocurrent of about 8×10^{-9} amp/cm^2 indicated. At low altitudes the measured potentials are more negative than anticipated. This is attributed to the effect of a radio-frequency plasma impedance experiment carried on the satellite. It is shown that near satellite perigee where the plasma frequency approaches the probe frequency of 6.5 Mc, the resonant increase of electron current to the probe can quantitatively account for the more negative potentials.

1. E. H. Walker, Plasma Sheath and Screening Around a Stationary Charged Sphere and a Rapidly Moving Charged Body, Ph.D. Thesis, University of Maryland, Physics Dept. (1964).

2. J. W. Freeman, Jr., J. Geophys. Res., 67, 921 (1962).

3. L. R. Davis and J. M. Williamson, Space Research III, (W. Priester, Editor, North-Holland Pub. Co., Amsterdam, 1963), p. 365.

REFERENCES

1. R. E. Bourdeau, E. C. Whipple, Jr. and J. F. Clark, J. Geophys. Res., 64, 1363 (1959).

2. L. Spitzer, Jr., Astrophys. J., 107, 6 (1948).

3. F. L. Whipple, Proc. Amer. Phil. Soc., 83, 711 (1940).

4. E. N. Parker, Astrophys. J., 139, 951 (1964).

5. S. F. Singer, Scientific Uses of Earth Satellites, (J. A. Van Allen, Editor, The U. of Mich. Press, 1956), p. 304.

6. B. Lehnert, Tellus, 8, 408 (1956).

7. R. Jastrow and C. A. Pearse, J. Geophys. Res., 62, 413 (1957).

8. D. B. Beard and F. S. Johnson, J. Geophys. Res., 65, 1 (1960).

9. L. Kraus and K. M. Watson, Phys. Fluids, 1, 480 (1958).

10. K. P. Chopra, Rev. Mod. Phys., 33, 153 (1961).

11. C. Y. Johnson and E. B. Meadows, J. Geophys. Res., 60, 193 (1955).

12. G. Hok and W. G. Dow, Rocket Exploration of the Upper Atmosphere, (R. L. F. Boyd and M. J. Seaton, Editors, Pergamon Press Ltd., London, 1954), p. 240.

13. R. L. F. Boyd, Rocket Exploration of the Upper Atmosphere, (R. L. F. Boyd and M. J. Seaton, Editors, Pergamon Press Ltd., London, 1954), p. 336.

14. W. R. Hoegy and L. H. Brace, The Dumbbell Electrostatic Ionosphere Probe: Theoretical Aspects, Sci. Rept. No. JS-1, Space Physics Research Lab., Univ. of Mich. (1961).

15. N. W. Spencer, L. H. Brace and G. R. Carignan, J. Geophys. Res., 67, 157 (1962).

16. B. Jung, Astron. Nach., 263, 426 (1937).

17. L. Spitzer, Jr., Astrophys. J., 93, 369 (1941).

18. F. Cernuschi, Astrophys. J., 105, 241 (1947).

19. L. Spitzer, Jr. and M. P. Savedoff, Astrophys. J., 111, 593 (1950).

20. E. J. Opik, Irish Astron. J., 4, 84 (1957).

21. K. I. Gringauz and M. K. Zelikman, Uspekhi Fiz. Nauk, 63, 239 (1957).

22. I. M. Imyanitov, Uspekhi Fiz. Nauk, 63, 267 (1957).

23. F. Whipple, Physics and Medicine of the Atmosphere and Space, (O. O. Benson and H. Strughold, Editors, John Wiley and Sons, Inc., New York, 1958), p. 48.

24. H. H. C. Chang and M. C. Smith, Jr., J. Brit. Interpl. Soc., 17, 199 (1959-60).

25. Aerospace Technical Intelligence Study, Soviet Geophysical Measurements with Sputnik III, Task Nr. 573102, Aerospace Technical Intelligence Center, (1960).

26. K. I. Gringauz, V. V. Bezrukikh and V. D. Ozerov, Iskusstv. Sputniki Zemli, 6, 63 (1961).

27. D. B. Beard and F. S. Johnson, J. Geophys. Res., 66, 4113 (1961).

28. P. D. Grannis, J. Geophys. Res., 66, 4293 (1961).

29. E. H. Walker, J. Geophys. Res., 67, 2586 (1962).

30. S. F. Singer and E. H. Walker, Icarus, 1, 112 (1962).

31. S. F. Singer and E. H. Walker, Icarus, 1, 7 (1962).

32. G. L. Gdalevich, Doklady AN SSSR, Geof. 146, 1064 (1962).

33. G. L. Gdalevich, Iskusstv. Sputniki Zemli, 17, 42 (1963).

34. I. M. Imyanitov, G. L. Gdalevich, and Ya. M. Shvarts, Iskusstv. Sputniki Zemli, 17, 66 (1963).

35. R. C. Sagalyn, M. Smiddy and J. Wisnia, J. Geophys. Res., 68, 199 (1963).

36. C. S. Shen and K. P. Chopra, J. Atmos. Sci., 20, 359 (1963).

37. K. Rawer, Radio Astronomical and Satellite Studies of the Atmosphere, (J. Aarons, Editor, North Holland Pub. Co., 1963), p. 385.

38. E. H. Walker, Plasma Sheath and Screening Around a Stationary Charged Sphere and a Rapidly Moving Charged Body, Ph. D. Thesis, Univ. of Md. Physics Dept. (1964).

39. R. T. Bettinger, An In Situ Probe System for the Measurement of Ionospheric Parameters, Ph. D. Thesis Univ. of Md. Physics Dept. (1964).

40. R. E. Bourdeau, J. L. Donley, G. P. Serbu and E. C. Whipple, Jr., J. Astronaut. Sci., 8, 65 (1961).

41. H. M. Mott-Smith and I. Langmuir, Phys. Rev., 28, 727 (1926).

42. K. T. Compton and I. Langmuir, Rev. Mod. Phys., 2, 123 (1930).

43. G. J. Schulz and S. C. Brown, Phys. Rev., 98, 1642 (1955).

44. H. E. Hinteregger, Private Communication (1961).

45. M. Kanal, Theory of Current Collection of Moving Spherical Probes, Sci. Rept. No. JS-5, Space Physics Research Lab., Univ. of Mich. (1962).

46. Ja. L. Al'pert, A. V. Gurevic and L. P. Pitaevskij, Space Sci. Rev., 2, 680 (1963).

47. H. E. Hinteregger, L. A. Hall and G. Schmidtke, Proceedings of the Fifth International Space Science Symposium, Florence (1964).

48. P. J. Nawrocki and R. Papa, Atmospheric Processes, GCA Rept. No. 61-37-A, Geophysics Corp. of Amer., Bedford, Mass. (1961).

49. H. E. Hinteregger and K. Watanabe, J. Opt. Soc. Am., 43, 604 (1953).

50. H. E. Hinteregger, K. R. Damon and L. A. Hall, J. Geophys. Res., 64, 961 (1959).

51. W. C. Walker, N. Wainfan and G. L. Weissler, J. Appl. Phys., 26, 1366 (1955).

52. H. C. Rentschler, D. E. Henry and K. O. Smith, Rev. Sci. Instr., 3, 794 (1931).

53. A. P. Lukirskii, M. A. Rumsh and L. A. Smirnov, Optics and Spectrosc., 9, 265 (1960).

54. R. Suhrman and J. Pietrzyk, Z. Physik, 122, 600 (1944).

55. H. de Laszlo, Phil. Mag., 13, 1171 (1932).

56. R. H. Fowler, Phys. Rev., 38, 45 (1931).

57. L. A. DuBridge, New Theories of the Photoelectric Effect, (Hermann and Cie, Paris, 1935).

58. A. H. Warner, Phys. Rev., 38, 1871 (1931).

59. O. Hachenberg and W. Brauer, Advances in Electronics and Electron Physics, (L. Marton, Editor, Academic Press Inc., New York, 1959), Vol. 11, p. 413.

60. H. S. W. Massey and E. H. S. Burhop, Electronic and Ionic Impact Phenomena, (Oxford Univ. Press, London, 1952).

61. R. Kollath, Handbuch Der Physik, (S. Flugge, Editor, Springer-Verlag, Berlin, 1956), Vol. 21, p. 232.

62. H. Bruining, Physics and Applications of Secondary Electron Emission, (Pergamon Press, New York, 1954).

63. A. J. Dekker, Solid State Physics, (F. Seitz and D. Turnbull, Editors, Academic Press Inc., New York, 1958), Vol. 6, p. 251.

64. A. R. Shulman and J. I. Myakinin, Doklady Akad. Nauk, USSR, 91, 1075 (1953).

65. G. A. Harrower, Phys. Rev., 104, 52 (1956).

66. H. Kanter, Phys. Rev., 121, 677 (1961).

67. A. A. Schultz and M. A. Pomerantz, Phys. Rev., 130, 2135 (1963).

68. C. Herring and M. H. Nichols, Revs. Mod. Phys., 21, 185 (1949).

69. E. Guth and C. J. Mullin, Phys. Rev., 59, 575 (1941).

70. H. Kanter, Phys. Rev., 121, 681 (1961).

71. H. D. Hagstrum, Phys. Rev., 96, 325 (1954).

72. H. D. Hagstrum, Phys. Rev., 89, 244 (1953).

73. J. H. Parker, Jr., Phys. Rev., 93, 1148 (1954).

74. L. B. Loeb, Basic Processes of Gaseous Electronics, (Univ. of California Press, Berkeley and Los Angeles, 1955), p. 778.

75. P. Cousinie et al, Comptes Rendus, 249, 387 (1959).

76. S. N. Ghosh and S. P. Khare, Phys. Rev., 129, 1638 (1963).

77. A. G. Hill, W. W. Buechner, J. S. Clark and J. B. Fisk, Phys. Rev., 55, 463 (1939).

78. S. N. Ghosh and S. P. Khare, Phys. Rev., 125, 1254 (1962).

79. B. Aarset, R. W. Cloud and J. G. Trump, J. Appl. Phys., 25, 1365 (1954).

80. N. N. Petrov, Bull. Acad. Sci. USSR, Phys. Series, 26, No. 11, 1350 (1962).

81. L. N. Large, Proc. Phys. Soc., 81, 1101 (1963).

82. M. L. E. Oliphant, Proc. Roy. Soc. A, 127, 373 (1930).

83. J. S. Allen, Phys. Rev., 55, 336 (1939).

84. H. D. Hagstrum, Phys. Rev., 123, 758 (1961).

85. J. S. Colligon, Vacuum, 11, 272 (1961).

86. W. Whaling, Handbuch Der Physik, (S. Flugge, Editor, Springer-Verlag, Berlin, 1956) Vol. 34, p. 193.

87. E. Anders, The Moon, Meteorites and Comets, (B. M. Middlehurst and G. P. Kuiper, Editors, The University of Chicago Press, Chicago, 1963), p. 402.

88. J. Wasson, J. Geophys. Res., 67, 3513 (1962).

89. W. M. Alexander, C. U. McCracken, L. Secretan and O. E. Berg, Space Research, (W. Priester, Editor, North-Holland Pub. Co., Amsterdam, 1963), Vol. 3, p. 891.

90. R. E. Bourdeau, J. E. Jackson, J. A. Kane and G. P. Serbu, Space Research, (H. K. Kallmann Bijl, Editor, North-Holland Pub. Co., Amsterdam, 1960), Vol. 1, p. 328.

91. K. Takayama, H. Ikegami and S. Miyazaki, Phys. Rev. Letters, 5, 238 (1960).

92. Y. Aono, K. Hirao and S. Miyazaki, J. Radio Res. Lab., 8, 453 (1961).

93. F. W. Crawford and R. S. Harp, J. Geophys. Res., 70, 587 (1965).

94. R. S. Harp and F. W. Crawford, J. Appl. Phys., 35, 3436 (1964).

95. L. G. Smith, Rocket Measurements of Electron Density and Temperature in the Nighttime Ionosphere, Tech. Report 62-1-N, Geophysics Corp. of America, Bedford, Mass. (1962).

96. R. E. Bourdeau and S. J. Bauer, Space Research III, (W. Priester, Editor, North-Holland Pub. Co., Amsterdam, 1963), p. 173.

97. S. Chandra, J. Geophys. Res., 68, 1937 (1963).

98. N. Sissenwine, Astronautics, 52 (August, 1962).

99. R. E. Bourdeau, Space Science Reviews, 1, 683 (1963).

100. S. J. Bauer, Nature, 197, 37 (1963).

101. S. J. Bauer, Hydrogen Ions, NASA Tech. Note X-615-64-48, Washington, D. C. (1964).

102. G. P. Serbu and E. J. Maier, Results from the IMP 1 Retarding Potential Experiment, presented at the Fourth Western National Meeting of the Am. Geophys. Union, Seattle, Wash. (1964).

103. V. G. Kurt and V. I. Moroz, Planet. Space Sci., 9, 259 (1962).

104. W. N. Hess, Space Science Reviews, 1, 278 (1962).

105. J. W. Freeman, Jr., The Morphology of the Electron Distribution in the Outer Radiation Zone and Near the Magnetospheric Boundary as Observed by Explorer XII, Ph. D. Thesis, State University of Iowa, Physics Dept. (1963).

106. H. H. Hilton, J. R. Stevens and A. L. Vampola, Observations of Large Fluxes of Low Energy Protons, presented at the Fourth Western National Meeting of the Am. Geophys. Union, Seattle, Wash. (1964).

107. B. J. O'Brien, Space Science Reviews, 1, 415 (1963).

108. L. R. Davis and J. M. Williamson, Space Research III, (W. Priester, Editor, North-Holland Pub. Co., Amsterdam, 1963), p. 365.

109. E. C. Whipple, Preliminary Electron Energy Spectra Below 30 eV in the Magnetosphere from OGO 1, presented at the Fourth Western National Meeting of the Am. Geophys. Union, Seattle, Wash. (1964).

110. J. W. Freeman, Jr., J. Geophys. Res., 67, 921 (1962).

111. E. N. Parker, Planet. Space Sci., 9, 461 (1962).

112. A. Bonetti, H. S. Bridge, A. J. Lazarus, B. Rossi, and F. Scherb, J. Geophys. Res., 68, 4017 (1963).

113. E. C. Whipple and B. E. Troy, Preliminary Data from the Ion-Electron Trap on OGO, presented at the Annual Meeting of the Am. Geophys. Union, Washington, D. C. (1965).

114. R. E. Bourdeau, J. L. Donley and E. C. Whipple, Jr., Instrumentation of the Ionosphere Direct Measurements Satellite (Explorer VIII), NASA Tech. Note D-414, Washington, D. C. (1962).

115. R. E. Bourdeau, E. C. Whipple, Jr., J. L. Donley and S. J. Bauer, J. Geophys. Res., 67, 467 (1962).

116. G. P. Serbu, R. E. Bourdeau and J. L. Donley, J. Geophys. Res., 66, 4313 (1961).

117. E. C. Whipple, Jr., Proc. I.R.E., 47, 2023 (1959).

118. J. V. Lincoln, J. Geophys. Res., 66, 979 (1961).

119. J. V. Lincoln, J. Geophys. Res., 66, 1279 (1961).

120. H. A. Whale, J. Geophys. Res., 69, 447 (1964).

121. F. W. Crawford, Private Communication (1965).

122. G. P. Serbu and E. J. Maier, Private Communication (1965).

123. H. Goldstein, Classical Mechanics, (Addison-Wesley Pub. Co., Cambridge, Mass., 1953) p. 63.